POLITECNICO DI TORINO

Collegio di Ingegneria Chimica e dei Materiali

Corso di Laurea Magistrale
in Ingegneria Chimica e dei Processi Sostenibili

Tesi di Laurea Magistrale

On the dehydration kinetics of liquid of alimentary and industrial interest: single droplet approach in acoustic levitation

Relatore

prof. Stefania Specchia

Candidato
Paolo Testa

October 2020

The project has been carried out at “Laboratoire Interfaces et milieu Divisés” (IMID) during an Erasmus project at UTC – Université de Technologie de Compiègne under the supervision of Prof. M. Saleh Khashayar

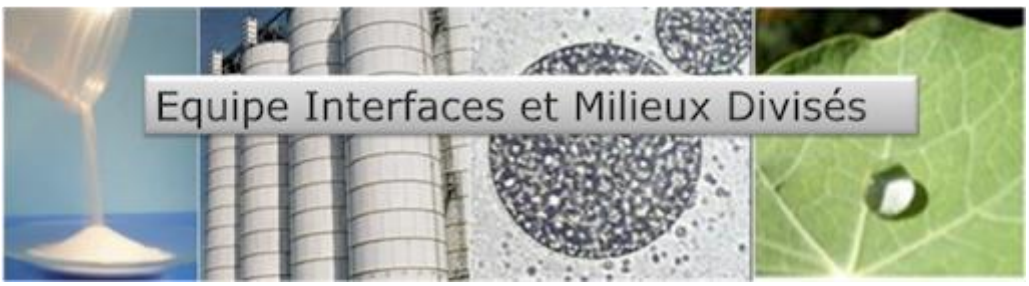

Table of content

1. Riassunto in italiano

1.1. Prefazione

L'idea e l'ispirazione per l'inizio di questa tesi finale è nata durante la mia permanenza all' UTC-Université de Technologie de Compiègne in Francia, durante l'anno accademico 2019-2020 da me trascorso all'estero come parte di un progetto Erasmus. Trovandomi a dover fare un piccolo lavoro di ricerca sperimentale durante il primo semestre, sono entrato in contatto con il direttore del dipartimento di GP (Génie des Pocédés, ingegneria di processo), M. Saleh Khashayar, che mi propose di continuare il lavoro precedentemente iniziato da una studentessa, che aveva raggiunto risultati interessanti, ma questionabili. L'argomento interessante e l'occasione ideale, spiegai a M. Saleh la mia particolare necessità quale studente italiano di trovare un argomento di tesi, ed egli si trovò d'accordo a continuare, approfondendo, questo lavoro per trasformarlo in un progetto finale. Dopo aver contattato la mia relatrice presso il Politecnico di Torino, Prof. Specchia, ed aver ricevuto l'approvazione, cominciai i miei esperimenti in febbraio, soltanto per doverli interrompere dopo un mese a causa della situazione di emergenza sanitaria, che ha causato la chiusura delle strutture universitarie, ivi compreso il mio laboratorio e il mio ufficio. Ciò che doveva essere un lavoro sperimentale di comparazione dei diversi comportamenti di vari liquidi di interesse industriale, tra i quali avevo pianificato acqua, caffè e latte, con l'intenzione di spingermi anche oltre qualora il tempo si fosse dimostrato sufficiente, si è trasformato perciò in un lavoro compilativo dei dati da me acquisiti in questo breve tempo, e di comento dei fenomeni osservati. Questo breve studio conferma i comportamenti già conosciuti, anche se rimangono alcuni interrogativi su alcuni comportamenti riscontrati, poiché il tempo e le condizioni di eccezionalità non hanno consentito di proseguire ulteriormente le investigazioni.

1.2. Introduzione

La tecnica di evaporare liquidi per ottenere dei prodotti polverulenti è molto comune e di grande interesse nella pratica industriale in diversi campi, spaziando dall'essicazione di prodotti alimentari, come latte, caffè, o anche più viscosi come albumi d'uovo, fino a campi più strettamente legati all'ingegneria di processo, come la produzione di laminati plastici o colle (WHITEHEAD, BALL, FINE, & LANGOLF, 2010). Questa essicazione è tipicamente ottenuta tramite la polverizzazione della miscela liquida in nuvole di spray, dove miliardi di micro e nano particelle vengono formate. Quindi, a partire dalle prime applicazioni fra il 1920 e 1930 (Bücks & Müller , 1933)questo processo ha dovuto affrontare il problema di gestire un numero estremamente grande di elementi, ciascuno con differenti traiettorie e comportamenti particolari. L'approccio e la descrizione del fenomeno furono quindi affrontati in maniera integrale, e il dimensionamento delle apparecchiature fu reso possibile grazie ad una approssimazione dell'intero processo (Masters, 1972). Vi è da dire che anche oggigiorno una descrizione qualitativa dell'intero processo non è completamente possibile, e numerose ricerche sono in corso per affrontare il problema tramite simulazioni CFD. Un nuovo metodo da diversi anni ha preso piede nella comunità scientifica, a partire dal lavoro e dalle correlazioni di Ranz e Marshall (Ranz & Marshall, 1952): si tratta dell' approccio *Single Droplet Drying* (SDD), nel quale una singola goccia e inserita in un ambiente controllato, il quale cerca di simulare le vere condizioni dell'ambiente di lavoro, ovvero l'umidità relativa, la temperatura e la presenza o meno di una corrente convettiva. Lo studio della singola goccia in evaporazione è quindi in grado di fornire dei risultati che, adeguatamente interpretati, possono portare a delle interpretazioni allargabili all'intera nuvola di spray.

1.3. I metodi

Per quanto riguarda quindi i metodi di applicazione di questa tipologia di studio sulla singola goccia, viene fatto riferimento a tre tecniche (Fu, Wai Woo, & Dong Chen, 2012): *Free-Falling Droplet, Glass Filament* e levitazione acustica. La presenza di vantaggi e svantaggi per ognuna di essa ha portato al fatto che ancora oggi non sia definita una tecnica standard, ma che in base alle necessità o alle particolari condizioni ne venga preferita una all'altra.

Nel metodo *Free-Falling*, il più vecchio ed anche il più semplice concettualmente, una goccia generata da un eiettore capillare viene fatta cadere attraverso una torre. Se in questo caso il grande vantaggio è quello di poter regolare in modo molto preciso la dimensione della goccia, il rateo di gocciolamento e le condizioni del gas interno alla torre, il problema è rappresentato dalla difficoltà di monitorare la caduta e ricavare informazioni dall'osservazione diretta, costringendo l'osservatore a piazzare diverse telecamere o ricavare dati tramite misurazioni indirette, come la velocità terminale della goccia.

Un metodo più fine ed elaborato, che ha riscosso un duraturo successo, è quello del *Glass Filament*. In questo caso la goccia viene sospesa alla punta di un finissimo filamento di vetro, con specifiche proprietà fisiche e geometriche. La goccia rappresenta un peso all'estremità della fibra vitrea, e causa una deflessione verso il basso; successivamente, evaporando il liquido, il filamento, scaricato del peso, ritorna alla sua posizione iniziale. Conoscendo esattamente le proprietà elastiche del filamento è facile, monitorandone la deflessione, estrapolare i dati cinetici sull'evaporazione. Inoltre, può essere una osservazione diretta dei cambiamenti di dimensione e di morfologia della goccia, ed anche facilmente, considerando che la goccia non è più in caduta libera. Lo svantaggio di questa tecnica è il fatto che la perturbazione rappresentata dalla punta vitrea all'interno della goccia può rappresentare un nucleo di germinazione di cristalli di solido dissolto.

Più recentemente, a partire dagli anni Novanta, la tecnica della levitazione acustica ha acquistato una popolarità sempre più crescente. Si tratta di un'altra tecnica in cui il campione è sospeso, ma la sospensione in questo caso è indotta grazie agli ultrasuoni. Questi sono in grado di generare dei nodi di pressione nel gas, grazie alla particolare disposizione degli altoparlanti. La gocciolina viene quindi portata in sospensione se la forza generata dal campo di pressione degli ultrasuoni è un grado di vincere la forza peso. Il grande vantaggio di questa tecnica è rappresentato dalla possibilità di osservare l'evaporazione, e l'eventuale formazione di una crosta solida, senza la perturbazione di un corpo esterno che possa stimolare fenomeni di germinazione. Inoltre, tale tecnica risulta relativamente semplice nella sua attuazione, anche per una persona non estremamente esperta. I punti deboli sono rappresentati dall'azione stessa del campo ultrasonico, che è causa principalmente di due effetti. Inizialmente, l'incidente campo ultrasonico causa una deformazione della goccia, portandola ad assumere una forma oblata. Questa forma, inoltre, cambia durante l'evaporazione, tendendo col tempo a divenire più sferica; questo fenomeno impedisce di considerare la goccia una sfera e ci costringere a tenere in considerazione l'evoluzione della forma. Secondariamente, è stato osservato che il campo ultrasonico forma delle zone di turbolenza attorno alla goccia (YARIN, BRENN, KASTNER, RENSINK, & TROPEA, 1999). Queste regioni di vorticosità implicano che è di fatto impossibile osservare l'evaporazione della goccia in un ambiente stagnante, ed inoltre rappresentano zone in cui l'umidità evaporante dalla goccia viene catturata e trattenuta, ostacolando, almeno in parte, la diffusione verso l'esterno.

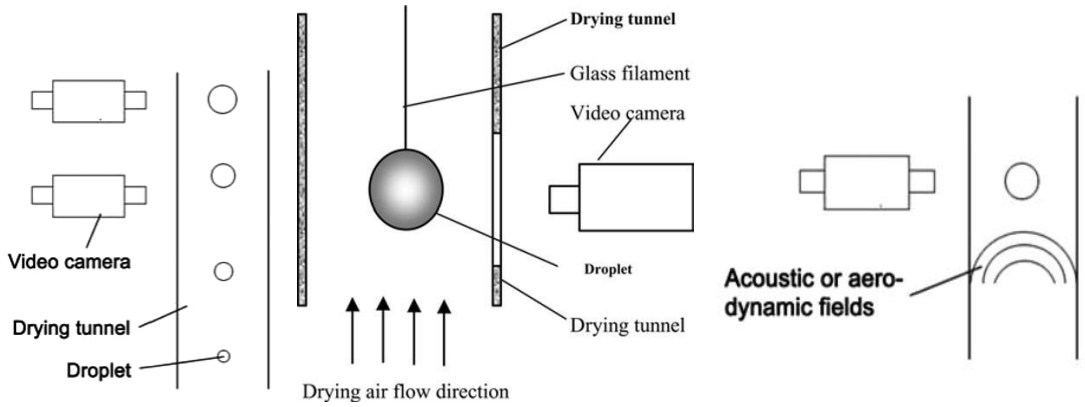

Figura 1.1 Le tre tipologie di SDD, da sinistra a destra: Free Falling, Glass Filament, levitazione acustica (Fu, Wai Woo, & Dong Chen, 2012)

Dopo aver illustrato ciò, e tenendo conto della grande quantità di letteratura prodotta sull'argomento, il mio lavoro si è avvalso della tecnica di levitazione acustica. Infatti, molto recentemente, grazie al miglioramento delle tecnologie di stampa 3-D e all'introduzione di nuovi altoparlanti miniaturizzati in grado di sostituire i vecchi e costosi emettitori piezoelettrici, un largo interesse si è sviluppato su questi dispositivi, grazie alla possibilità creatasi di costruire dei dispositivi estremamente economici e resistenti. Tale scelta si è rivelata anche forzata dal fatto che il laboratorio al quale ero assegnato poteva avvalersi soltanto di quel tipo di dispositivo.

1.4. Principi e strumentazione

1.4.1. Principi di levitazione acustica

La levitazione acustica, anche detta *acustoforesi* (Hilgenfeldt, Rallabandi, Agarwal, & Raju)consiste nel mantenere in sospensione un corpo, liquido o solido, in un mezzo gassoso. Ciò è possibile sfruttando la differenza di pressione nel gas stesso indotta dall'applicazione di un campo ultrasonico, con una frequenza quindi superiore almeno ai 20 KHz. Il suono si propaga nel mezzo gassoso tramite la formazione di zone di alta e bassa pressione; si noti che la differenza in pressione fra queste zone è estremamente bassa, circa diecimila volte inferiore della pressione atmosferica, ma sufficiente a indurre una vibrazione della membrana di un microfono, della corda di uno strumento o di un timpano umano. Inoltre, il suono, in quanto onda meccanica, è in grado di trasportare quantità di moto, grazie alla forza di radiazione acustica (Marzo, Barnes, & Drinkwater, 2017). Quando la forza esercitata su un oggetto è sufficientemente grande e converge da tutte le direzioni, le particelle possono essere fatte levitare e intrappolate (Brant, 2001).

Un'onda sonora stazionaria presenta una cresta, dove l'ampiezza dell'onda è massima per i valori positivi, e una valle, dove l'ampiezza è massima per i valori negativi. In mezzo troviamo un nodo di pressione, in corrispondenza del quale la pressione relativa è nulla. In questi punti non perturbati, è possibile far levitare un corpo esterno. Infatti, guardando la figura, si nota che al di sopra del nodo di pressione A si trova una zona di attrazione verso il nodo stesso, rappresentata da un valore negativo della forza di levitazione F_L, mentre al di sotto vi è una zona di repulsione, viceversa caratterizzata da valori positivi di F_L.. L'azione combinata di queste due zone è quella di mantenere la particella in posizione nel nodo di pressione. È evidente che la presenza di una sola onda non è in grado di permettere a un corpo esterno di rimanere in posizione stabile: per intuirlo facilmente, sarebbe come voler sistemare in equilibrio una sfera sulla punta di una ripida collina idealmente e perfettamente liscia. Sebbene posizionata in un punto virtualmente stabile, a sfera non è in una posizione di stabilità, e cadrà da una parte o dall'altra come conseguenza della minima perturbazione. Similmente, sono necessarie almeno due onde risonanti e che si intersechino in corrispondenza di un comune nodo di pressione. La configurazione più comune è quindi quella ad asse singolo, posizionata verticalmente.

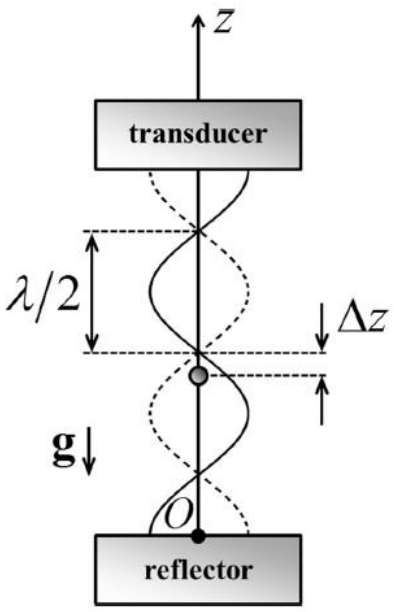

Figura 2 : sketch di un dispositivo trasduttore-riflettore. (Andrade, Pérez, & Adamowski, 2018)

1.4.2. Strumenti

La levitazione acustica ha rappresentato storicamente un tipo di tecnica elevata, di nicchia, soprattutto a causa degli alti costi dei dispositivi de dell'alto livello di formazione richiesto per operarli. Il nucleo costitutivo del dispositivo è l'emettitore piezoelettrico, in grado di generare onde ultrasoniche stabili, di fronte al quale si trova un riflettore concavo. Il principio di funzionamento si basa sull'emissione di onde applicando una tensione attraverso un cristallo piezoelettrico. Il campo elettrico applicato causa l'allineamento dei dipoli nel verso del campo, ed una conseguente espansione del cristallo. Regolando la chiusura e l'apertura del circuito è possibile ottenere specifiche frequenze. Questi tipi di cristalli sono una maniera efficace di convertire energia elettrica in energia meccanica. Questo tipo di tecnologia non è solo costosa da implementare, ma anche complessa da mettere in funzione, poiché l'emettitore deve essere regolato a distanza in maniera estremamente precisa, tramite una vite micrometrica, od altrimenti emergeranno problemi di instabilità.

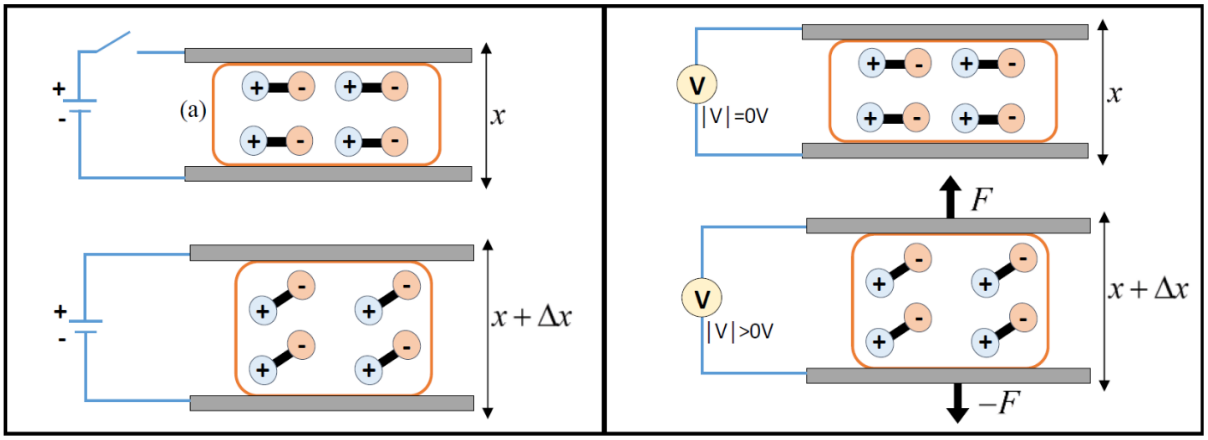

Figura 3 : sketch di funzionamento di un dispositivo a cristallo piezoelettrico. (Mecham, 2018)

Essendo questo tipo di tecnologia così problematico, recentemente un nuovo tipo di dispositivo ha fatto la sua comparsa nel campo. Si chiama TinyLev, e si tratta esattamente del tipo di dispositivo utilizzato per le mie osservazioni. Nel 2017, una pubblicazione del gruppo guidato da A. Marzo, dell'università di Bristol, descriveva il design e il funzionamento di un novo tipo di dispositivo di

levitazione acustica. In questo nuovo apparecchio, la scelta è slittata da un solo emettitore e uno specchio risonatore verso una configurazione di corone concentriche di emettitori posizionate al di sopra e al di sotto della particella in levitazione. Questi piccoli altoparlanti sono molto più economici dei vecchi emettitori piezoelettrici Langevin. Il nome stesso, TinyLev, è stato scelto per convogliare, anche grazie a una terminologia non strettamente scientifica, l'intenzione degli sviluppatori e la speranza che il futuro porti a una democratizzazione di questa tecnologia grazie alla miniaturizzazione e alla crescente popolarità degli hardware didattici e della stampa 3-D.
Nel progetto di Marzo, 72 trasduttori sono stati installati all'interno di due calotte semisferiche, distanziate di una distanza pari a un multiplo intero della lunghezza d'onda. Nel modello realizzato da M. Yorick Buot de l'Epine per il laboratorio dell'UTC, 120 trasduttori sono stati installati per motivi di sovradimensionamento precauzionale, all'interno delle due calotte separate di 110 mm. Inoltre, per evitare danni dovuti alla caduta delle gocce sulle parti elettroniche, un sottile strato di rete di nylon, tenuto in posizione da un supporto, era posizionato al di sotto della particella sospesa.

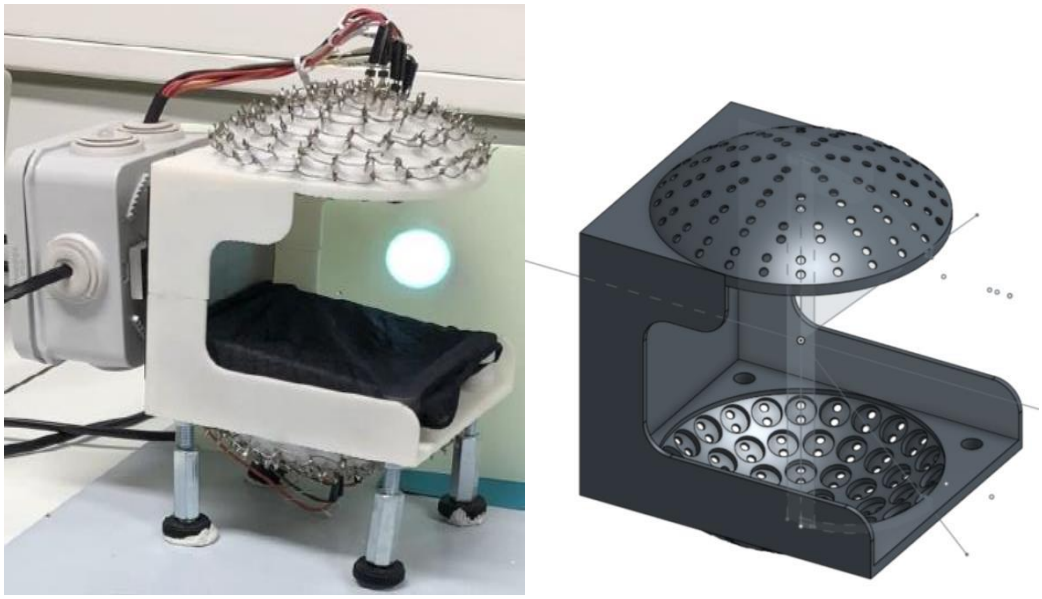

Figura 4 : immagine fotografica e del modello 3-D del dispositivo di levitazione

Per portare a termine le osservazioni mi sono potuto avvalere della seguente strumentazione di laboratorio:

- Un armadio ad atmosfera controllata, grazie al quale era possibile gestire le condizioni di umidità e temperatura. All'interno dell'armadio era inserito l'apparecchio di levitazione e veniva svolto l'esperimento vero e proprio di essicazione. Tutti gli esperimenti sono stati condotti a T=25°C e HR=38%, e questo per evitare di danneggiare la componentistica elettronica del levitatore.
- Un generatore di tensione ed un amplificatore, necessari al funzionamento del dispositivo di levitazione
- Un oscilloscopio, che permettesse di leggere il valore della frequenza e della tensione applicate
- Una telecamera e un treppiede da montarsi all'esterno dell'armadio, per registrare cosa accadesse durante l'esperimento. La cattura delle immagini era resa possibile dalle ante trasparenti dell'armadio.
- Un software di cattura e digitalizzazione delle immagini

Figura 5 : l'armadio ad atmosfera modificata e la telecamera posizionata sul treppiede

1.5. Metodi e sperimentazione

Scopo dell'esperimento è quindi quello di osservare direttamente l'evaporazione di una goccia in sospensione. Anzitutto è possibile fare un primo discrimine fra due grandi campi: liquidi puri e miscele.

Per i liquidi puri è ragionevole considerare che l'evaporazione avvenga a velocità costante. Di fatto, nessun altro fenomeno insiste sulla goccia, ed è stato provato che l'evaporazione di questi campioni di liquido segue linearmente una funzione del d^2 (Yarin, Brenn, Kastner, & Tropea, 2002). Questo significa che il quadrato del diametro della goccia decresce linearmente con il tempo, fino ad arrivare a completa evaporazione. La mia diretta esperienza ha in particolare provato che non è affatto banale arrivare a registrare una completa evaporazione della goccia, poiché questa tecnica di levitazione acustica deve sottostare a una varietà di instabilità. È allora molto più probabile che la goccia, dopo essersi quasi completamente consumata, imploda, o semplicemente cada dalla posizione di stabilità a causa delle oscillazioni.

La situazione cambia notevolmente quando si prende in considerazione un campione di miscela liquido-solido. Infatti, dopo un primo periodo in cui il rateo di evaporazione è praticamente costante, a causa dell'aumento della concentrazione dei solidi disciolti, l'evaporazione rallenta, e si forma un plateau. Si osserva così una evaporazione in due fasi. Nella prima, il liquido (nel nostro caso acqua) evapora dalla superficie, migrando dal corpo liquido verso l'ambiente circostante. In questa fase la legge del d^2 è rispettata. A partire da un certo punto, il meccanismo di evaporazione cambia, e l'effetto si può notare dalla forma del grafico volume/tempo (o area/tempo). Questo cambiamento nel rateo è dovuto alla formazione di una crosta superficiale, che ostacola l'evaporazione stessa; il liquido deve prima diffondere nella crosta solida e quindi dalla crosta all'ambiente. Al di là di un certo punto detto "locking point" (de Souza Lima, Ré, & Arlabosse, 2019), non è possibile osservare un'ulteriore diminuzione di dimensione, poiché la crosta è sufficientemente spessa da non potersi più compattare oltre. Questo studio si è concentrato sulla prima parte dell'evaporazione, per poterne dedurre il numero di Sherwood.

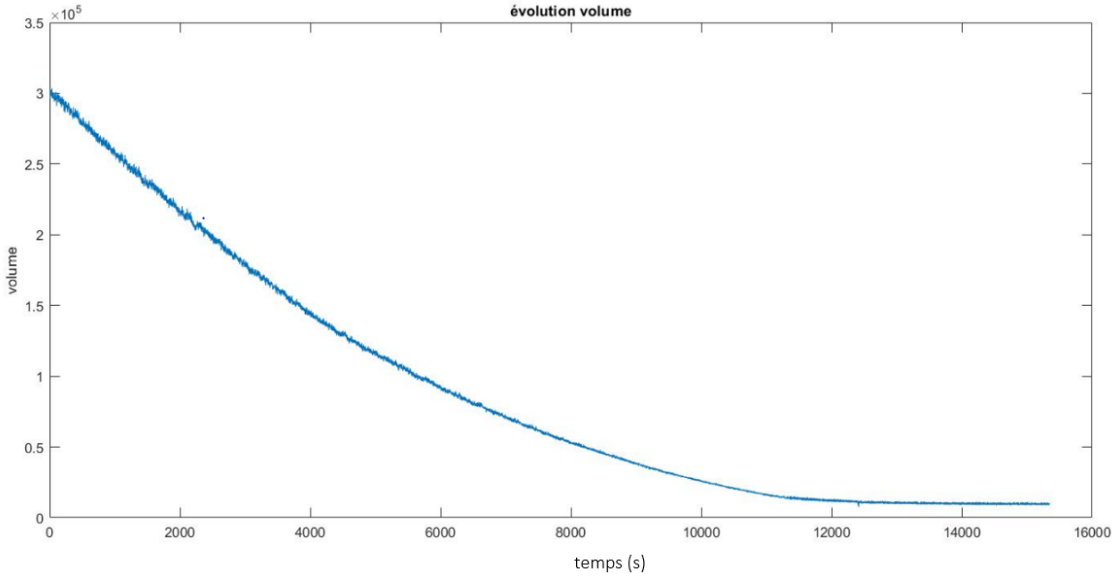

Figura 1.6 : esempio di evoluzione del volume nel tempo; campione di acqua pura

1.5.1. Preparazione dei campioni e procedura

Il periodo iniziale del lavoro è stato incentrato sulla stesura e la standardizzazione di una procedura, a partire dal lavoro precedentemente svolto, da seguire durante gli esperimenti. Tale procedura può essere schematizzata come qui riportato:

a) Preparazione del campione di miscela liquida
b) Posizionamento della goccia all'interno dell'armadio
c) Iniziare la levitazione e la cattura delle immagini, quindi l'esperimento
d) Attendere la consumazione completa della goccia
e) Trasferire i dati dal pc di laboratorio su uno più potente
f) Elaborare e interpretare i dati grazie a un modello di calcolo dedicato

I campioni di sono stati preparati con caffè macinato estratto in differenti maniere, anche tramite una caffettiera modello Moka Bialetti. Purtroppo, solo un tipo di osservazione è stata fatta per il latte intero, poiché il tempo è venuto a mancare.

Una volta preparati i campioni, era possibile passare al laboratorio ove si trovava l'armadio ad atmosfera controllata. Questo tipo di macchinario necessita di almeno tre ore per portarsi alle condizioni selezionate, ed è necessario programmare accuratamente gli esperimenti per evitare tempi morti. Anche il posizionamento della goccia è un momento cruciale, poiché risulta necessario aprire le ante trasparenti per accedere al dispositivo di levitazione; bisogna quindi essere estremamente rapidi per non modificare le condizioni di temperatura e umidità formatesi all'interno. Per facilitare la ricerca della posizione assiale dei nodi di pressione, è utile aiutarsi con una piccola biglia di polistirene. Questa riusciva ad essere posizionata facilmente, e rappresentava un utile punto di riferimento. Pur non essendo grande abbastanza per interferire con le onde ultrasoniche, era comunque preferibile posizionare la goccia di liquido, oggetto dell'osservazione, al di sotto della biglia, per evitare ulteriori interferenze.
Quindi, la goccia era posizionata tramite una pipetta microlitrica. Il volume impostato era di 5 µl; un volume relativamente grande come questo permetteva infatti l'uso di una pipetta usa e getta sufficientemente grande da non indurre fenomeni di capillarità che ostacolassero il distacco della goccia dalla plastica. Inoltre, 5 µl rappresenta un volume insolitamente grande, raramente oggetto di precedenti ricerche, perciò io ed il mio tutore abbiamo pensato fosse interessante osservare dei possibili fenomeni particolari legati a tale dimensione caratteristica. La cattura delle immagini cominciava nel momento in cui la goccia era piazzata, per periodi di tempo che andavano da un minimo di 1000 secondi fino a più di 3000. I dati erano raccolti sul momento, quindi trasferiti ad un pc dedicato per l'elaborazione.

1.5.2. Interpretazione delle immagini

Per interpretare le migliaia di immagini registrate è stato sviluppato, grazie all'aiuto del professore M. Mottelet Stephan del dipartimento di informatica, un codice Matlab in grado di prendere l'immagine digitale, isolare la sola goccia, quindi approssimarla come un' ellisse e memorizzare come elementi di un array i valori della lunghezza dell'asse maggiore e minore.

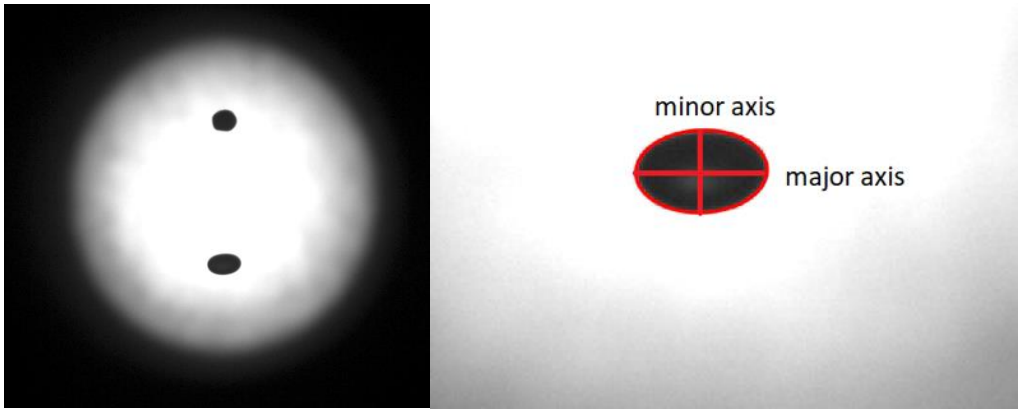

Figura 1.7 : (a sinistra) immagine catturata dalla telecamera, (a destra) immagine elaborata dal programma

Il programma legge le immagini dal file di input una per una, e calcola la superficie del solido di rotazione. In questo caso si considera che la goccia assuma la forma di ellissoide oblato, un solido quindi generato dalla rotazione attorno all'asse *z* di un'ellisse di semiassi maggiori e minori *a* e *b*, rispettivamente orientati secondo l'asse *x* e *y*. La formula per la superficie risulta essere:

$$S_{oblate\ spheroid} = 2\pi a^2 + \pi \frac{b^2}{e} \ln\left(\frac{1+e}{1-e}\right)$$

dove $e^2 = 1 - \frac{b^2}{a^2}$.

Acquisiti questi dati, il programma riporta i grafici della superficie rispetto al tempo, e dell'evoluzione dell'*aspect ratio*, cioè il rapporto tra l'asse maggiore e l'asse minore. Questo è un ulteriore fattore che permette di monitorare l'evaporazione della goccia, poiché progredendo nell'evaporazione la forma passa progressivamente da oblata a sferica. Ora, bisogna tenere conto del fatto che Matlab ottiene restituisce delle grandezze sotto l'unità di misura di pixel; è necessario allora convertirli in millimetri. Per fare ciò un altro codice è stato utilizzato, questa volta open-source, che prendendo a riferimento la pallina di polistirene, la quale aveva un diametro di 2.5 mm, poteva operare la conversione.

Infine, viene valutato il rateo di evaporazione. Per valutare la pendenza della curva generata dall' evoluzione della superficie, un terzo codice semplicemente calcolava

$$\frac{S_{n+1}-S_n}{t_{n+1}-t_n} = \frac{\Delta S}{\Delta t}$$

Quindi, se applicata a tutto l'array, questa formula riporterà la pendenza della linea interpolante tutti i dati. Perciò, dovendo acquisire la pendenza soltanto della prima fase di evaporazione, ho ristretto il calcolo ai dati tra 20 e 1500 secondi. Prima di 20 secondi possono esserci dei disturbi e delle oscillazioni dovute al posizionamento della goccia, quindi meglio escluderli, e fino a 1500 ho potuto sperimentare una sicura linearità, che era ciò che interessava.

1.6. Teoria e formule

Il modello matematico che rappresenta il processo di essicazione è rappresentabile con una tipica espressione di trasporto di massa, proveniente dalla teoria del boundary layer

$$\frac{dm}{dt} = -h_m A(\rho_{v,s} - \rho_{v,b})$$

dove:

- $\frac{dm}{dt}$ è il rateo di evaporazione [kg/s]
- h_m è il coefficiente di trasporto di materia [m/s]
- A è la superficie della goccia [m^2]
- $\rho_{v,s}$ e $\rho_{v,b}$ sono la densità di vapore alla superficie della goccia e nel bulk di aria [kg/m^3]

Ora, il coefficiente di trasporto di materia può essere considerato in termini del numero di Sherwood

$$h_m = \frac{Sh\ D}{d}$$

e quindi, tramite semplici passaggi matematici possiamo arrivare all'espressione:

$$Sh = -\frac{dA}{dt}\frac{\rho l}{4\ \pi\ D\ (\rho_{v,s} - \rho_{v,b})}$$

La quale per questo lavoro è stata riformulata come segue:

$$Sh = \frac{-\alpha\ \rho_{water}}{4\ \pi\ C_{total}\ D_{AB}\ M_{water}\ (x^i - x^\infty)}$$

Tramite una semplice analisi dimensionale è facile notare come le due espressioni siano identiche. I dati relativi alla formula si possono ritrovare in tabella:

Term	Expression	Value
P		101325 Pa
T_{ext}		25°C 298 K
HR		38%
$\Delta H_{v,\ water}$		2500 J kg^{-1} (273 K, 1 atm)
$T_{humid\ bulb} = T_h$		288.9 K
$T_{average}$	$T_{average} = \frac{T_h + T_{ext}}{2}$	293.53 K
T_{ref}		273 K
D_{ab} ($T_{average}$) **A=water** **B=air**	$D_{AB} = 0.0000212 \times P \times \left(\frac{T}{T_{ref}}\right)^{2.334}$	2.511E-05 $m^2\ s^{-1}$
R		8.31446 J $mol^{-1}\ K^{-1}$
C_{total}	$C_{total} = \frac{P_{total}}{R\ T_{ext}}$	40.874 mol m^{-3}
$P_w^{\infty} = P_v\ (T_{ext})$		1190.4 Pa
x^{∞}	$x^{\infty} = \frac{P_w^{\infty}}{P_{total}}$	0.01175 mol water/mol total
$P_w^i = P_v^*\ (T_{humid\ bulb})$		1790.8 Pa
x^i	$x^i = \frac{P_w^i}{P_{total}}$	0.01767 mol water/mol total
ρ_l		1000 kg m^{-3}
M_{water}		0.018 kg mol^{-1}

Tabella 1.1 : grandezze utilizzate

Questo numero di Sh può essere quindi valutato direttamente dall'interpretazione dei dati ottenuti sul campione sottoposto a sperimentazione.

È interessante comparare questo valore con quello ottenuto tramite l'espressione ricavata da Yarin et al., la quale è specificatamente studiata per casi di evaporazione tramite levitazione acustica. Si tratta di una equazione semi-empirica, ricavata dalla teoria e dall'analisi di numerosi esperimenti , la quale viene riportata come:

$$\langle \overline{Sh} \rangle = \left(\frac{45}{4\pi}\right)^{\frac{1}{2}} \frac{B}{(\omega D_0)^{\frac{1}{2}}} = K \frac{B}{(\omega D_0)^{\frac{1}{2}}}$$

$$B = \frac{A_{0e}}{\rho_0 c_0}$$

dove:

- D_0 è il coefficient di diffusione del vapore in aria [$cm^2\ s^{-1}$]
- ω è la frequenza angolare degli ultrasuoni [s^{-1}]

- B è la ampiezza di velocità della particella di gas nell'onda acustica [cm s^{-1}]
- A_{0e} è l'effettica ampiezza di pressione del campo acustico [dyne cm^{-2}]
- ρ_0 è la densità del gas non perturbato [g cm^{-3}]
- c_0 è la velocità del suono nel gas [cm s^{-1}]

1.7. Risultati

Procediamo quindi alla presentazione dei risultati. Tenendo conto del fatto che praticamente ogni campione è stato testato tre volte, per motivi di spazio non è possibile presentare tutti i grafici. Ad ogni modo, verrà rappresentata la tabella ricapitolativa riportante i risultati di tutti i campioni, cioè il numero di Sherwood e la deviazione standard. Lo scopo è qui quello di sottolineare differenze e particolarità.
Dopo ogni esperienza il seguente materiale era prodotto:

- Un certo numero di immagini catturate dalla telecamera
- Un foglio Excel riportante l'istante di tempo di cattura di ogni immagine
- Quattro grafici riportanti l'evoluzione della superficie, pura e normalizzata, l'aspect ratio e l'evoluzione del volume.

1.7.1. Acqua pura

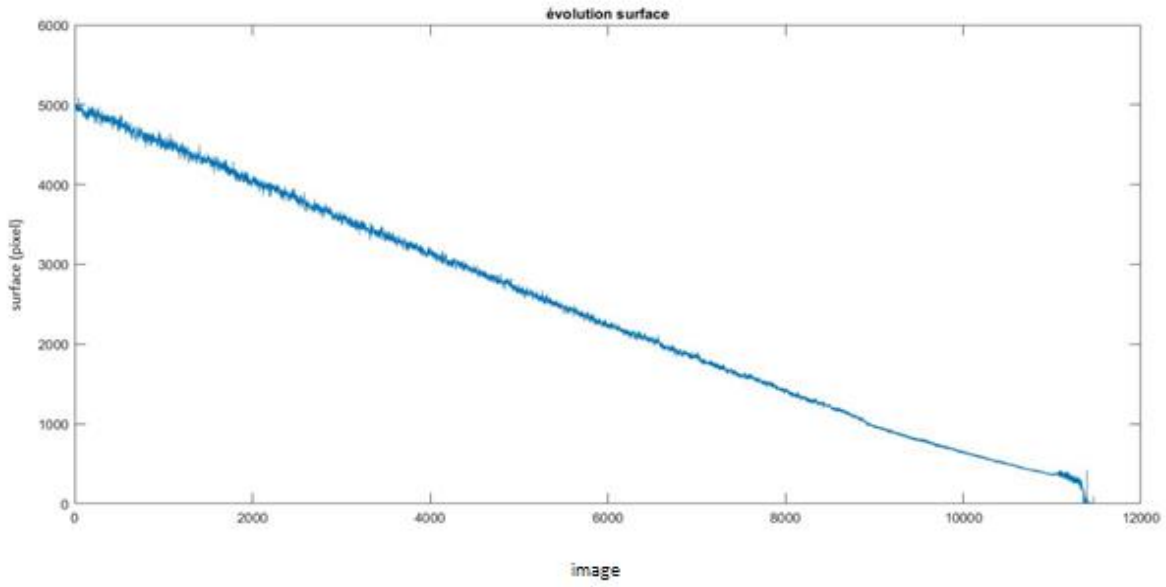

Figura 1.8 : evoluzione della superficie nel tempo; campione di acqua pura

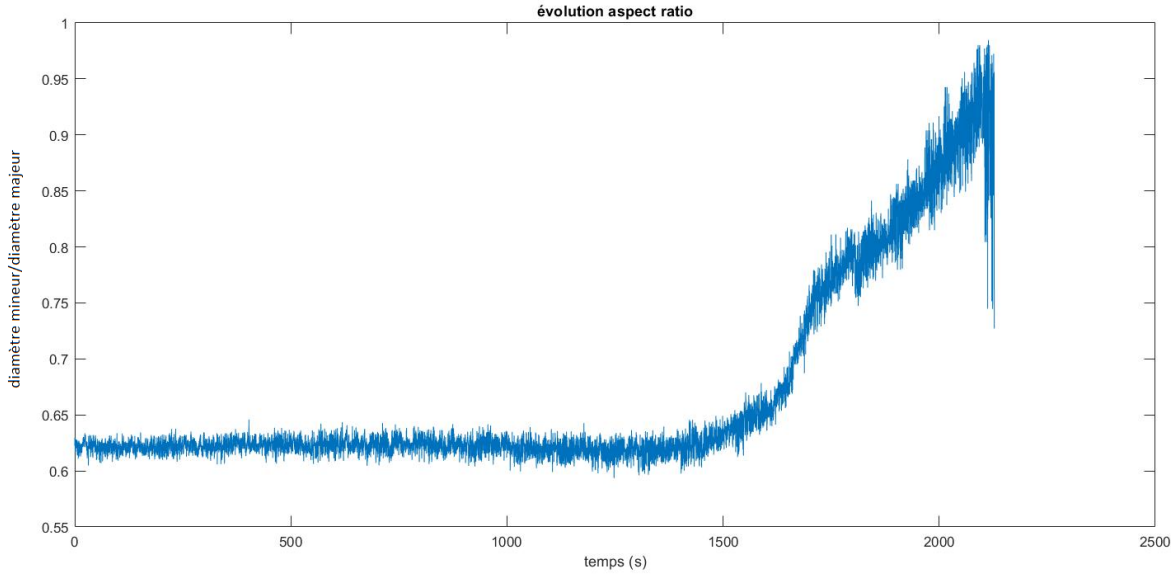

Figura 1.9 : evoluzione della aspect ratio nel tempo; campione di acqua pura

L'analisi del comportamento del campione di acqua pura è utile per avere un riferimento "bianco", per poter osservare i fenomeni che compaiono nel caso non ci siano solidi disciolti, ed anche per validare le ipotesi di teoria fatte all'inizio. Vediamo quindi che la legge del d^2 è valida, dato che la superficie decresce linearmente col tempo. Anche il grafico riportante l'aspect ratio ha una forma esattamente compatibile con le ipotesi di teoria, poiché la particella si ritrova all'inizio con una forma oblata, e con il tempo assume una forma via via più sferica. La zona finale del grafico è disturbata, rumorosa, e ciò è dovuto al fatto che il codice prende in considerazione ogni corpo con una sfumatura di nero. Questo significa che a volte può per errore prendere in considerazione una particella di polvere e non la goccia, e quindi restituire dei dati non corretti.

1.7.2. Caffè e latte

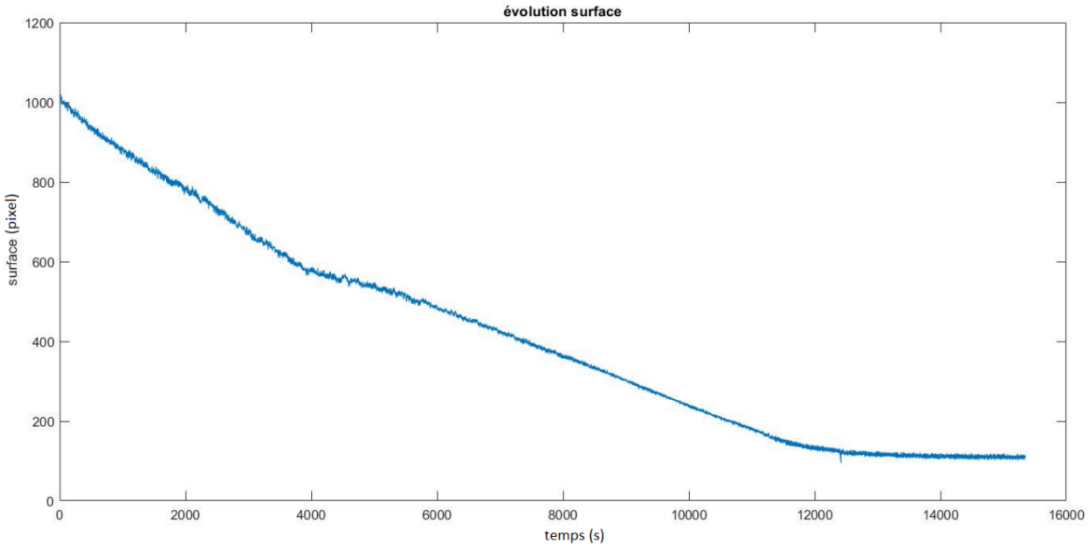

Figure 1.10: arabica, T=55°C, Centrifugato (a)

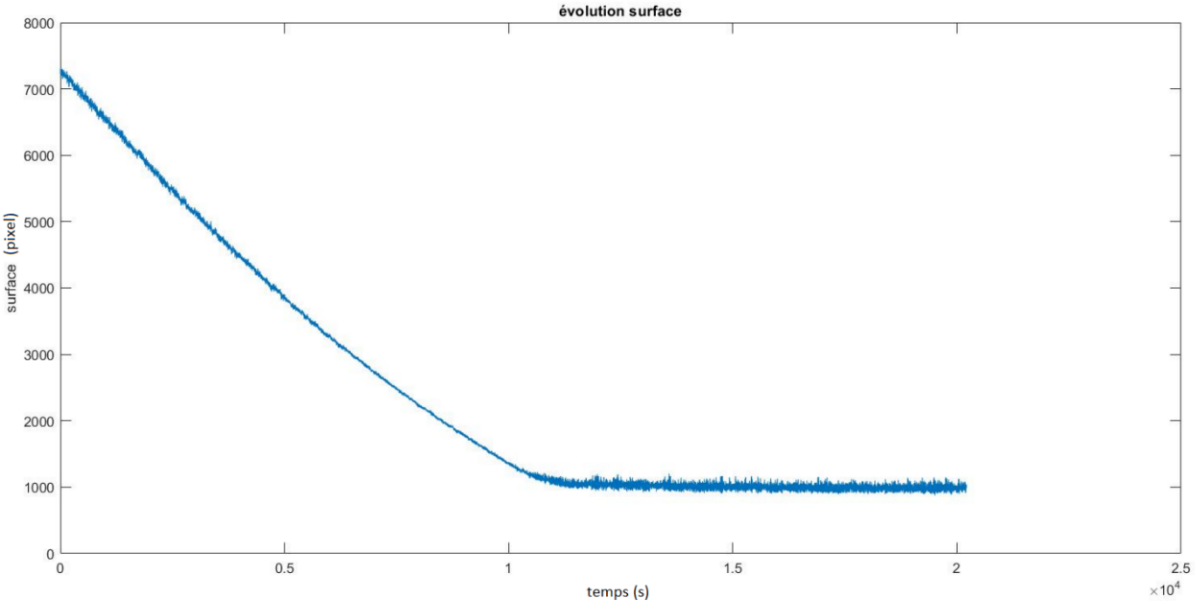

Figure 1.11: Arabica-Robusta , T=65°C , lasciato sedimentare (a)

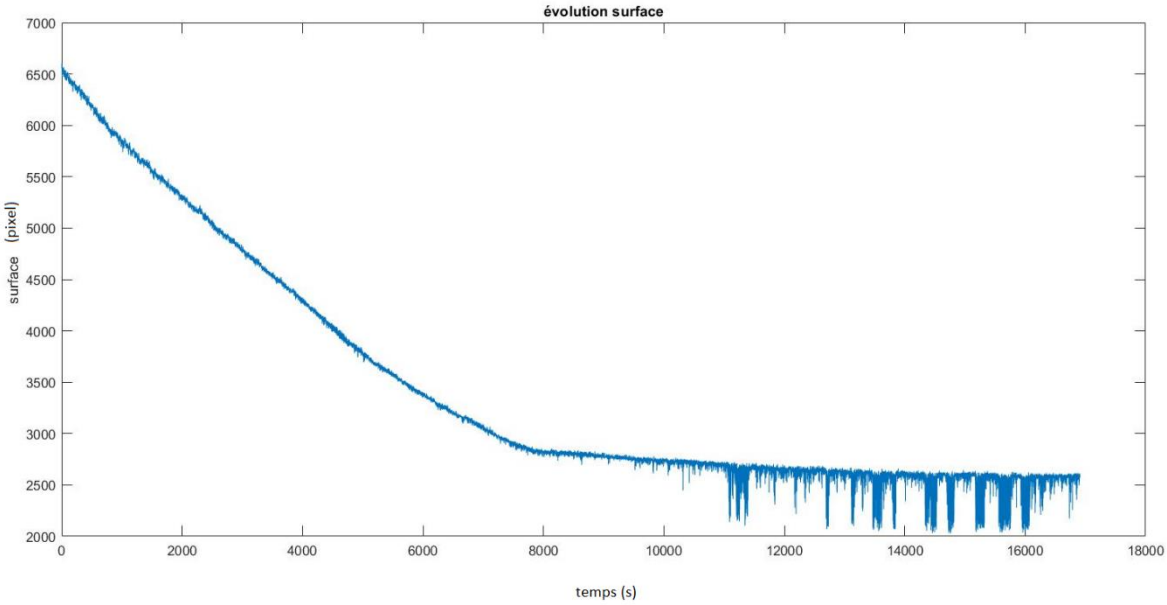

Figure 1.12: Latte intero

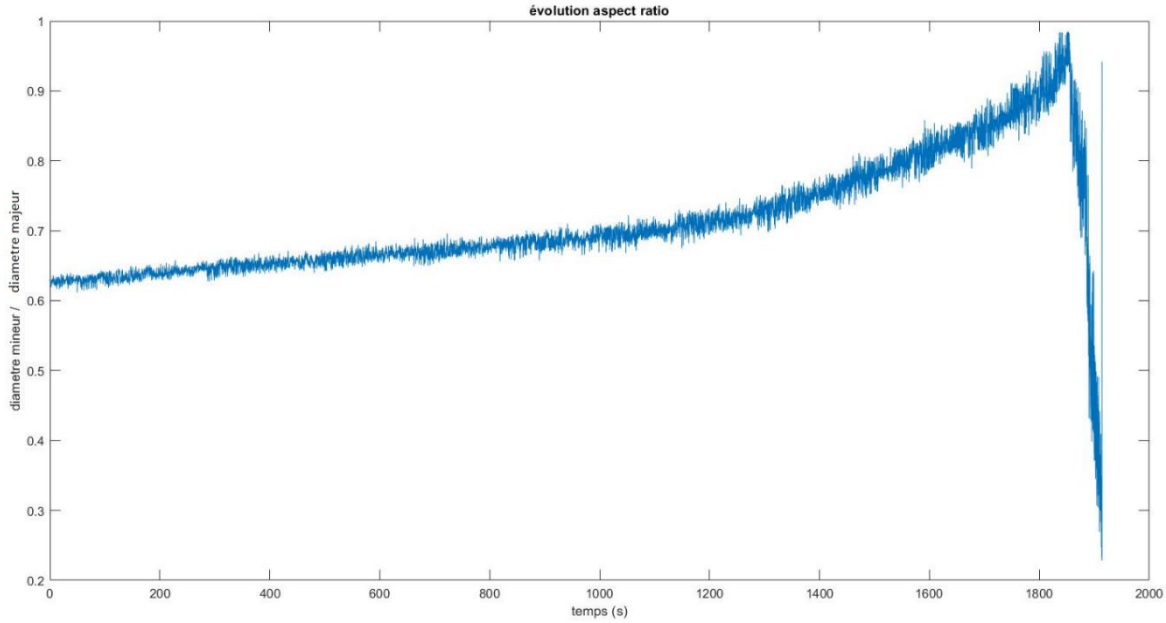

Figure 1.12: Caffè Robusta, T ambiente, lasciato sedimentare (b)

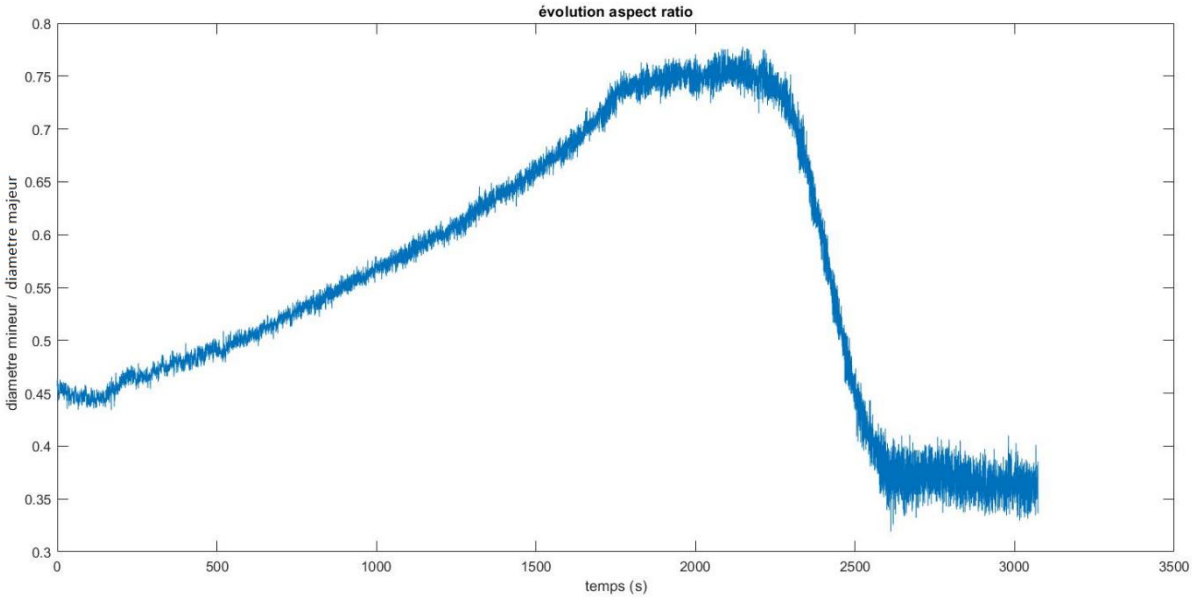

Figure 1.13: Miscela Granaroma Vergnano, via moka Bialetti

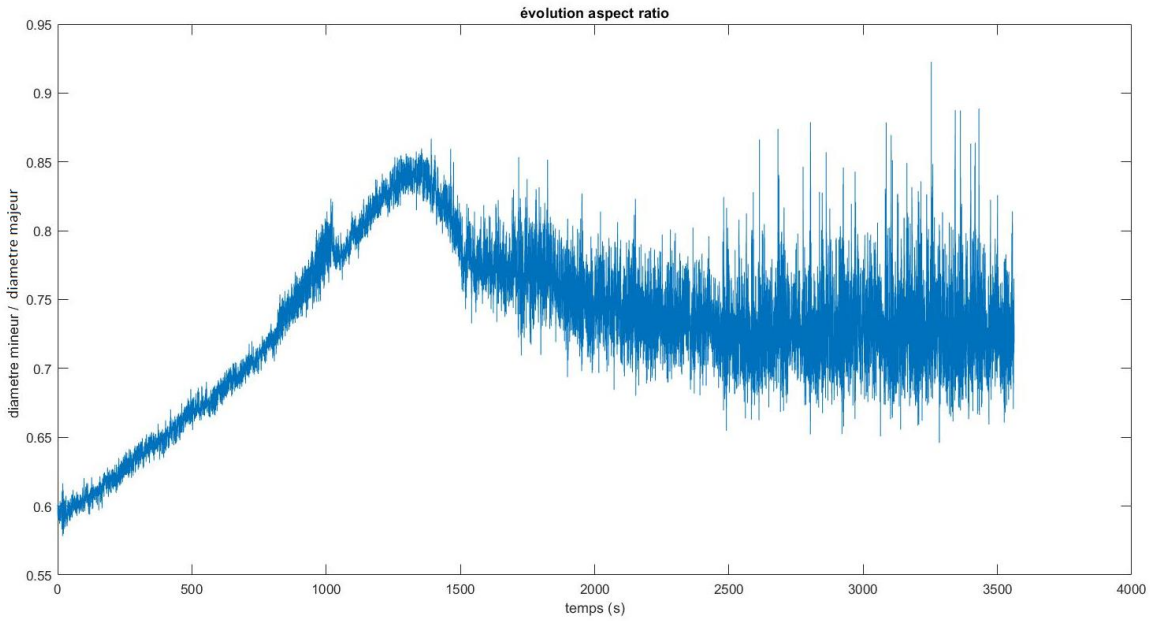

Figure 1.14: Latte intero

Si riportano qui alcuni grafici risultati di analisi. È anzitutto possibile notare le diverse casistiche che si possono riscontrare. Vi sono dei grafici di evoluzione superficiale estremamente lineari e puliti, altri meno lineari, altri ancora con un forte disturbo. Interessanti anche i grafici riportanti l'evoluzione dell'aspect ratio, grazie ai quali possiamo apprezzare i cambiamenti nella forma della goccia, ed anche la formazione di eventuali residuati solidi dell'evaporazione. Ad esempio, la figura 4 mostra un comportamento in linea con la teoria, ma la figura 6 no. Motivo di questi dati con disturbi così ampi può essere la formazione di una particella solida amorfa relativamente grande, ipotesi in linea con la natura del campione, in questo caso latte. Questa particella sarebbe messa poi in rotazione dal campo acustico, portando il programma a individuare dei valori rapidamente variabili degli assi maggiore e minore.

Label	Sample	Massic composition (g)				N°	slope α ($m^2.s^{-1}$)	Sh	St. Deviation
		Water	Arabica	Robusta	Milk				
1	Pure water	-	-	-	-	A	-1.13E-08	8.185	-
2	100% Arabica T=55°C centrifuged	50.0000	3.6100	-	-	A	-2.06E-08	14.964	2.8035655
						B	-1.25E-08	9.110	
						C	-1.23E-08	8.927	
3	100% Robusta T=43°C centrifuged	100.0000	-	7.1810	-	A	-1.10E-08	8.011	0.24109001
						B	-1.18E-08	8.576	
						C	-1.12E-08	8.144	
4	100% Arabica T=21°C centrifuged	50.0000	3.6031	-	-	A	-1.32E-08	9.617	0.87368041
						B	-1.03E-08	7.478	
						C	-1.17E-08	8.503	

5	100% Robusta T=21°C centrifuged	50.0000	-	3.6070	-	A B C	-1.40E-08 -1.44E-08 -1.31E-08	10.142 10.474 9.560	0.37799695
6	mix 50/50 Robusta Arabica T=21°C non centrifuged	50.0000	1.8000	1.8000	-	A B C	-1.46E-08 -1.21E-08 -1.14E-08	10.630 8.800 8.302	1.00084033
7	mix 50/50 Robusta Arabica T=59°C centrifuged	50.0000	1.8000	1.8000	-	A B C	-7.98E-09 -1.42E-08 -1.92E-08	5.799 10.291 13.964	3.33866186
8	mix 50/50 Robusta Arabica T= 65°c non centrifuged	50.0000	1.8000	1.8000	-	A B C	-1.56E-08 -1.62E-08 -1.69E-08	11.321 11.797 12.297	0.39861795
9	mix 7/3 Arabica Robusta T=21°C filtered	35.7000	3.5867	1.5371	-	A B C	-2.05E-08 -1.96E-08 -1.71E-08	14.911 14.280 12.398	1.06750155
10	Vergnano Granaroma Bialetti's Moka					A B C	-2.13E-08 -2.07E-08 -2.06E-08	15.495 15.059 14.987	0.22436549
11	Whole milk				50.0000	A B	-7.46E-09 -8.07E-09	5.420 5.865	0.22217746

Tabella 1.2 : tabella di riepilogo dei risultati ottenuti

La tabella mostra i risultati in maniera quantitativa. Si nota che per i campioni da 1 a 6 $Sh \cong 8$, simile perciò al risultato ottenuto per il campione di acqua pura. Ora, riconducendoci al significato del numero di Sherwood, più questo è grande, maggiore sarà il rateo di scambio di materia, quindi l'evaporazione. Secondo la teoria quindi, la goccia di acqua pura dovrebbe essere quella con rateo di evaporazione massimo, perché tale fenomeno non sarebbe ostacolato dalla presenza di solidi disciolti. Si nota però la presenza di valori ben al di sopra di 8. Tali risultati sono di dubbia interpretazione, e non sembrano causati da una manipolazione non corretta della procedura, poiché la deviazione standard non necessariamente mostra valori aberranti, come nel caso del campione 10.

Calcolando lo Sh teorico, proveniente dalla formula elaborata da Yarin et al., otteniamo:

Vincc (rms)	pressure (Pa)		ro air (kg m^{-3})	Co (m s^{-1})	K	D0 (m^2s^{-1})
6.35	2532.1895		1.177	340	1.89	2.63E-05
SPL (dB)		Aoe			B	
162.049324		25261.9114	dyne cm^{-2}		6.312637	
		2526.19114	Pa			
Sh						
11.32						

Tabella 1.3 : tabella riportante i dati utilizzati per ottenere il risultato di Sh teorico

Che è un valore distante da quello ottenuto per l'acqua pura, cui questa formula farebbe riferimento. In ogni caso questo risultato questo risultato distante da un dato sperimentale non deve spaventare, perché è stato ottenuto con notevoli approssimazioni e assunzioni, primo fra tutti l'attuale livello di pressione sonora (SPL), che non mi è stato possibile valutare direttamente, ma mi sono dovuto avvalere dei dati forniti dal costruttore dell'apparecchio. Con una operazione inversa, inserendo lo Sh ottenuto con il campione di acqua pura, è risultato un SPL di 150/160 dB, quindi certamente non lontano dall'ipotesi. Questo tipo di analisi comparativa serviva a verificare che il risultato teorico riportasse dei valori non troppo distanti da quelli ottenuti con l'esperimento. Una possibile ulteriore giustificazione di un valore di Sh così basso per il campione di acqua pura può essere ricercata nel fatto che tale campione è stato il primo ad essere testato da me, in un momento in cui ancora la mia manualità era relativamente scarsa, quindi potrebbe non essere del tutto affidabile.

1.8. Un sostanziale miglioramento all'esperimento

Durante le osservazioni, ho potuto notare un difetto importante della procedura. La formula per ricavare il valore dello Sh è basata sul calcolo della superficie della goccia, ma le immagini ottenute sono sempre proiezioni bidimensionali. Si è quindi costretti a procedere con delle approssimazioni, che possono indurre errori importanti, specie nel caso vi siano fenomeni di rotazione indotta dal campo acustico sulla goccia. Vi sarebbe perciò la necessità di acquisire immagini di due proiezioni della goccia, per poter ottenere un miglior risultato sul calcolo della superficie. Tale risultato potrebbe essere ottenuto con una configurazione come quella in figura 7, dove uno specchio posizionato opportunamente sarebbe in grado di riflettere una visione laterale della goccia. L'idea è stata discussa con il mio tutor, e trovata teoricamente realizzabile. Le due immagini potrebbero essere analizzate con un codice Matlab simile a quello già sviluppato. Sfortunatamente, ancora una volta, il tempo le condizioni eccezionali non ne hanno reso possibile l'implementazione.

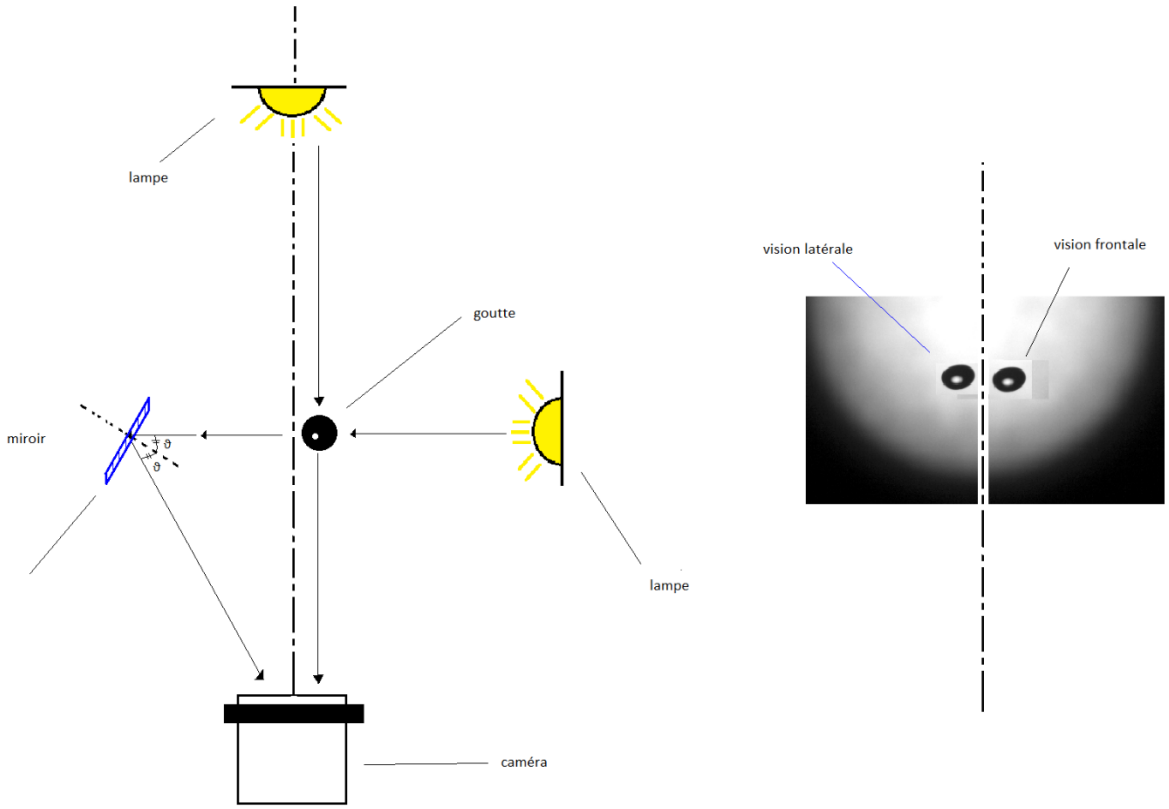

Figure 1.15: sketch di quello che avrebbe potuto essere il miglioramento implementabile al processo di cattura di immagini

1.9. Conclusioni e commenti

Gli esperimenti da me compiuti sui campioni di acqua pura confermano le ipotesi derivanti dalla teoria e le esperienze di studi precedenti. I test condotti sui campioni di latte confermano che la presenza di solidi disciolti inibisce il trasporto di massa dalla goccia all'ambiente, e ciò è confermato da un valore del numero di Sherwood inferiore a quello valutato nel campione di acqua pura. Esperimenti condotti su campioni di caffè hanno invece riportato un valore di Sh più elevato, suggerendo quindi un maggiore rateo di evaporazione. Questo risultato differisce da studi condotti precedentemente, ma numerosi fattori devono essere tenuti in considerazione, come un possibile errore umano, il quale non è da escludere data la mia relativa inesperienza in laboratorio, condizioni di sperimentazione notevolmente differenti da quelle ritrovate in letteratura, come l'assenza di una corrente convettiva interna all'ambiente ad atmosfera controllato o le particolari condizioni di temperatura e umidità relativa. Inoltre, la chiusura eccezionale delle strutture non ha consentito alla raccolta di ulteriori dati, né alla possibilità di condurre osservazioni particolari che potessero in qualche modo giustificare i comportamenti anomali osservati.

2. Preface

The idea for the beginning of this final thesis was born during my permanence at UTC – Université de technologie de Compiègne in France - as member of the ERASMUS program I was part of. Finding myself in the position of having to do a little research and experimental project during the first semester, I approached the department director of GP (Génie de Procédés, process engineering), M. Saleh Khashayar, who proposed me to continue the work already started by a student who by that time already got her degree, and had partially undergone this experimental study with the acoustic levitation device, obtaining interesting but questionable results. Immediately finding the project extremely interesting, I explained to M. Saleh my willingness to take over and continue this work, and also my need to find a subject for a final thesis for the spring semester, and, if possible, to further continue this topic to investigate its possibilities with others fluids and methods and transform that study in my final project. I have been cheerfully welcomed in the department and, after having contacted Professor Specchia here in Turin, and having received the approval, I started my experiments in February with the various devices that have been put at my disposal.

Unfortunately, after less than a month of experiments, the sanitary emergency the world has faced during this year caused the closure of all the university facilities, both of teaching and of research, causing my impossibility of accessing the laboratory before the end of my ERASMUS period and of the academic year.

What was intended to be an experimental work of comparison of different behaviours of various types of liquids on industrial interest, amongst them I planned water, coffee and milk, with the intention of going even beyond whether the time was reasonably sufficient, transformed in a work of compiling of the data acquired, and of comment of the observed phenomena.

This brief study well confirms the already known behaviours on this subject, yet other interpretations to obtained data have been acquired, for time and exceptional condition have not allowed to undergo into further investigation.

3. Introduction

The act of evaporating liquids to obtain a dust-like dried product is a very common and interesting industrial practise for a number of different fields, spacing from the drying of products for alimentary purpose, like milk, coffee, even more viscous liquids like egg whites (Fang, Rogers, Selomulya, & Chen, 2012), to fields related to the process industry like the production of plastic laminates or glues (WHITEHEAD, BALL, FINE, & LANGOLF, 2010). This drying is typically obtained via the pulverisation of the liquid mixture into spray clouds, where billions of micro and nanoscopical droplets are formed. So starting from its first applications between 1920 and 1930 (https://soe.rutgers.edu/sites/default/files/imce/pdfs/gset-2016/acoustic-levitation-theoretical.pdf, s.d.), this process had to face the problem of dealing with an extremely big number of elements, each one with different trajectories and particular behaviours. The approach to and the description of the phenomenon was then taken as an integral one, and dimensioning was made possible thanks to the approximation on the whole process (Masters, 1972). It has to be said that still today the quantitative description of the whole process is not completely possible, and numerous researches are on their way to approach to the problem via CFD simulations, still subjected to a certain degree of uncertainty.

Starting from the work of Ranz and Marshall (Aissa, ABDELOUAHAB, NOUREDDINE, EL GANAOUI, & PATEYRON, 2015), a new method of analysis has started to gain interest by the scientific community: we are talking about the Single Droplet Drying (SDD) analysis. In SDD, as the name itself illustrates, a single droplet is placed in a controlled environment that is set to be as similar to the actual working environment as possible, properly tuning the conditions of relative humidity, ventilation, and temperature. Initially this technique was introduced to study the behaviour of droplets

of pure liquids or of mixture and to measure accurately the drying kinetics. In the last years, with the improving of the image capturing related technology, such as the digitalisation and miniaturisation of devices, this study was sided with the observation of the morphological changes of the sample. (de Souza Lima, Ré, & Arlabosse, 2019)

The SDD analysis relies on three different techniques: the free fall, the glass filament method and the acoustic levitation.

3.1. The methods

3.1.1. The Free-Falling Droplet

The first and conceptually easier method is the free-falling droplet monitoring, that simply consists, as suggested by the name itself, of a droplet generated by a capillary nozzle, let falling through a tower. Whether the main advantage is on the possibility to precisely tune the size and the rate of dripping along with the conditions of the gas inside the tower, allowing to well simulate the conditions of an actual spray drying, the main problem is represented by the difficulty in monitoring the actual process and to obtain information from the direct observation, forcing to place numerous cameras and capturing devices, or either to extrapolate the data from indirect measurements, like the terminal velocity of the droplet.

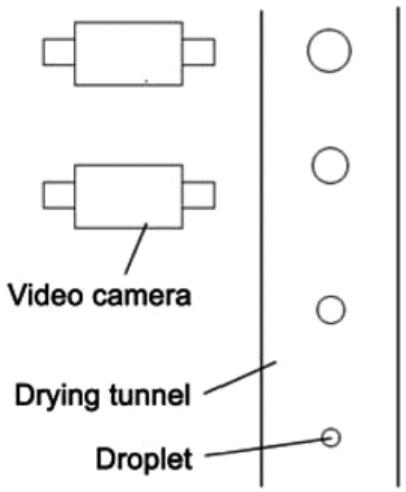

Figure 3.1: the free-falling droplet technique *(Fu, Wai Woo, & Dong Chen, 2012)*

3.1.2. The Glass filament method

A more fine and elaborated method is represented by the glass filament one. In this case, a droplet of the desired dimension is suspended at one end of a thin glass filament. This glassy filament is tailor-made on this purpose, with specific geometric and physical properties. With the knowledge of those properties, the desired data from the evaporating droplet can be obtained in two different ways.

First, by observation of the change of the position of the thin rod as the drop gest smaller and smaller. In fact, when suspended, the droplet represents a quote of added weight to the filament, that from perfectly horizontal is forced to deflect downwards. If, as said above, we know exactly the elastic properties of the filament, it's easy, monitoring the slope, to extrapolate the kinetic data we look for, if it's true that during evaporation the droplet loses liquid mass, thereby getting lighter. (QI Lin & Chen, 2002)

Secondly, a direct observation of the changes in dimension and morphology of the droplet itself can be carried out, in this case obtaining direct data. This can be made easily, considering that the droplet is suspended and still, not anymore falling through a tube. Also, the main advantage of this second approach is that both the direct and indirect observation can be made simultaneously, without interfering, in fact corroborating one the measure of the another.

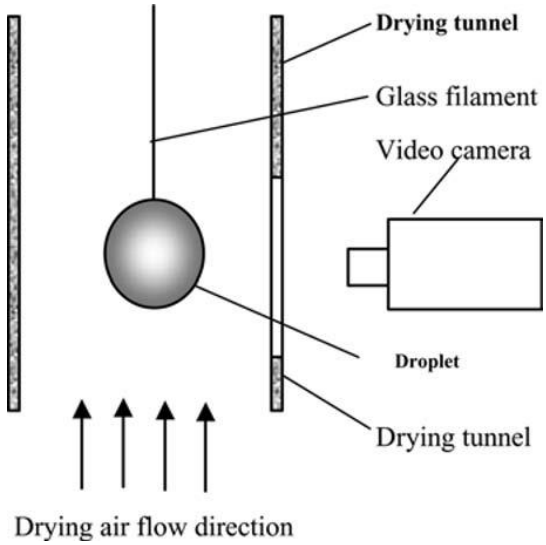

Figure 3.2: the glass filament method *(Lin & Chen, 2004)*

Drawbacks on this method are represented mainly by the numerous factor insisting on the observation of the changing of the slope of the filament, such as the drag force applied on the droplet when a flow of air is sent in the testing equipment, that interferes with the effect that the weight would have if alone, and has to be corrected. Also, this more elaborated method requires high skills in manipulation, for the size of the droplet to be suspended on the glassy tip is by the order of less than a microliter: hence, considering a spherical droplet, assumption not so far from the truth for extremely small samples, we are talking of diameters of about half a millimetre. This implies a number of steps to follow in order to successfully deposit the fluid sample. Last, the influence of the tip itself represents a perturbance. If it has been proved that the glassy end occupies only 0.2% to 1% of the microscopical volume, and so bringing little to negligible influence on the temperature of the drop, the presence of a pointy edge is undeniably germ for crystallisation of the solid dissolved in the liquid, causing the appearing of the solid aggregation before what we could expect in a spray evaporation. (de Souza Lima, Ré, & Arlabosse, 2019)

3.1.3. Acoustic levitation

More recently, and in particular starting from de ‘90s thanks to the studies carried out by Yarin, Pfaffenlehner and Tropea, that still today represent the most complete and detailed on the subject, a new methodology has started to gain popularity: the study of those phenomena via the acoustic levitation with ultrasounds. We are talking here of another sample-suspended method, but the suspension here is induced by the creation of pressure nodes in the gas medium thanks to properly placed ultrasound loudspeaker inside a device, and placing into those nodes a droplet or a particle, that will be actually suspended if the force exerted by the pressure wave is sufficient to balance the weight of said bodies. Details of the functioning of the device will be presented in a following section.

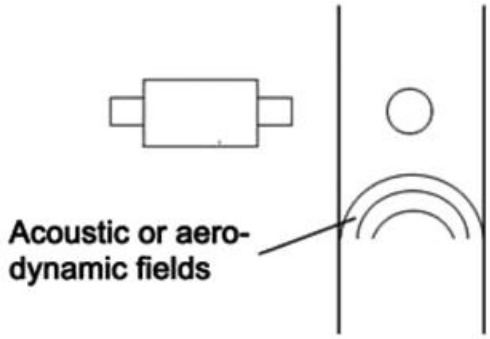

Figure 3.3: the acoustic levitation *(Fu, Wai Woo, & Dong Chen, 2012)*

The great advantage of this technique is represented by the possibility of observation of the evaporation, and the consequent solid crust formation, without the perturbation of an external body that could stimulate phenomena not actually happening in the industrial reality. This may be confirmed by the fact that the evaporation kinetics generally remain linear longer during the acoustic levitation with respect to the filament method, because of a delayed apparition of the solid crust that, causing an obstacle to the internal and external diffusion of the liquid, deviates the behaviour introducing a non-linearity (Al Zaitone & Tropea, 2011). Not trivial is the easiness of this type of observation, that requires little to no particular skills to be carried out, and also the good degree of repeatability obtained if the conditions of the experiment are well respected time to time.

Drawbacks on this method are represented by the action of the acoustic field itself causing at least two perturbing effects. Firstly, the ultrasonic incident wave insisting on the droplet causes a deformation, bringing the shape from an ideal sphere to an oblate spheroid. Furthermore, the deformed shape changes during the evaporation, and so what at the beginning of the experiment was an ellipsoidal body, along with the shrinkage and the loss of mass tends to return to the shape of a sphere. This phenomenon can be monitored evaluating time by time the ratio of the minor semiaxis b over the major a; calling then $\frac{b}{a}$ *aspect ratio* we can observe this value to change from an initial number ranging from 0.4 to 0.6 at the beginning of the experiment to 0.8 to 1 at the end Hence the actual impossibility of considering the drop as a sphere but rather an ellipsoid of evolving shape, of which the sphere represents a particular case when the two semiaxis are coinciding. (Giorgiutti-Dauphiné & Pauchard, 2018)

Secondly, the effect of the ultrasonic field is proved to create zones of turbulence surrounding the droplet. Those zones, symmetrically placed on the two hemispheres, assume the shapes of toroids, that even in the case of a still gas medium, where the turbulence should be absent, contribute to enhance the local Reynolds number, preventing *de facto* an evaporation in a stagnant or laminar environment. Then, if with the glass filament method we can discriminate between two types of evaporation, one diffusion-driven in a stagnant environment and one convection-driven in case of high Reynolds numbers of the gas medium, for the acoustic levitation the experiment is inevitably subjected to an acoustic-driven evaporation even in case of stagnant gas medium, like in my observations, for the main driving force of is represented by the effect of the ultrasonic toroids. In addition to that, the effect of this acoustic vortexes is dual, meaning an enhanced turbulence and consequent evaporation at the surface, but a retention of the gas moisture on the surroundings of the droplet, causing a weakening of the diffusive force (YARIN, PFAFFENLEHNER, & TROPEA, On the acoustic levitation of droplets, 1998) (YARIN, BRENN, KASTNER, RENSINK, & TROPEA, 1999)

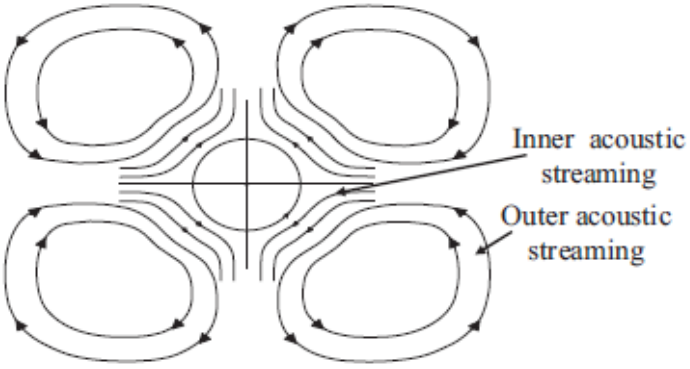

Figure 3.4: the surrounding acoustic streams generated by the effect of the acoustic wave on the gas medium *(Al Zaitone & Tropea, 2011)*

3.2. The choice

Large quantities of studies have been made and articles have been published on this topic. However, a sort of a preference seemed to have established for the glass filament method. Reliability, relatively low-cost material and easiness of extrapolating the required data apparently are sufficient to balance the intrinsic interference of the method and the high skill level required for its application.

This considered, an undeniably important work has been made on the acoustic levitation method too, but only recently the full potential of this speculation has been really made clear. The continuous improvement on the 3-D printing technology of these late years has now allowed to build devices extremely cheap with the intuitive use of software and printers that are more and more common and available. Moreover, the acoustic field, time ago generated via an expensive single piezoelectric Langevin horn emitter, can be now obtained thanks to a series of miniaturised loudspeakers, cheap and robust. Details of the device used in this research will be exposed in a following section.

Comparisons have been made between those two methods, showing that the behaviour differs depending by the gas stream blown into the device. Particularly, a threshold of the blowing rate was highlighted, below which the evaporation is faster for the glass filament than the one of the acoustic levitation, and when surpassed brings to an equal evaporation rate for the two compared methods. This is due to the particular effect of the acoustic vortexes, that will be explained later. Those slightly diverging effects and the interpretations of the phenomena intrigued me, capturing my attention.

Not secondarily, the choice of investigating the application of the acoustic method onto the study of the kinetics of evaporation of a suspended droplet was due to the interest of the GP department of the University, that had in place a, so far rarely used, levitation device

PROS	Drying condition induced closely follows that of a spray dryer	Measurements on the drying kinetics and visualization of the droplet during drying are relatively less complex	Measurements on the drying kinetics and visualization of the droplet during drying are relatively less complex
CONS	Measurements on the drying kinetic and visualization of the droplet during drying is complex and difficult	Possible effect of the acoustic waves affecting the mass transfer process	Intrusion of filament into the droplet (however, effect on heat and mass transfer can be minimized)
MEANS OF SUPPORT	No support	By acoustic field	By inserting the tip of a fine glass filament
INTRUSIVE INTO DROPLET	No	No	Yes
POSSIBLE METHODS OF DRYING RATE MEASUREMENT	Usually by indirect methods such as measuring the distance that the droplet travelled inside the tower, or collecting droplets at different heights of the tower	Usually by indirect methods such as converting the droplet diameter changes or droplet positions changes into mass changes	- Capable of using direct methods such as connecting the glass filament to a microbalance - Capable of realizing continuous measurement during drying
SIMILIARITY TO ACTUAL SPRAY DRYING PROCESS	Very similar; can be improved to act as an advanced spray-drying	Drying kinetics affected by the acoustic field	Drying kinetics affected by the intrusive glass filament
REPRODUCIBILITY OF KINETICS MEASUREMENT	–	–	- Temperature and diameter measurements: within 3% - Mass measurement: within 6%

Table 3.1: comparation of the mentioned techniques *(Al Zaitone & Tropea, 2011)*

4. Principles and instrumentation

4.1. Principles of acoustic levitation

The acoustic levitation technique, otherwise said *acoustophoresis* (Hilgenfeldt, Rallabandi, Agarwal, & Raju) consists into maintaining in suspension a body, liquid or solid, in a gaseous medium, like air in this case. This is obtained using the pressure differences in the gas itself induced by the application of an ultrasonic field. The application of said sonic fields of frequency superior to 20 kHz is necessary to overcome the gravitational force. It has to be said that there are records of experiences and observations of levitation using sonic waves belonging to the hearing spectrum. However, those accounts are part of a merely oral tradition, related to some oriental religious rituals, and without any reliable proof, little to no credit can be given to those stories. The first documented experience dates of 1933, when Bücks and Muller achieved to levitate an alcohol droplet between a piezoelectric emitter, quartz in that case, and a parabolic reflector (Bücks & Müller , 1933)

Sound propagates in the gaseous medium thanks to the formations of high- and low-pressure zones: we can thus talk of acoustic pressure. Note that the difference between the high- and low-pressure zones is extremely little, roughly ten thousand times below the atmospheric one, but sufficient to induce vibration on a microphone membrane, a string of an instrument or the human tympanum. Also, sound, as a mechanical wave, is able to carry momentum that can act on bodies and particles thanks to the acoustic radiation force (Marzo, Barnes, & Drinkwater, 2017). When the forces exerted on an object are strong enough and converge from all directions, the particles can be levitated and stably trapped (Brant, 2001)

An incident standing wave presents two characteristic zone: a crest, where the amplitude of the wave is maximal for the positive values, and a valley, where the amplitude is maximal for the negatives. Between those two points we find a pressure node, where the gauge pressure is equal to zero.

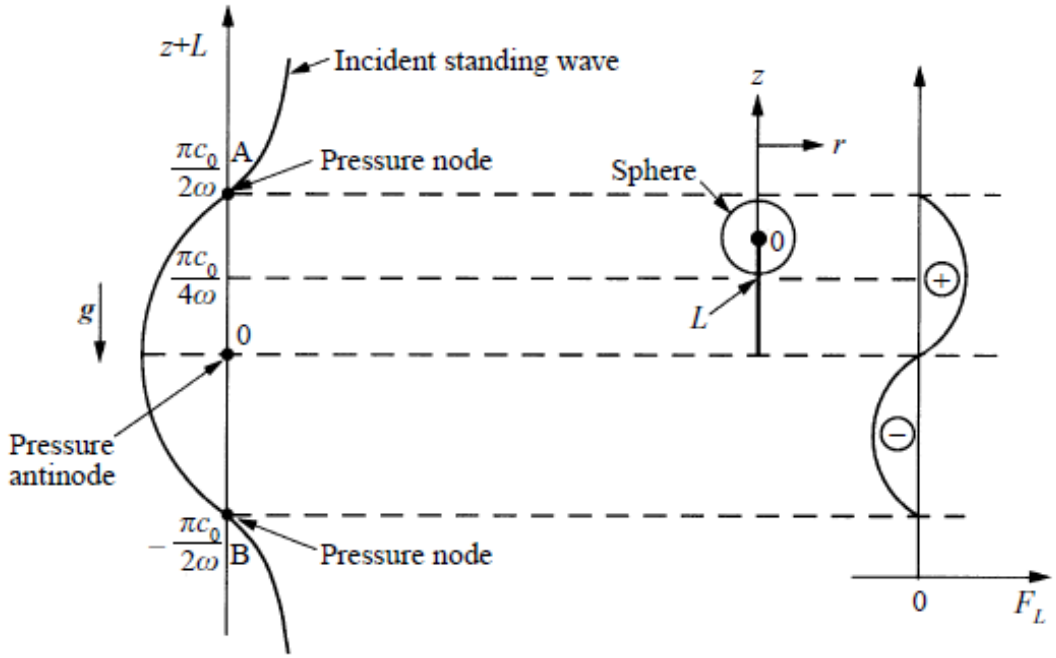

Figure 4.1: scheme of an acoustic wave. Here F_L is the acoustic levitation force acting on a rigid sphere. *(YARIN, PFAFFENLEHNER, & TROPEA, On the acoustic levitation of droplets, 1998)*

Inside those unperturbed points, an external body could be virtually levitated. We see from the Figure 3.1 that, calling the wavelength λ, between to pressure nodes we have a distance of λ/2. Let us

consider the middle point between two nodes, calling it antinode, as the origin of our reference. This system will be vertical, with the positive z axis pointing upward, the positive verse of the gravity force g pointing downward. Thus, the z-positive part included between an antinode and a node will be a zone of repulsion force, so a suspended body will receive a force directed upward. On the other hand, the z-negative part between an antinode and a node will be an attractive-force sone, where the body will sense a force directed downward. Those two zones have the combined effect to keep in place the particle in the pressure node.

It is evident that the presence of a single wave is not sufficient to allow a stable positioning of the particle. To easily understand the phenomenon, it is much like trying to position a sphere on the vertex of an ideally smooth and steep hill. Although placed in a virtually stable point, the sphere is not in a true stable position, and will fall with the occurrence of the slightest perturbance. That is why a single wave is not sufficient, but we need at least two waves, resonating and both intersecting in correspondence of the pressure node. To achieve this the most common and simple configuration to these days is the single-axis configuration (Whymark, 1975) where the device is typically placed vertically, with the suspended body axially aligned with the wave sources.

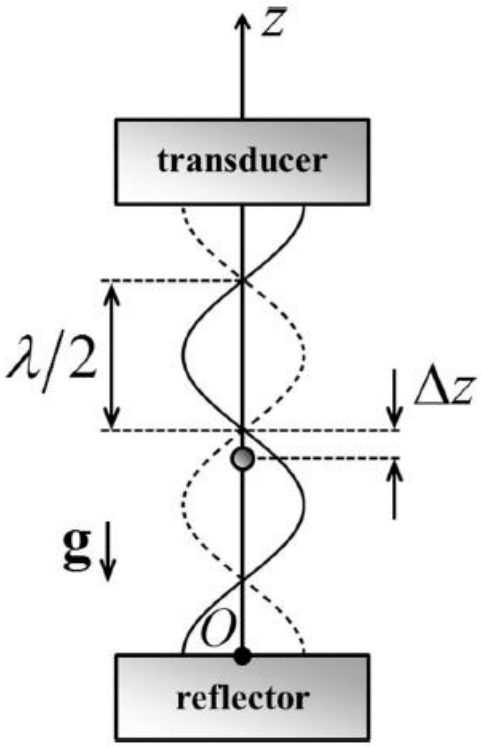

Figure 4.2: sketch of a transducer-reflector levitation device. It is shown that the position of the suspended body, subjected to its own weight, is slightly below the theoretical point of stability. *(Andrade, Pérez, & Adamowski, 2018)*

However, as the sketch in Fig 3.2 illustrates, it has been noted by many authors (Trinh & Hsu, 1986) (Foresti, Nabavi, & Poulikakos, 2012) that the position of the suspended particle is slightly below the pressure point. This is due to the weight of the particle itself, and for the case of observation of an evaporating or sublimating sphere, the knowledge of Δz and the monitoring of its changing can be useful to extrapolate data on the observed phenomenon. In fact, while evaporating, the particle loses mass and so weight, shifting then towards the upper node. Also, this variable can be used to evaluate the mass of the particle, which can give information on the density or the volume respectively.

4.2. The acoustic radiation force

If the particle has to defeat the gravitational pulling to be able to properly levitate, a force has to be applied on it in the opposed direction. As said, the effect of the vibrating sonic or ultrasonic transmitter is to produce an acoustic wave, so a pressure front moving in the gaseous field. The force in this case is the result of the pressure. It is then necessary to show briefly the definition and the obtention of this mentioned force.

Starting from the continuity equation for the gaseous medium, the Euler's equation for the conservation of momentum, and the equation of state, that for simplicity purposes can be taken as the ideal gas law, and by the pressure, velocity and density fields in the gas that can be described as

- $p = p_0 + p_1$
- $\boldsymbol{u} = \boldsymbol{u}_0 + \boldsymbol{u}_1 = \boldsymbol{u}_1$ given that the gas is at rest at the initial conditions,
- $\rho = \rho_0 + \rho_1$

with some passages we can obtain the linear wave equation, that reads as

$$\nabla^2 p_1 = \frac{1}{c_0^2} \frac{\partial^2 p_1}{\partial t^2} \quad (3.1)$$

Where c_0 is the sound velocity and p_1, u_1 and ρ_1 are the first order perturbation fields, meaning the first order term of the Taylor's series.

The acoustic radiation force is related to the acoustic radiation pressure $\langle p_2 \rangle$, a nonlinear phenomenon that can be derived from the linear fields p_1 and u_1. Its definition reads as

$$\langle p_2 \rangle = \frac{1}{2\rho_0 c_0^2} \langle p_1^2 \rangle - \frac{\rho_0}{2} \langle \boldsymbol{u}_1 \cdot \boldsymbol{u}_1 \rangle \quad (3.2)$$

From this, we derive the acoustic radiation force ($\mathbf{F_{rad}}$)

$$\mathbf{F_{rad}} = -\iint \langle p_2 \rangle \, \mathbf{n} dS \quad (3.3)$$

An easier approach to the obtention of an expression for $\mathbf{F_{rad}}$ can be found in a 1962 publication by Gor'kov, where is derived an expression for the acoustic potential for a spherical particle of radius (R) much smaller than the acoustic wavelength. To introduce this, we have to take admit that the fields insisting on the particle are the sum of an incident ad an scattered field, indicated here with the apexes *in* and *sc* respectively. That said, this potential according to Gor'kov is expressed by:

$$U = 2\pi R^3 \left[\frac{f_1}{3\rho_0 c_0^2} \langle \left(p_1^{in}\right)^2 \rangle - \frac{f_2 \rho_0}{2} \langle \mathbf{u}_1^{in} \cdot \mathbf{u}_1^{in} \rangle \right] \quad (3.4)$$

With

$$f_1 = 1 - \left(\frac{\rho_0 c_0^2}{\rho_p c_p^2} \right) \quad (3.5)$$

$$f_2 = 2 \left(\frac{\rho_p - \rho_0}{2\rho_p + \rho_0} \right) \quad (3.6)$$

Where ρ_p and c_p are the sphere density and speed of sound in the sphere, respectively, and the subscript 0 indicates the gas.

It is easy to see that in case of a liquid (or solid) particle, because of the great discrepancy between the densities, we can reasonably approximate $f_1 = f_2 = 1$.

Then, we find the expression for p_1^{in} by solving the linear wave equation previously mentioned obtaining

$$p_1^{in} = p_0 \cos(\omega t) \cos(kz) \quad (3.7)$$

with:

- p_0 the pressure amplitude
- ω the angular frequency of the wave
- $k = \frac{\omega}{c_0}$

Substituting this in the Euler's equation we find

$$\mathbf{u_1^{in}} = \frac{p_0}{\rho_0 c_0} \sin(\omega t) \sin(kz)\ \hat{\mathbf{k}} \quad (3.8)$$

that is the particle velocity. Time averaging those equations, we find the terms:

$$\langle \left(p_1^{in}\right)^2 \rangle = \frac{p_0^2}{2} \cos^2(kz) \quad (3.9)$$

$$\langle \mathbf{u_1^{in}} \cdot \mathbf{u_1^{in}} \rangle = \frac{1}{2} \left(\frac{p_0}{\rho_0 c_0}\right)^2 \sin^2(kz) \qquad (3.10)$$

that can be substituted in the Gor'kov equation (Andrade, Pérez, & Adamowski, 2018). Thus, following the mentioned approximation of the two characteristic functions we obtain

$$U = \frac{p_0^2 \pi R^3}{\rho_0 c_0^2} \left[\frac{\cos^2(kz)}{3} - \frac{\sin^2(kz)}{2}\right] \qquad (3.11)$$

Finally, given that the radiation force can be expressed as the divergence of its potential $\mathbf{F_{rad}} = -\nabla U$, we obtain a final and useful expression for the force that reads as

$$\mathbf{F_{rad}} = \frac{5\pi R^3 k p_0^2}{6\rho_0 c_0^2} \sin(2kz)\ \hat{\mathbf{k}} \qquad (3.12)$$

4.3. Device theory: the Langevin transducer

The acoustic levitation represented historically a high-level investigation technique, mostly because of the high cost of the device and the high skill level required to tune and use the device itself. The functioning core of the device is in the emitter. This is constituted by a piezoelectric transducer capable of emitting stable ultrasonic waves, in front of which we find a concave reflector. For a long time, the emitter was the of the Langevin type.

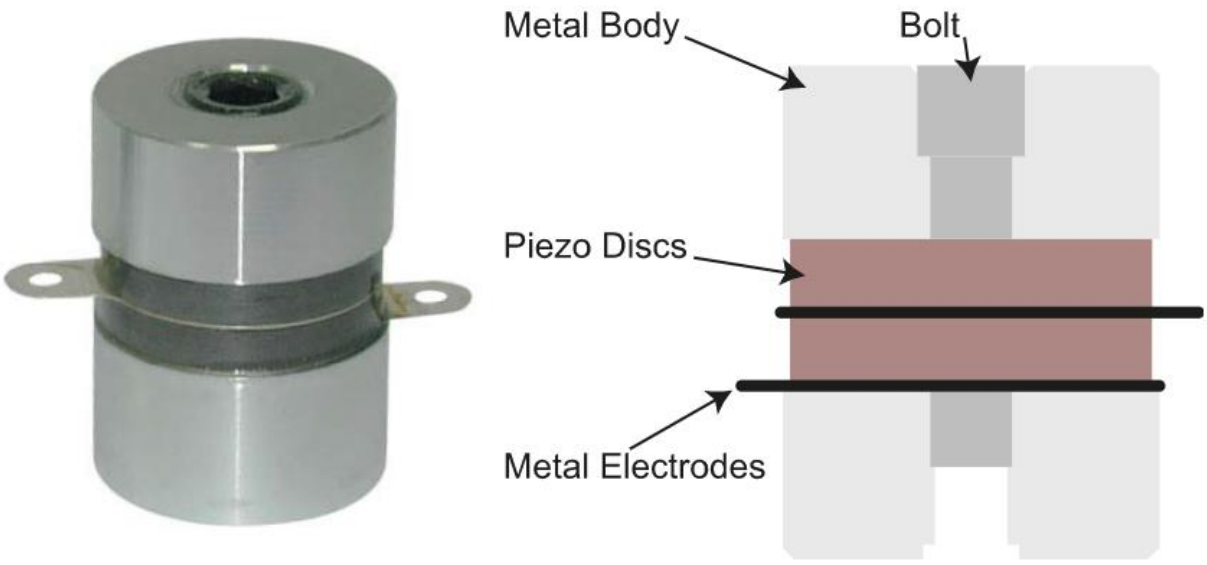

Figure 4.3: example and sketch of the piezoelectric transducer. *(https://www.piezodrive.com/ultrasonic-drivers/intro-ultrasonic/, s.d.)*

This transducer works by having a voltage applied across a piezoelectric material. If a voltage is applied across the crystal, the dipoles will align themselves with the electric field and the crystal expands. Similarly, when pressure is applied to the crystal the electric dipoles within it re-orient, thus creating a voltage.

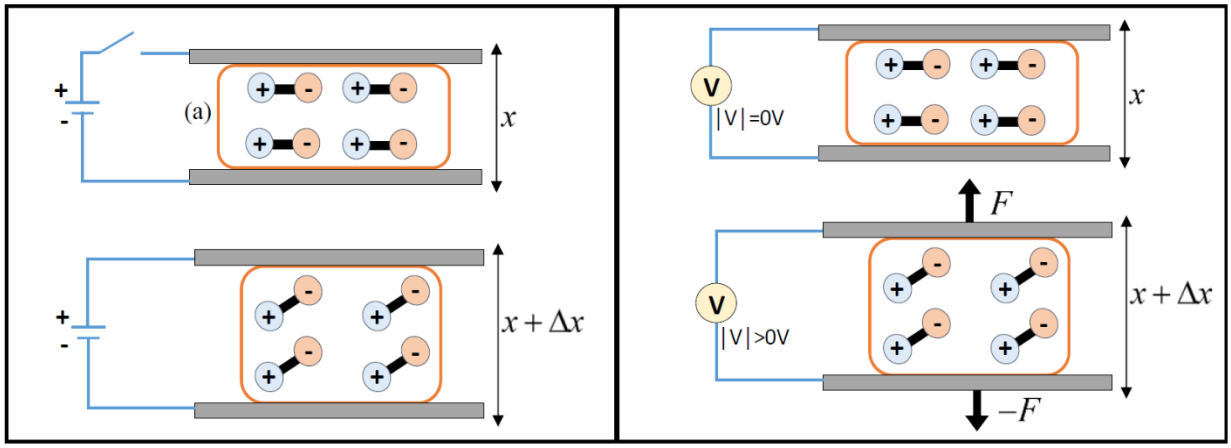

Figure 4.4: (left) When a voltage is put across a piezoelectric crystal (a) the electric dipoles within the crystal will align themselves with the electric field, thus expanding the crystal. If a force, F, is exerted on the crystal (right) causing it to expand, the displaced charges will create a voltage difference. *(Mecham, 2018)*

These piezo crystals are an effective way of converting electrical energy into mechanical energy and will serve as the driver for the transducer's motion. A steel bolt holds the transducer together and also completes the circuit between the two piezos. In this experiment we used a sinusoidal current to drive the piezo. The transducers behave like a spring with free, equal masses on each end, that can be of different shape and material. (Moreno, Acevedo, & Leija, 2005)

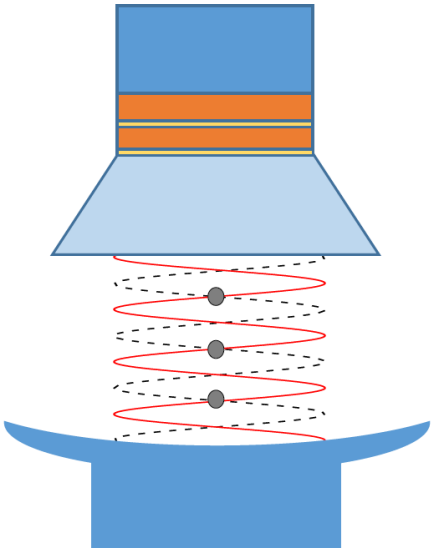

Figure 4.5: the formation of the nodes thanks to the emitter and reflector *(Mecham, 2018)*

By placing at a precise distance, meaning at an integer number of half wavelength, the reflector, we can than obtain the stable pressure nodes and allow the particle to levitate. The problem arising in this operation is that the tuning of the reflector distance is an extremely delicate operation. In fact, if the frequencies typically used in the ultrasonic levitation range from 28 to 40 kHz, this means a wavelength from 12 to 9 millimetres (air, 20°C, $c_0 = 343\ m/s$). Hence it is required the use of a micrometric screw to properly set the distance, that has to be perfectly adjusted in order to avoid problems of instability due to the imperfect resonance.

This technology being expensive to set up and to operate, very recently a new type of device has been gaining importance in this field. It is called TinyLev and, since is the type of instrument I used in my observation, a following section will be dedicated to its illustration

4.4. Plausible and validated future applications

The acoustic levitation technique, that spans far beyond the basic example of a single axis configuration for the mere static levitation of a particle, is extremely intriguing and scientist are working to find appropriate applications for this technology. Contactless manipulation and containerless transportation are the main features that are appealing the most. This perk is a unique feature of this technique, allowing for example of manipulating and mixing living cells and DNA plasmids (Vasileiou, 2016). Great enthusiasm was recently shown due to the improving of 3-D printing techniques, so that now scientist, researchers but even students can self-produce an effective, precise yet low cost device.

It seems by the great interest of researcher on the subject and by the possible implications of the discovery that the next main goal will be represented by the achievement of manipulating multiple samples and systematically mixing and splitting them. All this will be done in the millilitric or microlitric scale.

4.5. Instrumentation used

For the purposes of this study, I was mended to use the instrumentations of the laboratory. The study of the drying kinetics through levitation was then realised with the following elements:

- a climatic chamber, with controllable and adjustable temperature and humidity
- a generator, sending the required tension for the functioning of the levitation device
- a frequency amplifier
- an oscilloscope, allowing to read the applied frequency and tension
- an optical system composed of a light source and of a camera and a tripod
- image capturing software (HIRIS and Camera Tool)
- the acoustic levitation device

Figure 4.6: the climatic chamber

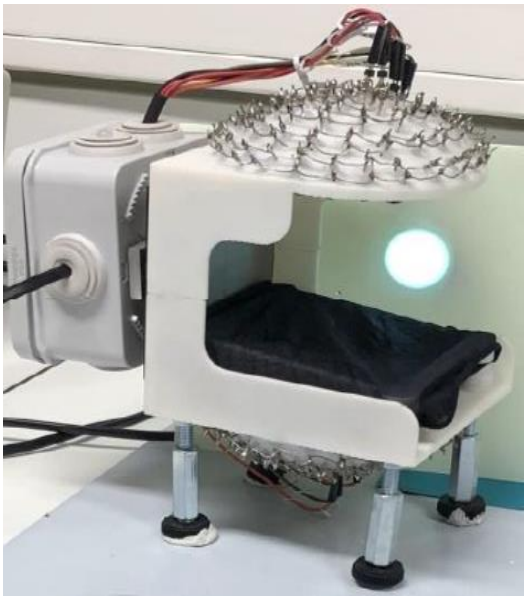

Figure 4.7: the acoustic levitation device on the type of TinyLev

Here are more specifically described parts of the instrumentations used, and how they were operated.

4.5.1. The climatic chamber

This element is simply a closet-like device, where it is possible to regulate and obtain specific conditions of temperature and humidity.

Figure 4.8: The output interface of the climatic chamber

For the purposes of this experiment, a fixed set of temperature and humidity was decided, together with the tutor and the developer of the device, M. Yorick Buot de l'Epine, PhD. These values were of T = 25°C and HR = 38%. This was taken to avoid problems to occour to the ultrasonic transducers that, although robust and reliable, are anyway electronic components, subjected do the influence of high temperature and humidity conditions. Possibilities to safely broaden the range of environmental conditions wan not taken in consideration for this study, for it

should be purpose of a dedicated research, involving more skilled people, as the technology of the transducer is very recent and little literature or publications on its applications is available.

4.5.2. The PIV camera and setup

With the acronym PIV, we typically mean Particle Image Velocimetry (Goharzadeh & Molki, 2015). It is a modern and interesting method for studying the behaviour of a fluid of gaseous flow. Normally, the PIV technology uses laser or light pulses as source of illumination, and the timing between the pulses represent the elementary time interval Δt. A CCD camera (charged couple device) captures the images of the developing phenomenon occurring and then the data are computed and correlated by software of image interpreting.

For this application, the camera was filmed with a pre-determined frame rate, and the light source was fixed, as a lightbulb dampened by a semi-opaque layer, like a paper sheet, in front of it. This was because the phenomenon of evaporation is noticeable in a medium to long period of time, with little necessity of a high frequency pulsed light emitting source.
In a CCD camera, an array of coupled capacitors is mounted on an integrated circuit. Illustrating the precise functioning of this complex, yet so common nowadays, device is far beyond the purpose of this work and the skills of the writer. Essentially, each pixel of the final image is represented by a capacitor. Those capacitors are made of a semi-conductive alloy that can be excited by incoming photons, causing the discharge of the plates, thus generating an electric impulse that can be processed and transformed into an image.

Figure 4.9: the PIV camera

Figure 4.10: the camera mounted on the tripod

The camera was equipped by a system of lenses to magnify the image and then mounted on an adjustable tripod. In this case precision in the setting was of primary interest, as a misplacement or a setting not on bubble level will certainly lead to an error of parallax.
Eventually the setting was placed in front of the transparent glass door of the climatic chamber, axially aligned with the levitating sample ant the light source, as showed on the figure.

Figure 4.11: the final setting of the PIV device ready to start the image capturing process

4.5.3. The acoustic levitation device: the TinyLev

In 2017 a ground-breaking article was published by the team of A. Marzo from the university of Bristol. It described the design and the functioning of a new device for the acoustic levitation of small samples. Instead of sticking to the well-known technology of an axial resonant apparatus with Langevin type transducer, it introduced a new configuration, where resonance was completely put aside. In fact, instead of single emitter with a concave surface for reflection and focusing of the wave, Marzo's experiment was on a new instrument with multiple emitters placed above and below the levitating sample. After perfecting the technology, he interestingly came out with an original and programmatic name: TinyLev. This bizarre name is in fact able to convey the idea of compactness and robustness of the configuration, but also, with a non-strictly-scientific terminology, it can express the willing of the maker, that is the hope of a future democratisation of this technique thanks to the miniaturisation of the devices, and the popularity of didactic hardware and 3-D printing.

This system relies on the placing in parallel of ultrasonic distance sensors (emitting type). Those emitters consume little electric current thanks to their high impedance and can obtain high pressure level. In Marzo's project, 72 transducers are installed on two hemi-spheres, devided by a distance multiple of the length of a wave signal.
In the model realised by M. Yorick Buot de l'Epine for the UTC laboratory, 120 transducers and not 72 were placed, for purpose of precautionary overdimensioning, with the following disposition for each hemisphere:

- 1st ring: 6 transducers
- 2nd ring: 12 transducers
- 3rd ring: 18 transducers
- 4th ring: 24 transducers

Figure 4.12: the configuration of the transducers in the device

Figure 4.13: CAD sketch of the device for the 3D printing. A not better specified epoxydic resin was used for the printing, that showed good properties to humidity and temperature.

The distance of 110mm was chosen between the two parts, as it gives an uneven number of wavelengths. Eventually, in order to prevent damages to the emitters of the lower array from the falling of the small levitated bodies, particularly liquid droplets, a thin layer of nylon was kept in position by an equally printed support (Buot de l'Epine, 2017).

5. Methods and experimentation

In this section the purpose of the experiment will be shown, together with the methods used to prepare the samples, procedure of the experiments and image interpreting.

5.1. The drying process

When levitating a liquid droplet, evaporation from the sample takes place. Here already a major distinction arises between two fields: pure liquids and mixtures.

For pure liquids it is reasonable to consider evaporation with a constant rate from the particle. In fact, no other phenomena are insisting on the droplet, and it has been proved that the evaporation of those pure liquid samples follows linearly a d^2 law function (Yarin, Brenn, Kastner, & Tropea, 2002). This means that the square diameter of the drop decreases linearly with time, eventually arriving to completely evaporate. In particular, for the case of acoustic levitation, as I experienced, getting to a complete evaporation for a pure sample is a non-trivial task, as the technique is intrinsically subjected to a number of instabilities. Direct observation showed that the most common ending for the droplet is its implosion, when not simply a fall from its position due to increasing

oscillations that move it away from the node.
The situation changes significantly when we come to the study of non-pure liquid samples, in particular liquid-solid mixtures. We cannot admit anymore that no third phenomenon is acting on the suspended liquid. Then, after a first period when the evaporation rate is practically constant, with the increasing importance of the effect of the diluted solids, the rate gradually decreases, and a plateau is formed. Details will be presented in following subsections.

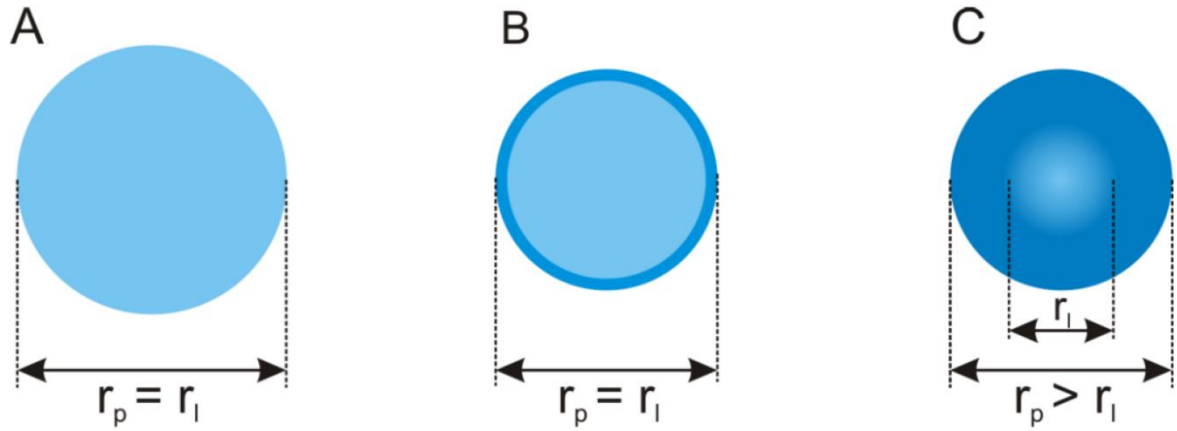

Figure 5.1: Constant drying stage (A), transition point (B) and shell formation in second stage (C) *(Thu Hang, Jaskulski, & Peglow, 2015)*

5.1.1. Physical and geometrical estimates

Studies have been made in the past years to set out some parameters together with orders of magnitude to deduce an interpretation for experimental results (Sloth, et al., 2006) (YARIN, BRENN, KASTNER, RENSINK, & TROPEA, 1999).
The problem of the evaporation of a droplet, suspended or not, is typical template in the field of transport phenomena, as mass and heat transfer are occurring in the process (Renksizbulut, Nafziger, & Li, 1991) (Mezhericher, Levy, & Borde, 2020). So then let us take some insight in the geometry, and in the characteristics of a generical sample.

It is by now clear that the droplet we are talking about is of a spherical shape. If fact the assumption of a spherical geometry is reductive, because during the experiment the sample undergoes a deformation due to the force exerted by the ultrasonic field. So, the actual shape is more like an oblate spheroid. Details on how the geometry was taken into account will be shown accurately later, aside with the computational model.
However, as first approach to the subject, a spherical hypothesis can hold. For this sphere, we can consider the volume-equivalent radius as characteristic size, of the order of $a \sim 10^{-3}$ m. The thermal diffusivity α_l of such liquids as water has the magnitude of $\alpha_l \sim 10^{-7}$ m^2 s^{-1}. Considering the characteristic heat transfer time for such droplets ad the ratio between those two quantities, we obtain

$$\tau_1 = \frac{a^2}{\alpha_l} \sim 10\ s \qquad (4.1)$$

Also, consider that the typical lifetime of an acoustically levitated droplet is on the order of $\tau_2 \sim 10^2 - 10^3\ s$; in particular, my experiments spanned from any value between 1000 to >3000 seconds. It is then clear that $\tau_2 \gg \tau_1$. Hence, we can consider the $temperature\ inside\ the\ droplet$ as uniform, particularly $T \equiv T_s$, where T_s is the $surface\ temperature$. Note that $\tau_2 \sim \langle \overline{h_c} \rangle^{-1}$, were h$c$ is the time average mass transfer coefficient for the acoustically driven evaporation, also averaged over the droplet surface (YARIN, BRENN, KASTNER, RENSINK, & TROPEA, 1999). To these days the most detailed and complete work on

the acoustic levitation has been done by researchers Yarin and Tropea. In theirs work, it is possible to find a definition for the mass transfer coefficient as:

$$\langle \overline{h_c} \rangle = \frac{D_0}{2a} \left(\frac{45}{4\pi}\right)^{\frac{1}{2}} \frac{B}{(\omega D_0)^{\frac{1}{2}}} \quad (4.2)$$

$$B = \frac{A_{0e}}{\rho_0 c_0} \quad (4.3)$$

where:

- D_0 is the diffusion coefficient of vapor in air [$cm^2\ s^{-1}$]
- ω is the angular frequency of the ultrasound. [s^{-1}]
- B gas particle velocity amplitude in the acoustic wave [$cm\ s^{-1}$]
- A_{0e} is the effective pressure amplitude of the acoustic field [$dyne\ cm^{-2}$]
- ρ_0 is the unperturbed gas density [$g\ cm^{-3}$]
- c_0 is the gas sound velocity [$cm\ s^{-1}$]

In that paper, units of measure are presented as shown above. No particular justification is given for this choice. Nonetheless, those units are coherent and mutually simplify when coming to the investigation of dimensionless numbers.

Recalling that the Sherwood number is defined as $Sh = \frac{h\,L}{D}$, in our case we have

$$\langle \overline{Sh} \rangle = \langle \overline{h_c} \rangle \frac{2a}{D_0} = \left(\frac{45}{4\pi}\right)^{\frac{1}{2}} \frac{B}{(\omega D_0)^{\frac{1}{2}}} = K \frac{B}{(\omega D_0)^{\frac{1}{2}}} \quad (4.4)$$

where the group K is introduced for the sake of abbreviation. For acoustically driven evaporation, this Sh was found to be of the order of 10, result that is in part confirmed by my experiments.

The study of the Sherwood is not by chance, as this dimensionless number is indicator of the mass transfer rate.

It can be noted that the expression found above is way different from the more common, and validated too, according to Ranz and Marshall (Ferrari, 1989)

$$Sh = 2 + 0.6\, Re^{\frac{1}{2}} Pr^{\frac{1}{3}} \quad (4.5)$$

because, for example, a limiting value of 2 shall be observed in cases of stagnant gaseous medium. In reality, as I experienced with my own experiments, even in the not so commonly studied case of a quiescent surrounding gas, such a little value for the mass transfer cannot be obtain. This is justified by the action of the acoustic stream around the droplet, so that is incorrect to consider a diffusion driven evaporation mechanism.

5.1.2. The two-stages drying

As mentioned before, the evaporation of a droplet can be described as a two stages process. Let us consider the case I examined, namely the one with a liquid matrix with dissolved solids. In the first part, water is evaporating from the surface, migrating from the liquid body to the surrounding environment. In the same time, the content in solid increases inside. For this whole period, the rate of evaporation, and of shrinkage too, is constant with time, following the d^2 linear law. The rate of diminishing in moisture content can be considered in a similar way.

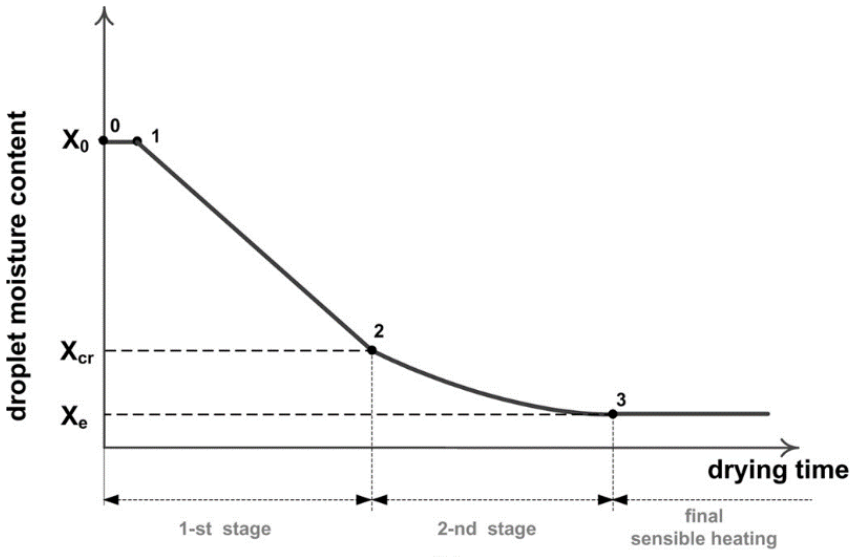

Figure 5.1: sketch of the behaviour of the moisture content *(Mezhericher & Borde, 2010)*

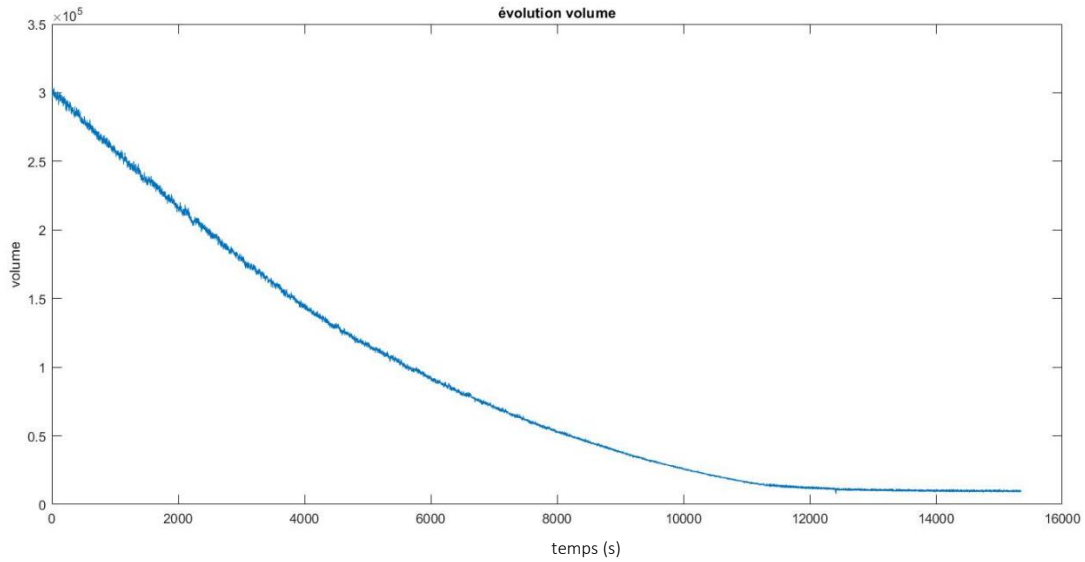

Figure 5.2: graph for the volumic shrinkage of an analyzed sample (arabica coffee in water)

Starting at a certain point, the mechanism of evaporation changes, and it is evident from the change in the shape of a graph volume/time (or area/time). In fact, due to the evaporation carried out, the increased solid concentration leads to the formation of an actual crust on the surface, that includes the liquid part. At this point evaporation still continues, but at a lower rate, because the liquid has first to diffuse through the pores of the solid crust, and then leave the surface. For a certain period this slow-rate evaporation can be still monitored by observation of the diminishing dimension. When the particle reaches the "locking point" no further shrinkage can be noticed, even if evaporation is occurring (Shamaei, et al., 2016). At that point, the porous crust is sufficiently thickened to prevent itself from shrinking more. Indirect clues from ongoing evaporation can be collected from the axial displacement of the particle, that getting lighter and lighter, is able to move upwards. However, this was not considered during my experiments, due to a lack of initial hints and time.

The computational part of this work was focused on the first stage, aiming to deduce the Sherwood number and to produce conclusions on those observations.

5.2. Samples preparation and procedure

As mentioned at the very beginning of this paper, the aim for the investigation of this work was to study different types of liquid mixtures, in some way related to the alimentary field and applications. Due to my poor laboratory skills by that time, there was a preliminary period at the beginning of the research during which I focused on the mastering of the laboratory facilities and standardising a new procedure. So, I took in heritage the previously done work, accomplished during the previous semester by a graduating student, and studied it.
Together with my tutor we agreed on some major points about the procedure. The setup of the procedure can be summarised as it follows:

a) Preparation of the sample
b) Placing of the sample in the climatic chamber
c) Starting the levitation and the image capturing, thus starting the experiment
d) Waiting until complete destruction of the droplet
e) Transferring the data from the laboratory computer to a more powerful one
f) Elaborating and interpreting the data with a dedicated calculation model

The preparation of the sample to be tested, although not a very hard task, was an issue of precision and patience. The main aim wat to reach the highest degree of precision possible and to standardise the step, trying also to make it faster.

First, a list of the desired mixtures was taken down. When dealing with dissolved solids like salts or sugars, it is easy to understand that the percentage indicated are index of the mass concentration. Not so straightforward is the definition for the water-coffee mixture. In this case, the weight written indicates the amount of powder used in the preparation of the coffee itself. I preferred not to use instant coffee, but rather use different types of grounded coffees. For the milk, time ran out when I just could finish a single experiment on the only one sample of whole milk. The preparation for this type of sample was without doubt the easiest one, as the milk was simply poured from the bottle to the test tube used for transportation and then into the micro syringe.
Here a table with the samples prepared

Sample type	Sample name	Characteristics	Date
100 % arabica coffee	*A_h_c_a*	Water : 100ml Coffee : 7.181 g T_{in}=21 °C T_{fin}=55°C Time : 1h centrifuged	04/03/2020
	A_h_c_b		04/03/2020
	A_h_c_c		04/03/2020
	A_nh_c_a	Water : 100ml Coffee : 7.181 g T_{amb}=21°C Time : 1h centrifuged	05/03/2020
	A_nh_c_b		05/03/2020
	A_nh_c_c		05/03/2020
100% robusta coffee	R_h_c_a	Water : 100ml Coffee : 7.181 g T_{in}=30 °C T_{fin}=43°C Time : 1h centrifuged	04/03/2020
	R_h_c_b		04/03/2020
	R_h_c_c		04/03/2020
	R_h_c_d		07/03/2020
	R_h_c_e		07/03/2020
	R_h_nc	Water : 100ml Coffee : 7.181 g	04/03/2020

		T_{in}=30 °C T_{fin}=43°C Time : 1h Not centrifuged - filtered	
	R_nh_c_a	Water : 100ml Coffee : 7.181 g T_{amb}=21°C Time : 1h centrifuged	06/03/2020
	R_nh_c_b		06/03/2020
	R_nh_c_c		06/03/2020
50% robusta-arabica mixture	0.5_RA_nh_nc_a	Water : 50ml arabica coffee : 1.8g robusta coffee :1.8g T_{amb}=21°C Time : 2h Not centrifuged - filtered	06/03/2020
	0.5_RA_nh_nc_b		06/03/2020
	0.5_RA_nh_nc_c		06/03/2020
	0.5_RA_h59_c_a	Water : 50ml arabica coffee : 1.8g robusta coffee :1.8g T_{in}=22 °C T_{fin}=59°C Time : 1h Not centrifuged - filtered	09/03/2020
	0.5_RA_h59_c_b		09/03/2020
	0.5_RA_h65_nc_a	Water : 50ml arabica coffee : 1.8g robusta coffee :1.8g T_{in}=22 °C T_{fin}=65°C Time : 1h Not centrifuged - filtered	09/03/2020
	0.5_RA_h65_nc_b		09/03/2020
	0.5_RA_h65_nc_c		09/03/2020
30% - 70% robusta – arabica mixture	3.7_RA_h65_f_a	Water : 50ml arabica coffee : 5.0267g robusta coffee :2.1543g T_{in}=25 °C T_{fin}=65°C Time : 1h Not centrifuged - filtered	11/03/2020
	3.7_RA_h65_f_b		11/03/2020
	3.7_RA_h65_f_c		11/03/2020
Vergnano's "*Granaroma*" grounded coffee mixture	granaroma_moka_a	Coffee prepared with a Bialetti's espresso machine "Moka"	12/03/2020
	granaroma_moka_b		12/03/2020
	granaroma_moka_c		12/03/2020
Whole milk	lait_entier_a		12/03/2020
	lait_entier_b		**12/03/2020**

Table 5.1: table showing the prepared samples for the experiment

Once finished the preparation, it was time to move to the climatic chamber.
This type of instrumentation needed time to reach the operative conditions. Despite being placed in a basement, the conditions of humidity and temperature were variable day by day. The machine needed at least three to four hours to set correctly, so to avoid dead times it was crucial to carefully schedule the experiments. The positioning of the droplet was a skill to be mastered too. The flaw of the whole process of positioning is the necessity to open the glass door of the chamber. In fact, this modifies and interfere with the set conditions inside, but with the physical impossibility of piercing

a hole or to operate the positioning by distance, the sole possible improvement is to be as fast as possible.

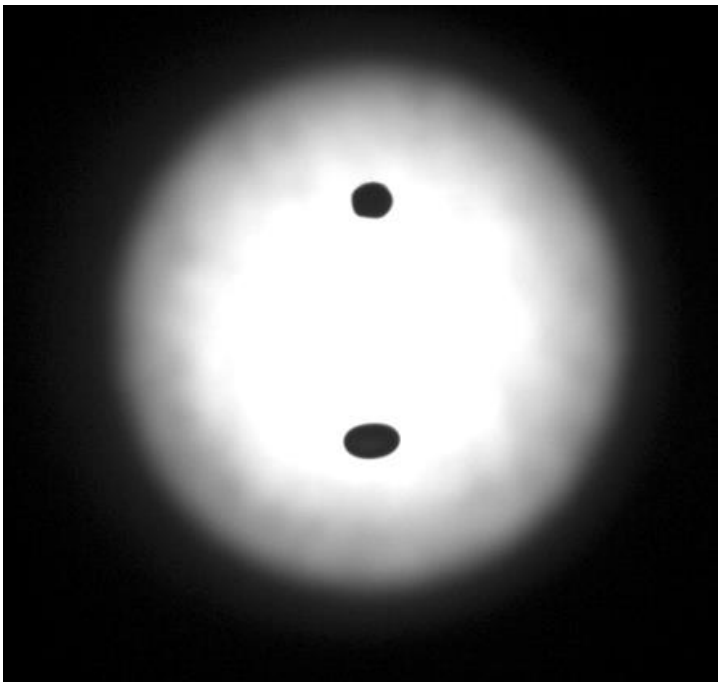

Figure 5.3: the two suspended bodies, the polystyrene bead (above) and the droplet (below)

In order to help to find the axial positioning of the pressure nodes, a good approach was to position a small polystyrene bead in the levitation device. It was to be placed on a node that would result above the droplet. This is because even if the dimension of the bead is small enough (on average never more than 2.5 mm) to not interfere with the waves, placing it above the droplet, true object of interest of the research, would definitely prevent interference. Moreover, being a solid body, the bead has a stable dimension overtime, and could be taken as a reference point, at least for some characteristic lengths. Changing in the shape of the bead were observed, but this was due to the rotation triggered by the ultrasonic waves.
Then, using the bead as reference point, the droplet was positioned using a microlitric pipette. The volume was set to 5 µl. No specific reason related to the nature of the experiment was taken into consideration for the choice of this volume. However, for a non-specialist like me, this relatively large volume allowed the use of a pipette with disposable tips big enough not to introduce strong capillary forces that could lead to obstacles in the ejection and the positioning of the droplet. In fact, adhesive forces between the liquid and the plastic of the tip are already big enough to sometimes avoid the detachment of the droplet towards the pressure node, thus forcing to change the tip, reclose the door of the chamber and lose time waiting for the controlled condition to set again. Working with a microlitric syringe, with smaller volumes, would have been harder to do quickly, considering all the time to spend to clean the instrument after every single use. Finally, and more interestingly, a volume as large as 5 µl was rarely object of research, and scarce documentation is available. So, I and my tutor thought it would have been interesting to see if there was any particular phenomenon to observe or to make comparison with.

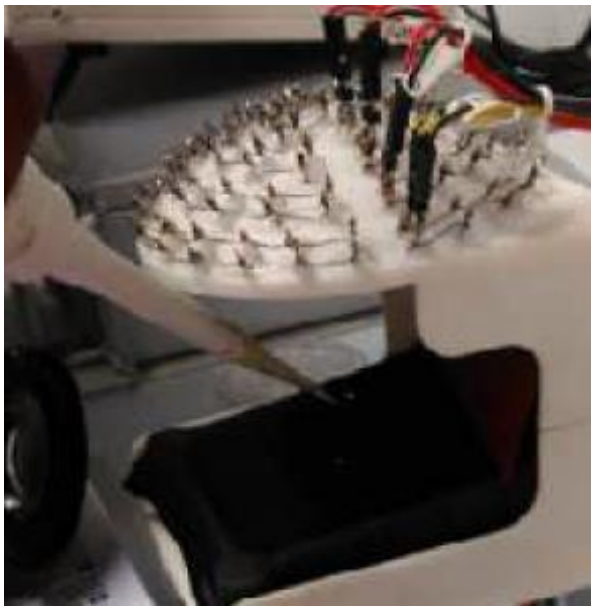

Figure 5.4: placing a droplet

The image capturing started the very moment the droplet was placed, and the glass door was closed. As said before, this part could last for a variable time, spanning from at least 1000 seconds to more than 3000. It was observed that experiments that stopped before 1500-2000 seconds were few, and carried an intrinsic flaw, like an excessively deformed shape. The data were processed on the moment by a dedicated pc, and then transferred to my own, more powerful. Eventually, the final step was represented by the numerical elaboration. Being this operation the core of the experiment in terms of extrapolation of information and interpretation, a dedicated subsection will show the details.

5.3. Image capturing and elaboration

Two software were then used for the image capturing: Hyris and CameraTool. When started, the recording tool acquires the images with a set frame rate, and stores them as separate files, with a relatively high definition.
As shown, each image is composed by a luminous circle, the backlight source, and two objects, a plastic bead used as spatial and dimensional reference, and a droplet. The observation of the ongoing experiment shows a progressive shrinkage of the droplet until it complete disappearing, for the case of pure liquid, or definitive stabilisation at a certain dimension of the remaining solid particle. At that point, manual intervention is required to stop the recording.

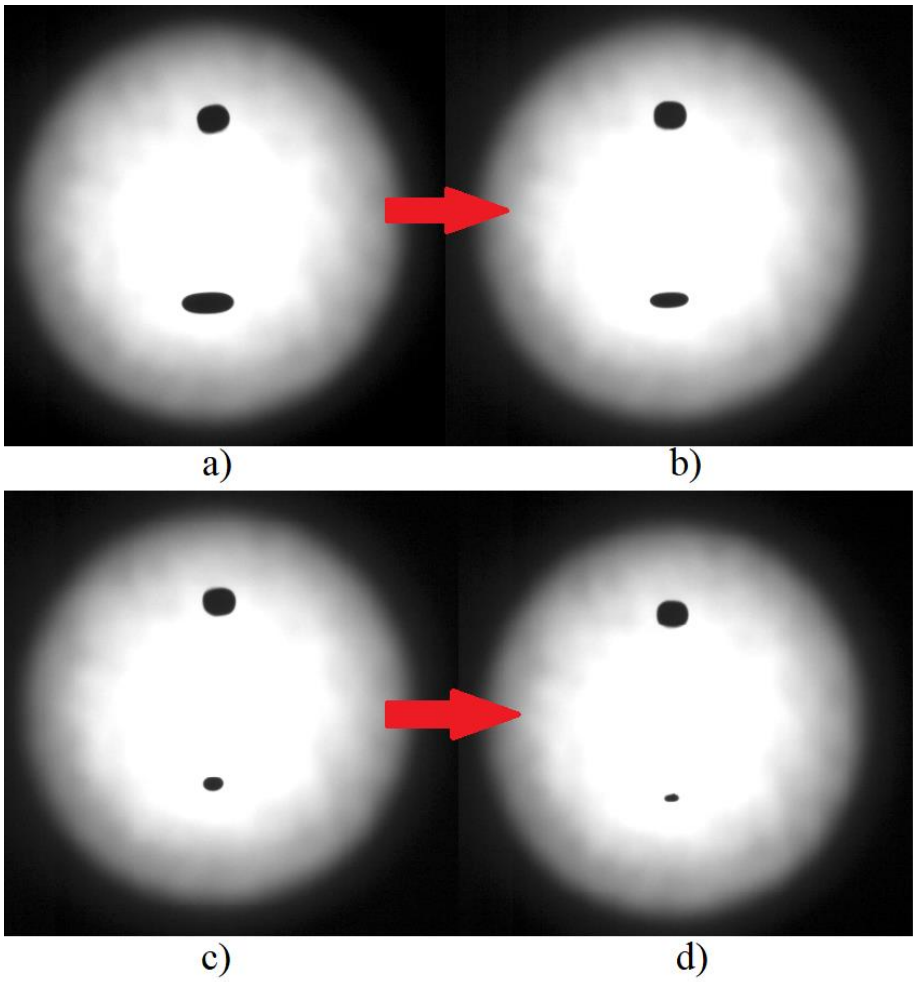

Figure 5.5: example of the evolution in the form and dimension of a droplet during the experiment (arabica coffee mixture)

5.3.1. Theory and formulae

To end up with an interpretation, a mathematical model has to be set out. The expression representing the drying process can be found on multiple sources and studies, and has the form of a typical mass transfer expression from the boundary layer theory

$$\frac{dm}{dt} = -h_m A\left(\rho_{v,s} - \rho_{v,b}\right) \quad (4.6)$$

where:

- $\frac{dm}{dt}$ is the drying rate [kg/s]
- h_m is the mass transfer coefficient [m/s]
- A is the surface of the droplet [m^2]
- $\rho_{v,s}$ and $\rho_{v,b}$ are the vapor density at the surface of the droplet and in the bulk of air [kg/m^3]

Now, the mass transfer coefficient can be considered in terms of the Sherwood number

$$h_m = \frac{Sh\ D}{d} \quad (4.7)$$

and by saying so we are considering that for the moment the hypothesis of a particle perfectly spherical yields. Then following this simple math

$$\frac{4}{3}\,\pi\,\rho_l\frac{d(r^3)}{dt} = -h_m 4\,\pi\,r^2\left(\rho_{v,s}-\rho_{v,b}\right) \quad (4.8)$$

$$\frac{d(r)}{dt} = \frac{-h_m}{\rho_l}\left(\rho_{v,s}-\rho_{v,b}\right) \quad (4.9)$$

$$A = 4\,\pi\,r^2 \quad (4.10)$$

$$\frac{dA}{dt} = -8\,\pi\,r\frac{h_m}{\rho_l}\left(\rho_{v,s}-\rho_{v,b}\right) = -8\,\pi\,r\,\frac{Sh\,D}{2r}\left(\rho_{v,s}-\rho_{v,b}\right) \quad (4.11)$$

$$Sh = -\frac{dA}{dt}\frac{\rho l}{4\,\pi\,D\,(\rho_{v,s}-\rho_{v,b})} \quad (4.12)$$

So then by knowing basic information on the sample we can deduce an a-dimensional number, index of the mass transfer. It is interesting then to compare this *Sh*, obtained practically by tracing the evolution of the surface during the time and observing its slope, with the value that comes from the expression of Yarin et al., that takes into account only the acoustic field.

For the purposes of this experiment, the above expression was slightly modified in the terms. Table 5.2 shows the list of the used terms.

Instead of using the vapour density, I used the combined terms of the molar concentration C_{total}, the molar mass M_{water}, and the molar fraction x^i and x^∞. From an easy dimensional analysis, it is clear that the two ways of operation are coincident, for the final result is always a mass over volume. Noting the group $\frac{dA}{dt}$ with the letter α, the new expression will read

$$Sh = \frac{-\alpha\,\rho_{water}}{4\,\pi\,C_{total}\,D_{AB}\,M_{water}\,(x^i - x^\infty)} \quad (4.13)$$

Term	Expression	Value
P		101325 Pa
T_{ext}		25°C 298 K
HR		38%
$\Delta H_{v,\,water}$		2500 J kg^{-1} (273 K, 1 atm)
$T_{humid\ bulb} = T_h$		288.9 K
$T_{average}$	$T_{average} = \frac{T_h + T_{ext}}{2}$	293.53 K
T_{ref}		273 K
D_{ab} ($T_{average}$) **A=water B=air**	$D_{AB} = 0.0000212 \times P \times \left(\frac{T}{T_{ref}}\right)^{2.334}$	2.511E-05 $m^2\,s^{-1}$
R		8.31446 J $mol^{-1}\,K^{-1}$
C_{total}	$C_{total} = \frac{P_{total}}{R\,T_{ext}}$	40.874 mol m^{-3}
$P_w^\infty = P_v$ (T_{ext})		1190.4 Pa

x^{∞}	$x^{\infty} = \frac{P_w^{\infty}}{P_{total}}$	0.01175 mol water/mol total
$P_w^i = P_v^*$ (T humid bulb)		1790.8 Pa
x^i	$x^i = \frac{P_w^i}{P_{total}}$	0.01767 mol water/mol total
ρ_l		1000 kg m^{-3}
M_{water}		0.018 kg mol^{-1}

Table 5.2 : list of the used terms

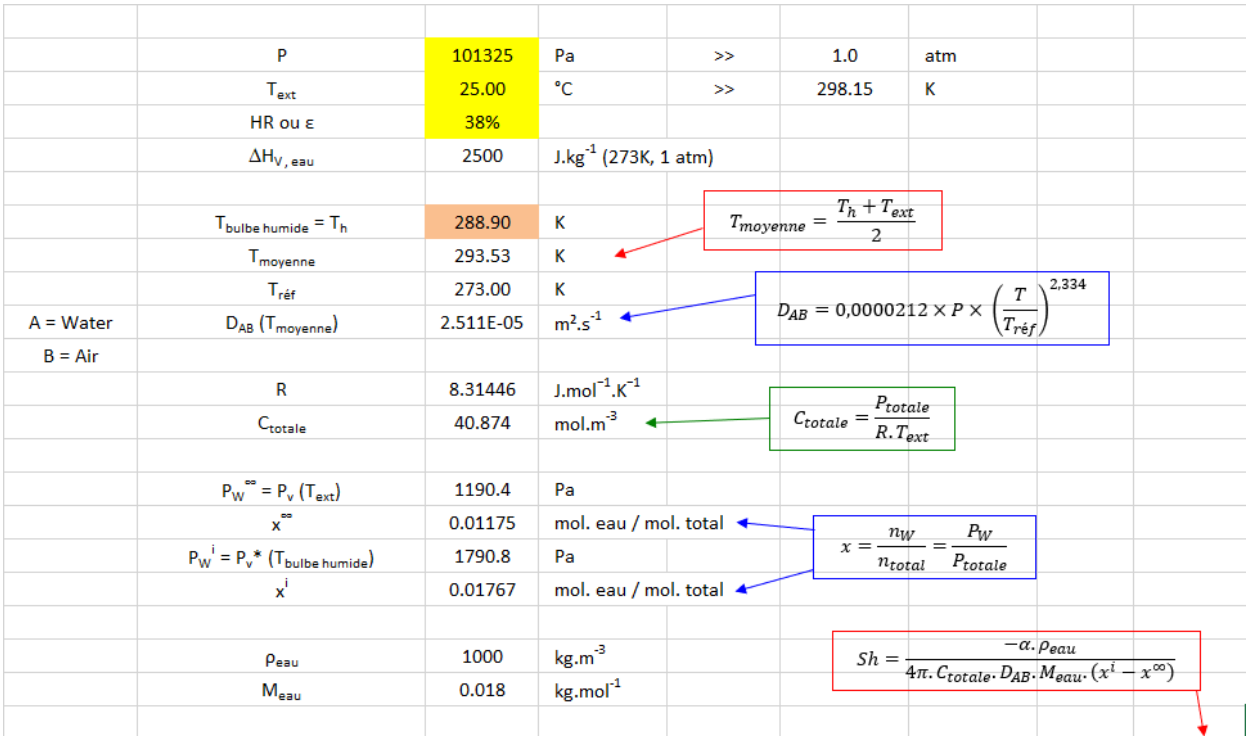

Figure 4.6: snapshot of what the excel table looks. The wet bulb temperature is highlighted differently because is obtained from a calculation in a second excel sheet

5.3.2. Image interpretation

Purpose of the calculation part was to evaluate the rate at which the droplet was shrinking. To do so, a MATLAB code was developed together with the informatic department, thanks to the aid of Professor M. Mottelet Stephan. This program is able to take the digital image, to isolate the droplet, and then to assign as an element of array the value of the length of the minor and major axis, the surface and the volume.

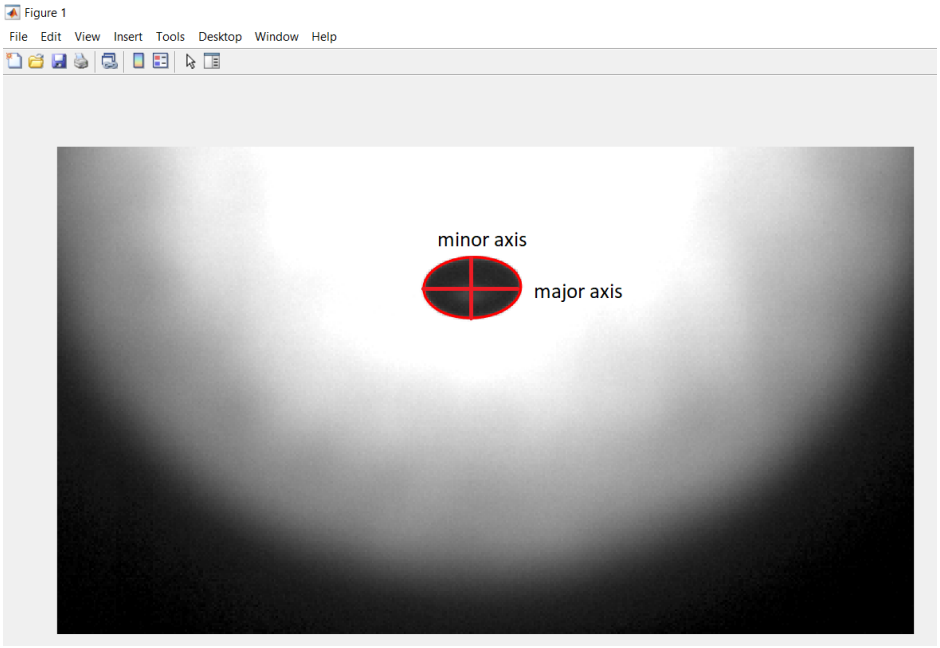

Figure 5.7: picture of what the code interprets as an image. The droplet 2-D projection is approximated to an ellipse

The program reads all the images from the input folder and process them one by one. At the end, for each picture, it obtains the numerical value of the major and minor axis. So it calculates the surface by considering the droplet as an oblate spheroid, thus a solid generated rotating about the *z*-axis an ellipse with the semi-minor axis *b* and semi-major axis *a*, being *a* laid on the *x*- and *y*-axis and *b* on the *z*-axis. The formula for the surface reads as

$$S_{oblate\ spheroid} = 2\pi a^2 + \pi \frac{b^2}{e} \ln\left(\frac{1+e}{1-e}\right) \quad (4.14)$$

where $e^2 = 1 - \frac{b^2}{a^2}$

This part finished, the program plotted the evolution for the surface and of the volume on a graph. Also, it evaluated the evolution of the aspect ratio, namely the ratio between the major and minor axis. This value is another indicator of the behaviour of the droplet during the evaporation, how "well" the droplet passes from an oblate form to a more spherical form.

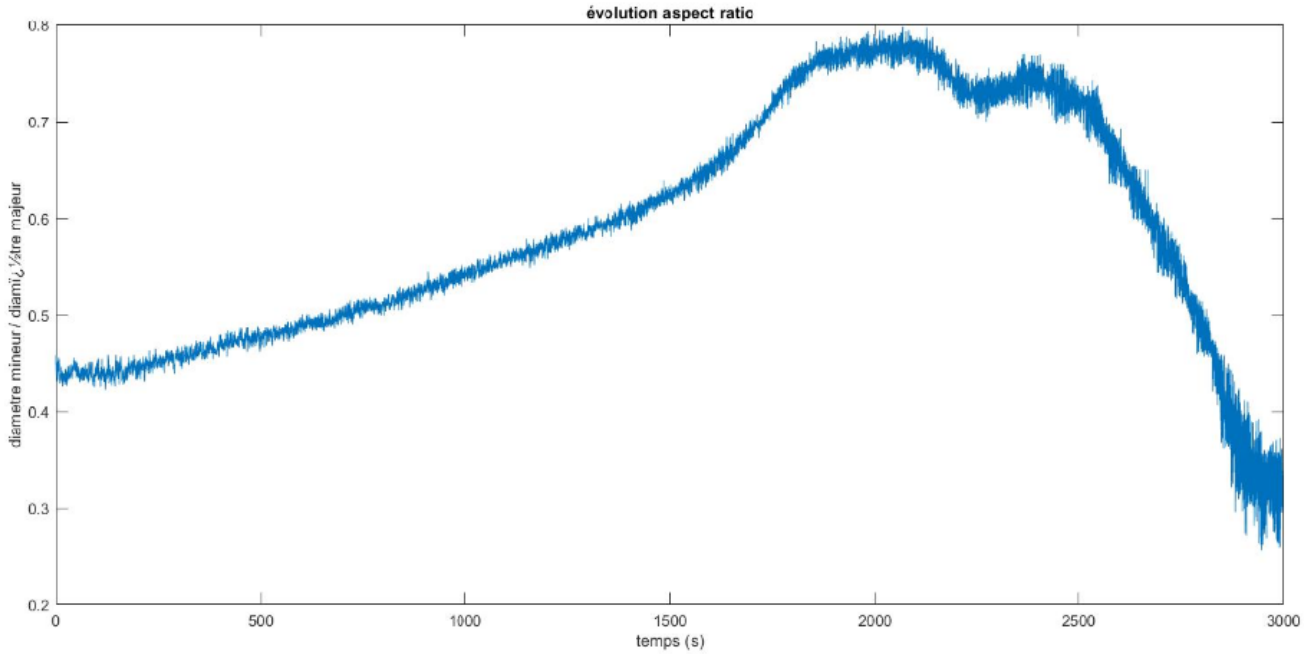

Figure 5.8: Plot of the evolution of aspect ratio.

Finally, the evaluation of the rate of evaporation.
As said before, the program is able to collect data on the surface of the droplet. What is important to notice though is that the area evaluated by Matlab is expressed in pixels. But to apply the formula for the Sh above, units have to be coherent, so we need to convert them into metrical system. This is the purpose of a second code, which once inserted a known real distance, gives back the equivalence pixel-millimetres (or metres). The set distance was taken on the polystyrene bead, evaluating the diameter as 2.5 mm. The conversion was then done, and the surface could be written as an actual value in mm^2 or m^2.

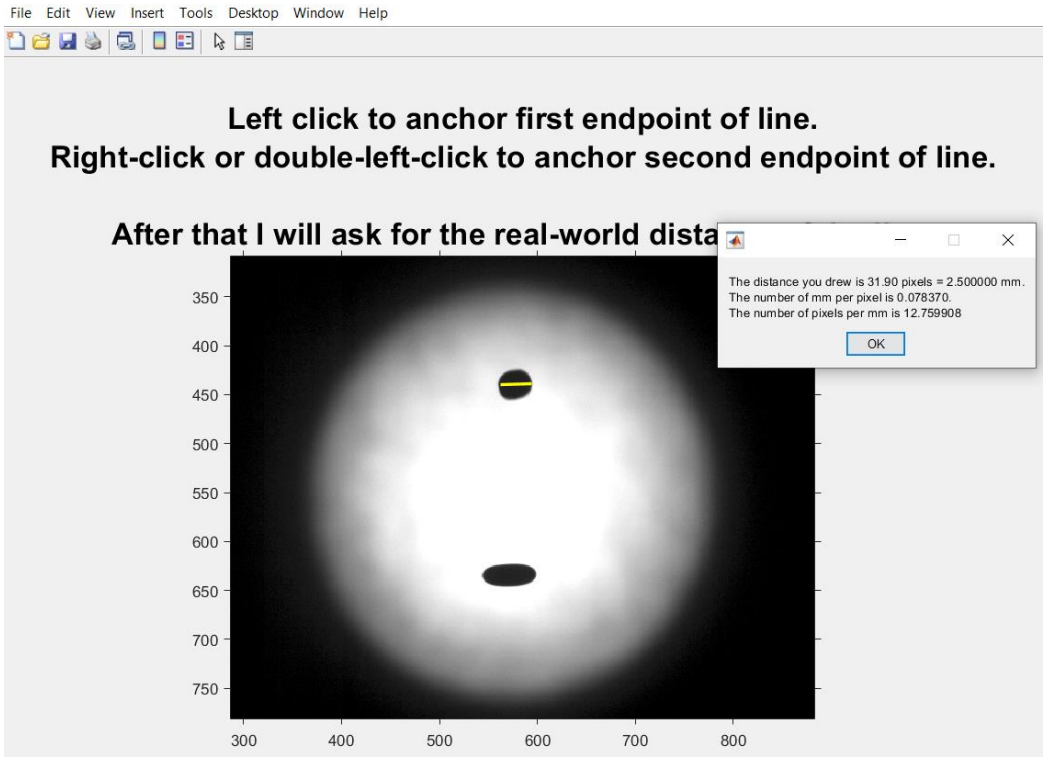

Figure 5.9: Snapshot of the interface to the user that appears when calibrating the conversion between pixels and millimetres

To evaluate the slope of the curve generated by plotting the evolution of the surface, a third and last program simply calculated

$$\frac{S_{n+1} - S_n}{t_{n+1} - t_n} = \frac{\Delta S}{\Delta t} \quad (4.15)$$

If this is applied on the whole array, the slope will be the one of the lines interpolating all the data. So, I decided to take into consideration as significative data only the ones from 20 to 1500 seconds. Excluding the data after 1500 s allows to be sure to obtain data on the first drying stage, that is the one interesting for this study, but also excluding the ones before 20 s avoids data corrupted by a still not stable position of the droplet or not correctly set conditions due to the quick opening and closing of the door.

6. Results

The following section will present the results of the research. Taking into account the fact that practically every sample has been tested three times, not all the graphs and table will be exposed here for space issues. However, a recap table will show the final result, namely the number of Sherwood and the standard deviation, for all the samples. Firstly, the results for the pure water samples are presented extensively, then other interesting samples. The aim is here to try to highlight differences and particularities.

After every experience, a folder with this material inside was produced:

- a certain number, variable with respect to each particular case, of pictures
- an Excel sheet reporting the time instant of recording associated with each picture
- four graphs reporting the evolution of the surface, brute and normalised, the aspect ratio and the volume

Then the data concerning in particular the time and the evolution of the surface were extracted and coupled to evaluate the slope of the curve in time.

6.1. Pure water

The purpose of observing the behaviour of a droplet of pure water is to, first of all, validate the hypothesis stated at the beginning of the research, then to have a white reference to compare all the other results.

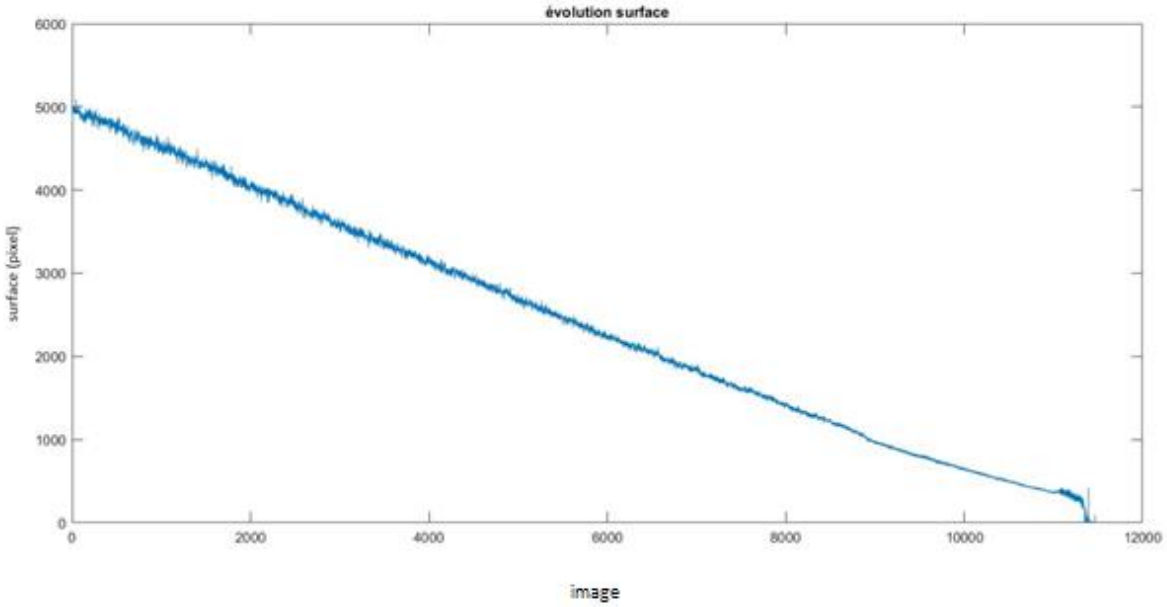

Figure 6.1: The surface of the droplet with respect of time, here indicated with respect to the image taken. The unit of measure here for the surface area are pixels

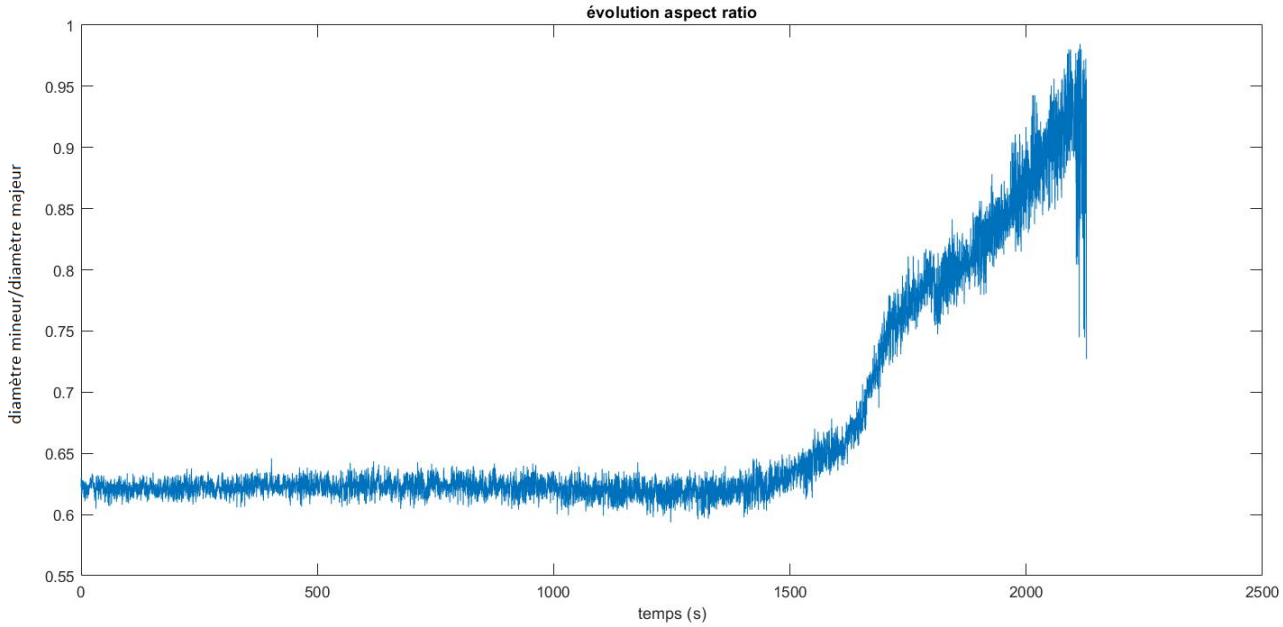

Figure 6.2: The evolution of the aspect ratio.

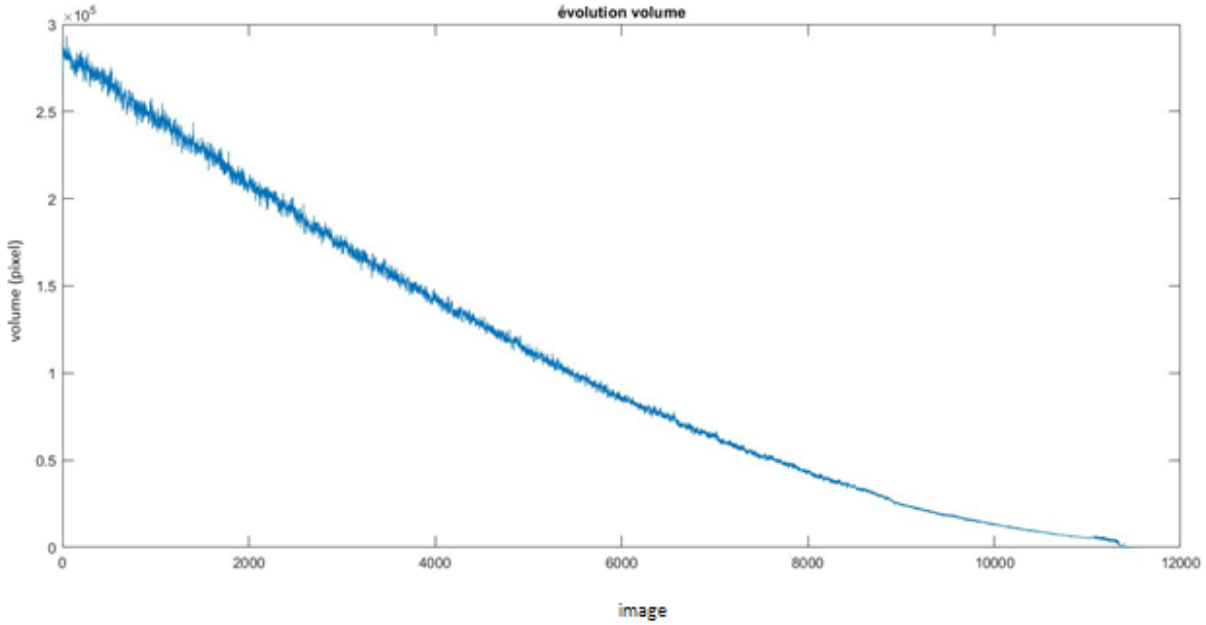

Figure 6.3: The evolution of the volume

Now, from figure 1 it is clear that one of the beginning hypotheses of the d^2 law holds, as the surface decreases linearly with the time. On the other hand, the volume does not show the same linearity. Also, the behaviour of the aspect ratio is perfectly in line. It begins with an oblate ratio, 0.65 c.a., but with the time it steadily goes to one, meaning that the droplet gets more and more spherical. The right-hand part of the graph in figure 5.2 shows noisy data; this is due to the fact that from the moment the droplet disappears, the program still considers every body with shades of black. Thus, any bit of powder, floating or on the lens, is taken as a valid input. This is the disturbance at the end of each experience, and it is not important at all, for that reason the last bit of data are usually excluded since they are not reliable nor interesting.

At the end, the analysis for the droplet of pure water returns:

Date	Sample	N°sample	Slope (m^2s^{-1})	Sh
04/03/2020	Pure water	a	-1.13E-08	8.185

Table 6.1

Conclusions that can be made on this result will be discussed at the end of the section, comparing the results of also the other samples

6.2. Coffee samples

In order to produce coffee samples that could be of some interest and embrace the different types of coffee-making and brewing, I chose to diverse the choice. The amount of grounded coffee powder used was always the same proportionally to water; the two were mixed via magnetic agitation. Samples were prepared with both hot and cold water. The separation of the water from the remaining solid consumed coffee was also done with multiple methods. Some samples were centrifuged, some were filtered, and some others were left still to sediment with natural speed.

Practically every experience was repeated three times, to verify whether or not a degree of repeatability was established. Here I am showing graphs of some experiences, labelling precisely each one. As did for water, the general recap for the slope and data will be presented at the end.

6.2.1. Arabica coffee

6.2.1.1. Hot brewed (T_{fin}=55°C)– centrifuged

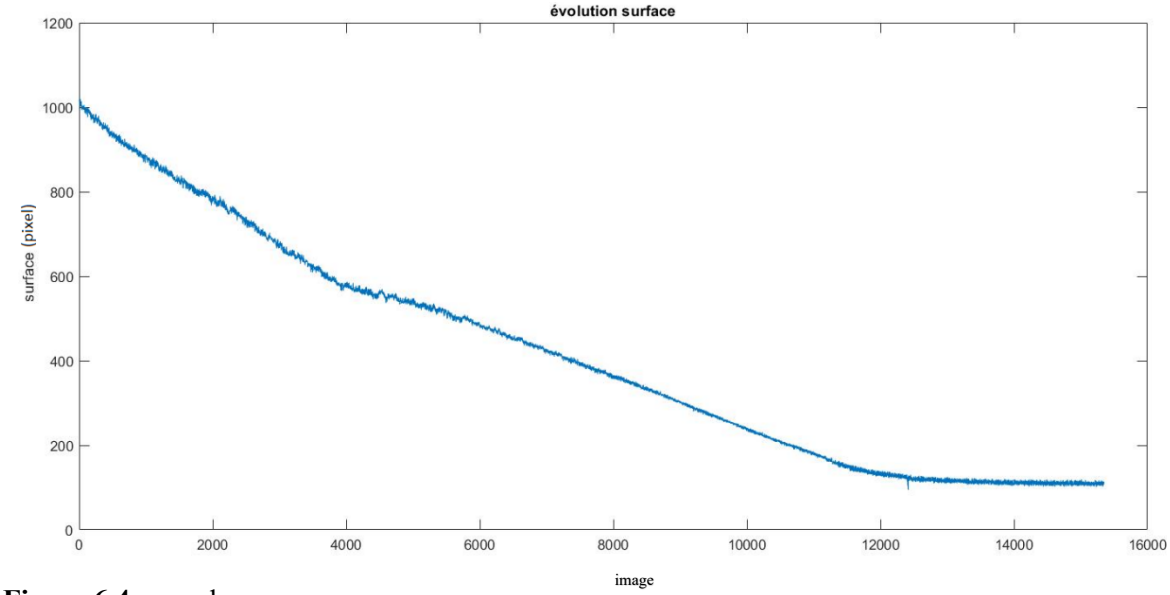

Figure 6.4: sample a

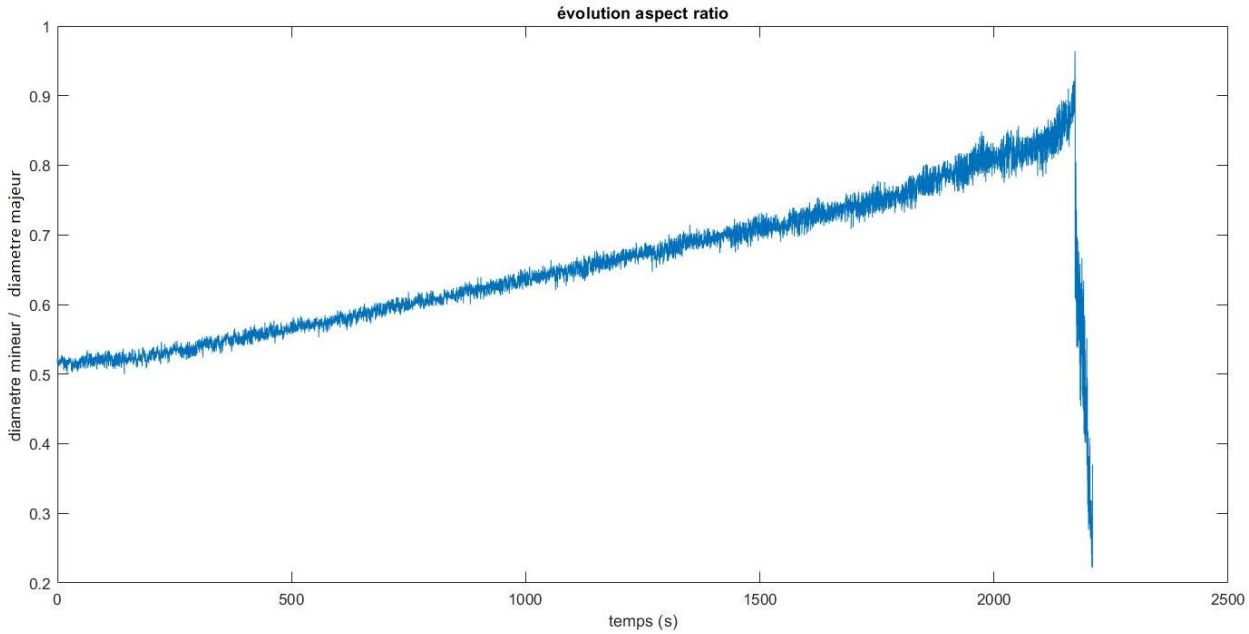

Figure 6.5: Sample b

6.2.1.2. Cold brewed – centrifuged

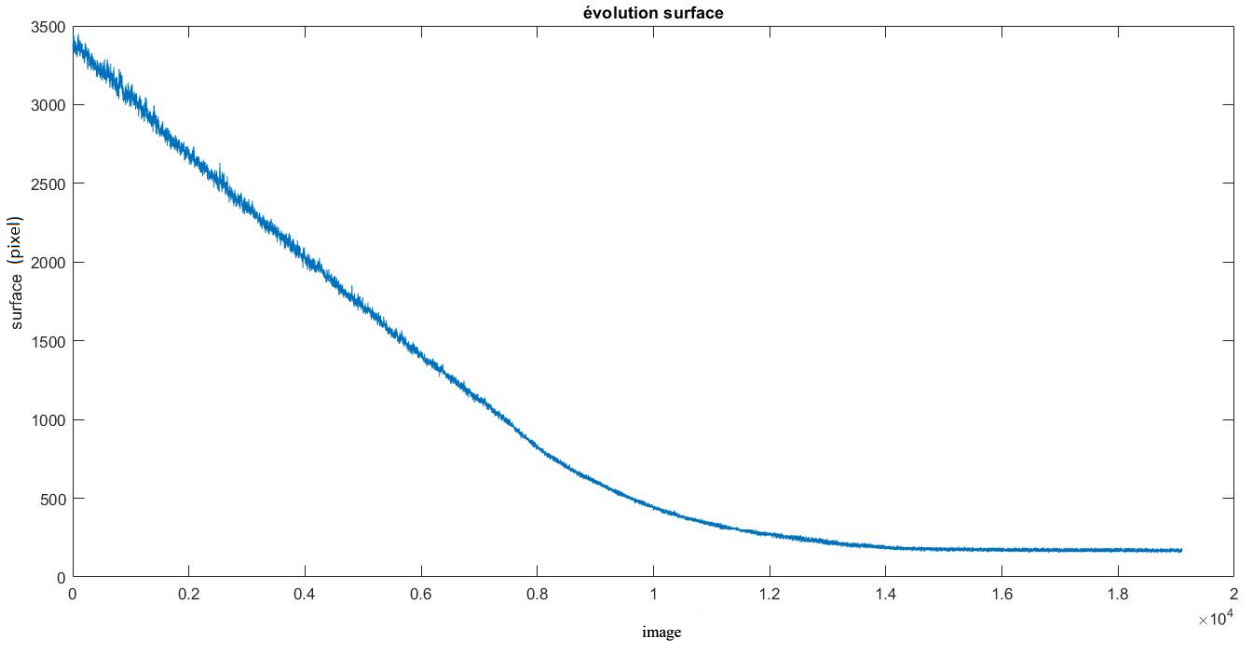

Figure 6.6: Sample c

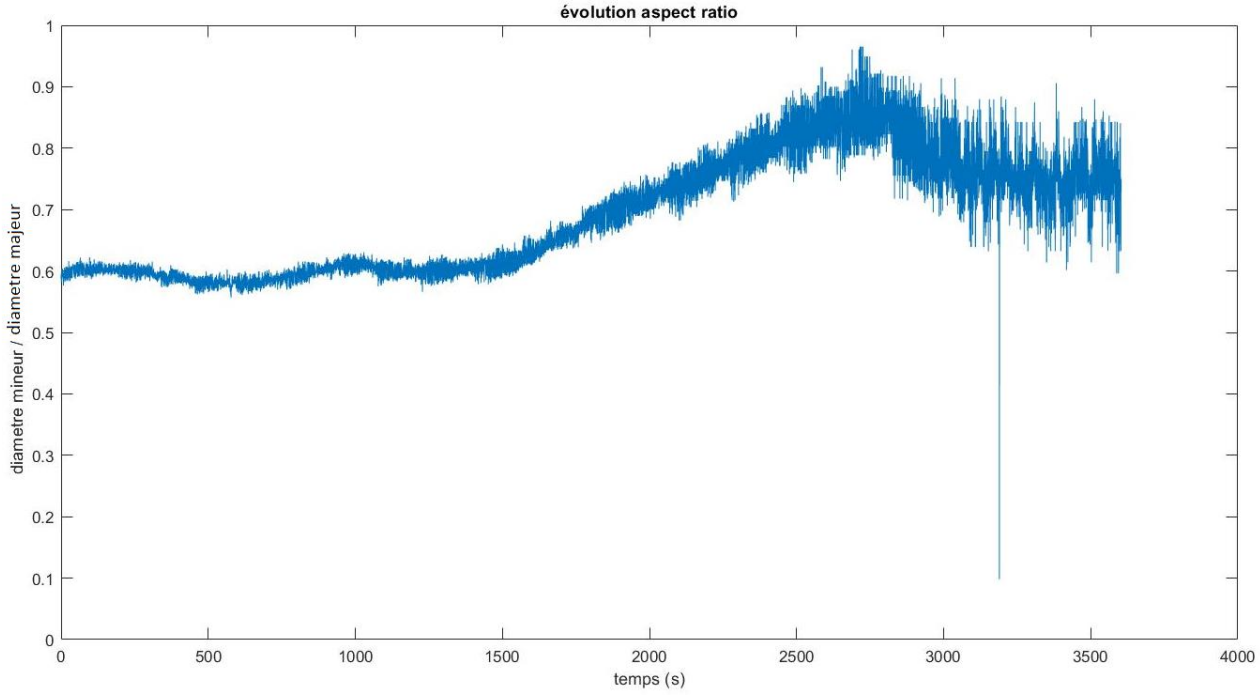

Figure 6.7 Sample b

6.2.2. Robusta coffee

6.2.2.1. Hot brewed (T_{fin}=43°C) – centrifuged

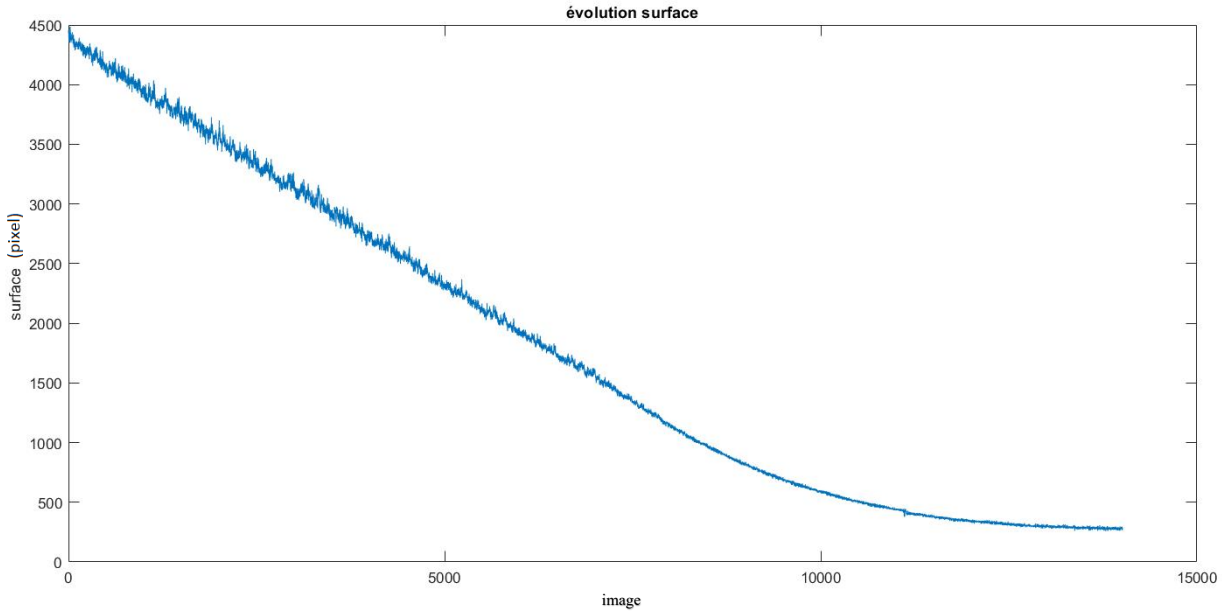

Figure 6.8: Sample a

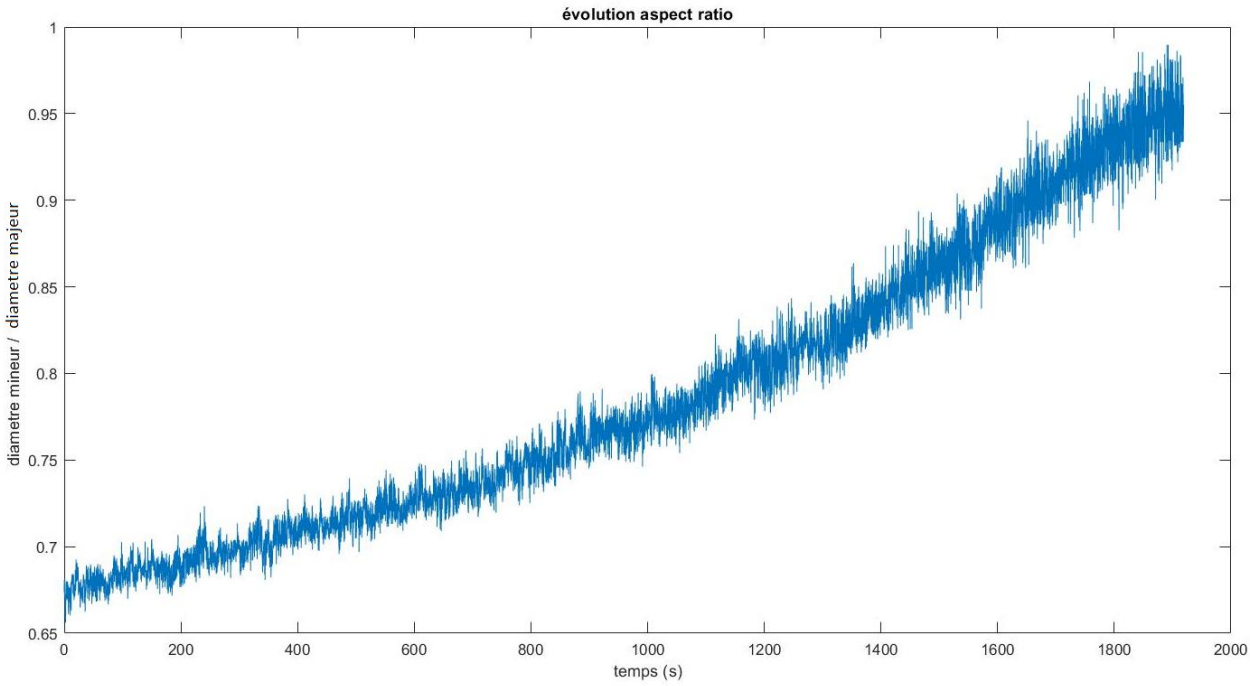

Figure 6.9: Sample b

6.2.2.2. Hot brewed – not centrifuged, let sediment naturally

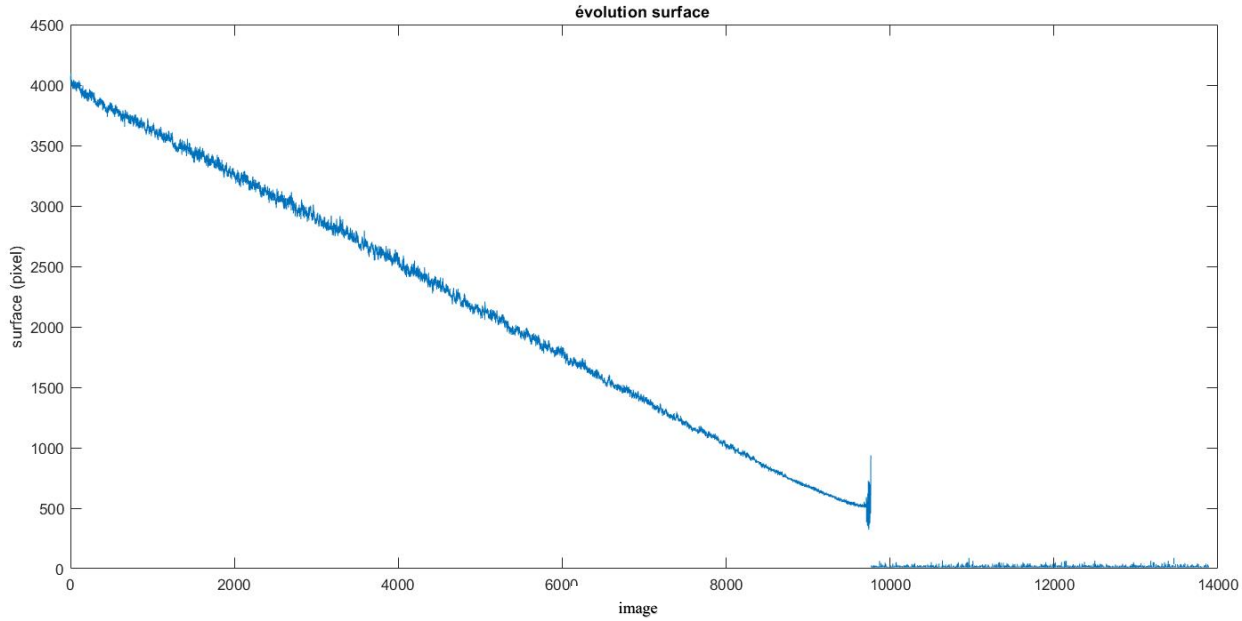

Figure 6.10: Sample a

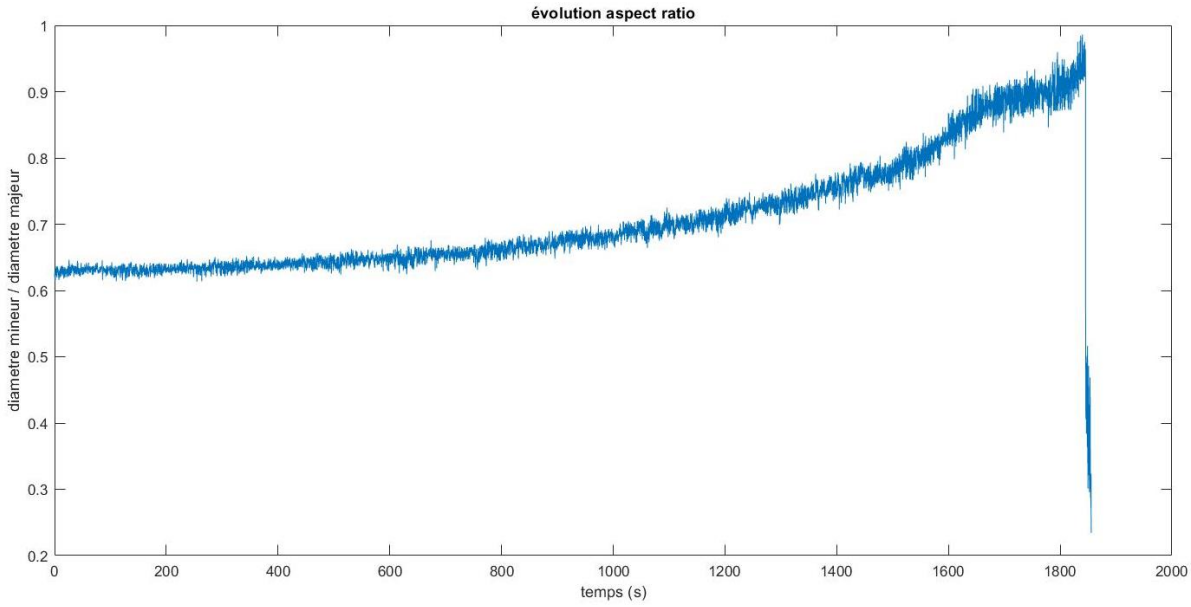

Figure 6.11: Sample a

6.2.2.3. Cold brewed – centrifuged

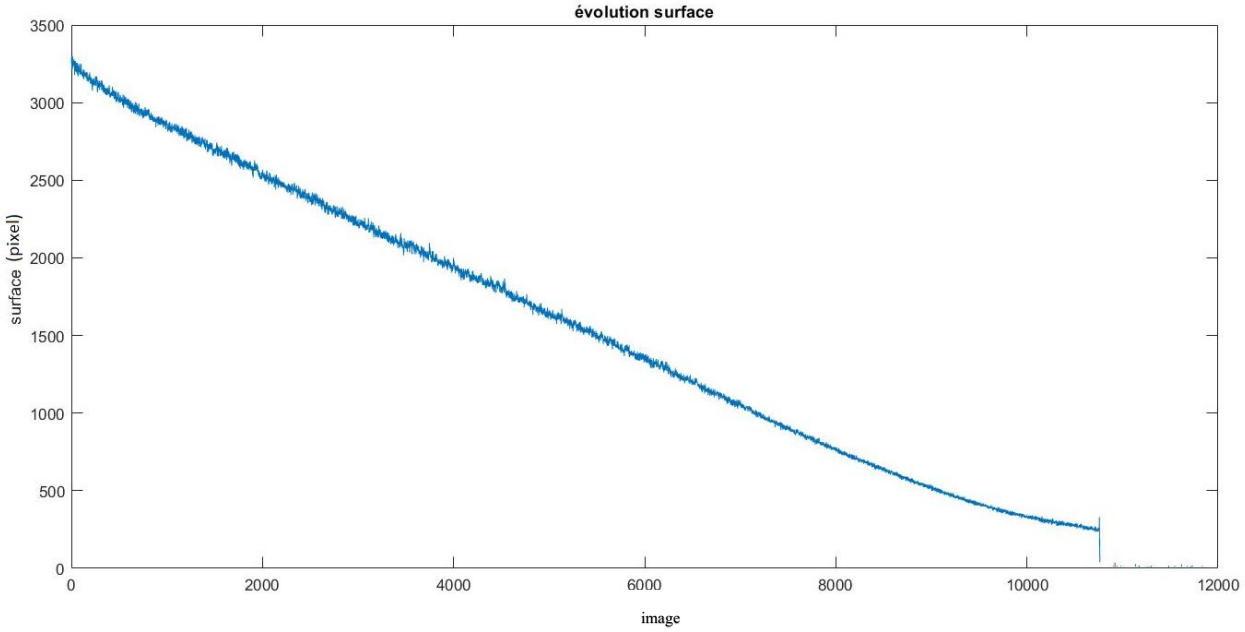

Figure 6.12: Sample b

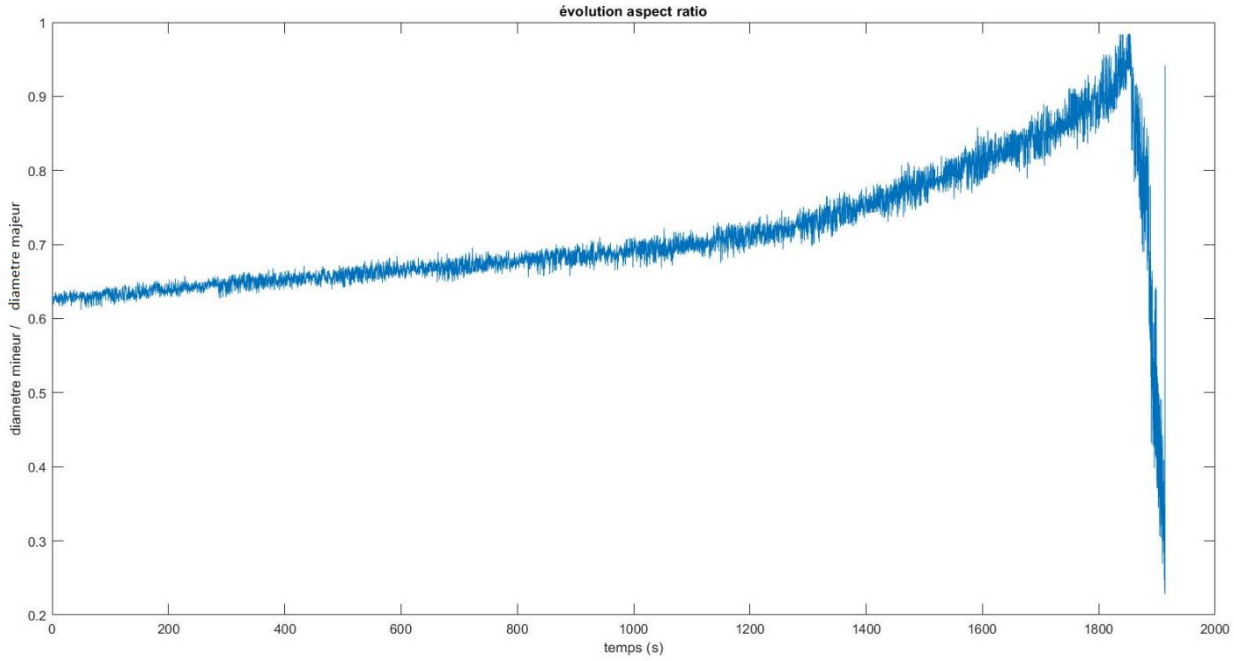

Figure 6.13: Sample a

6.2.3. Arabica-Robusta 50% mix

6.2.3.1. Hot brewed (T_{fin}=59 °C) – centrifuged

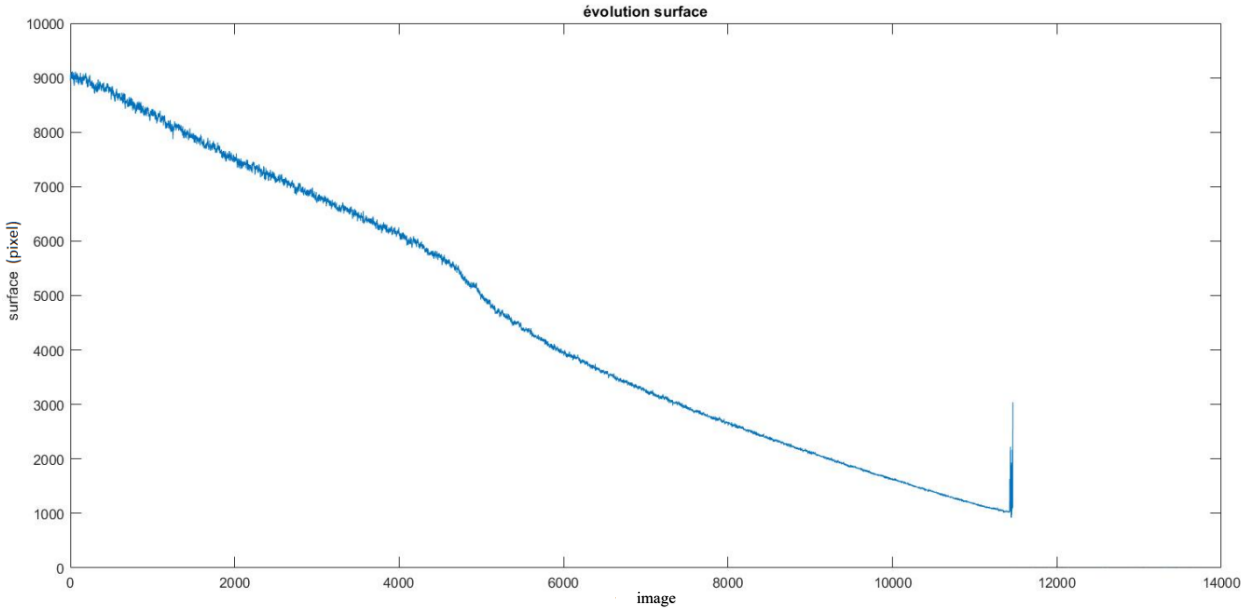

Figure 6.14: Sample c

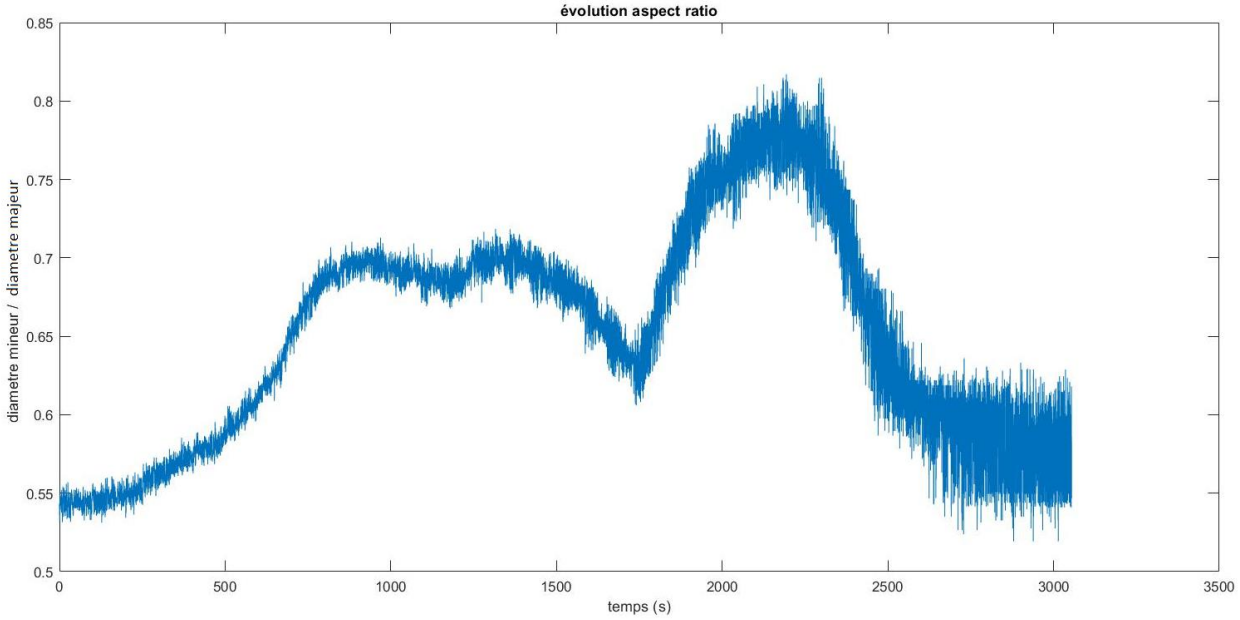

Figure 6.15: Sample c

6.2.3.2. Hot brewed (T_{fin}=65 °C) – not centrifuged, let sediment naturally

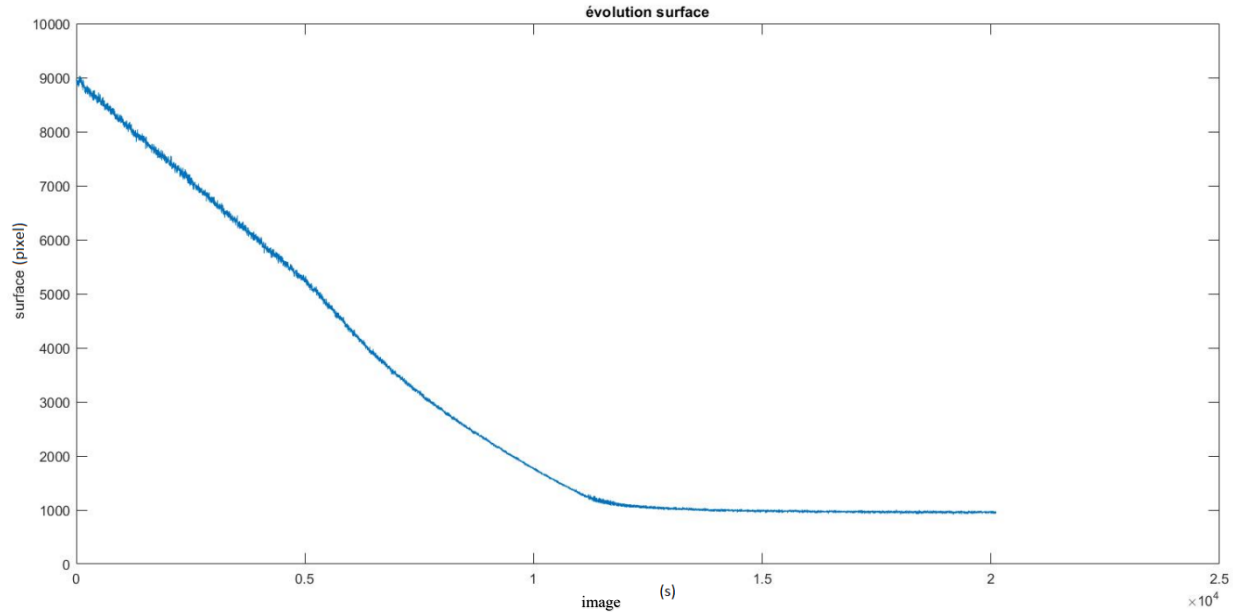

Figure 6.16: Sample a

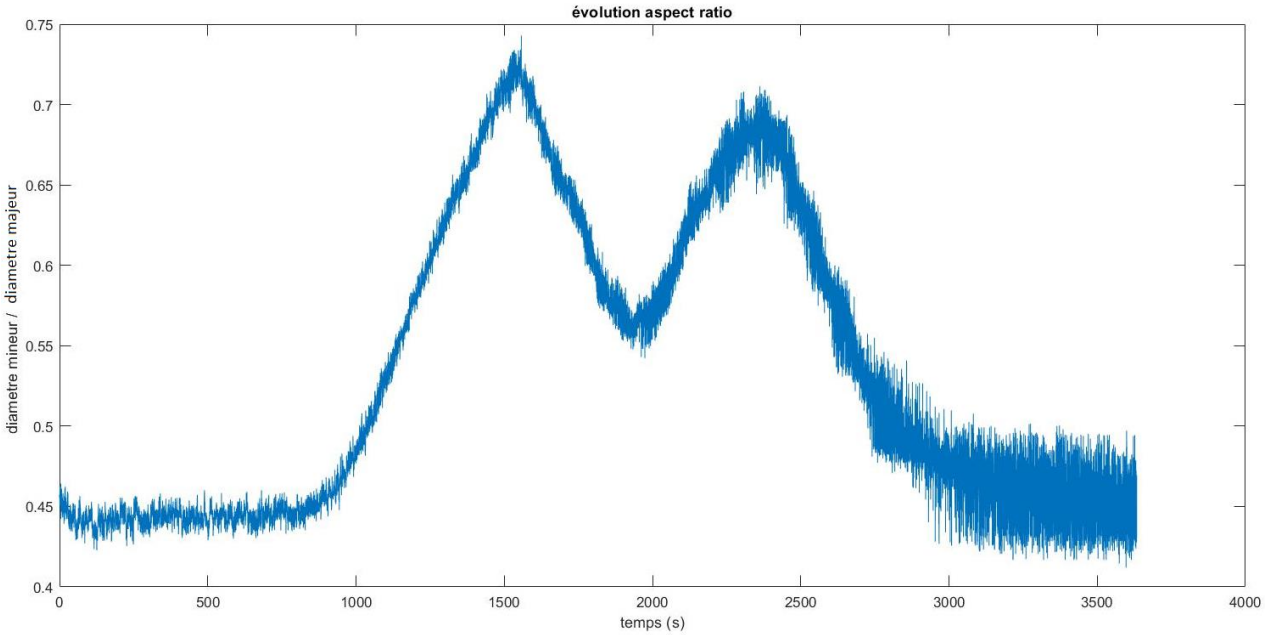

Figure 6.17: Sample c

6.2.3.3. Cold brewed - not centrifuged, let sediment naturally

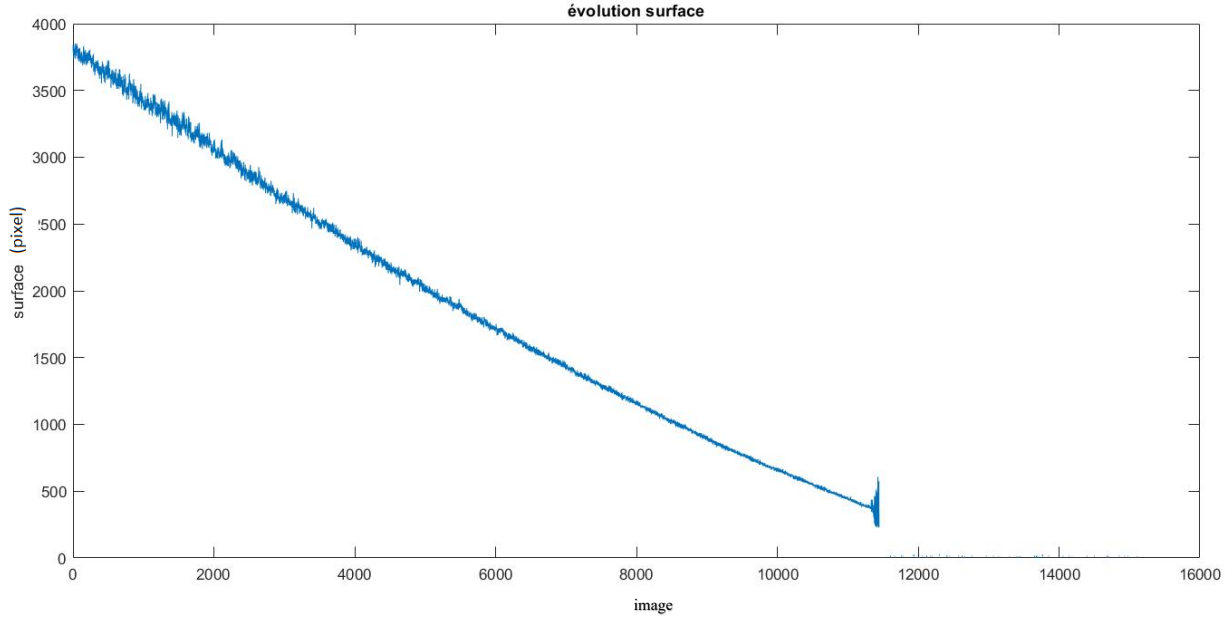

Figure 6.18: Sample c

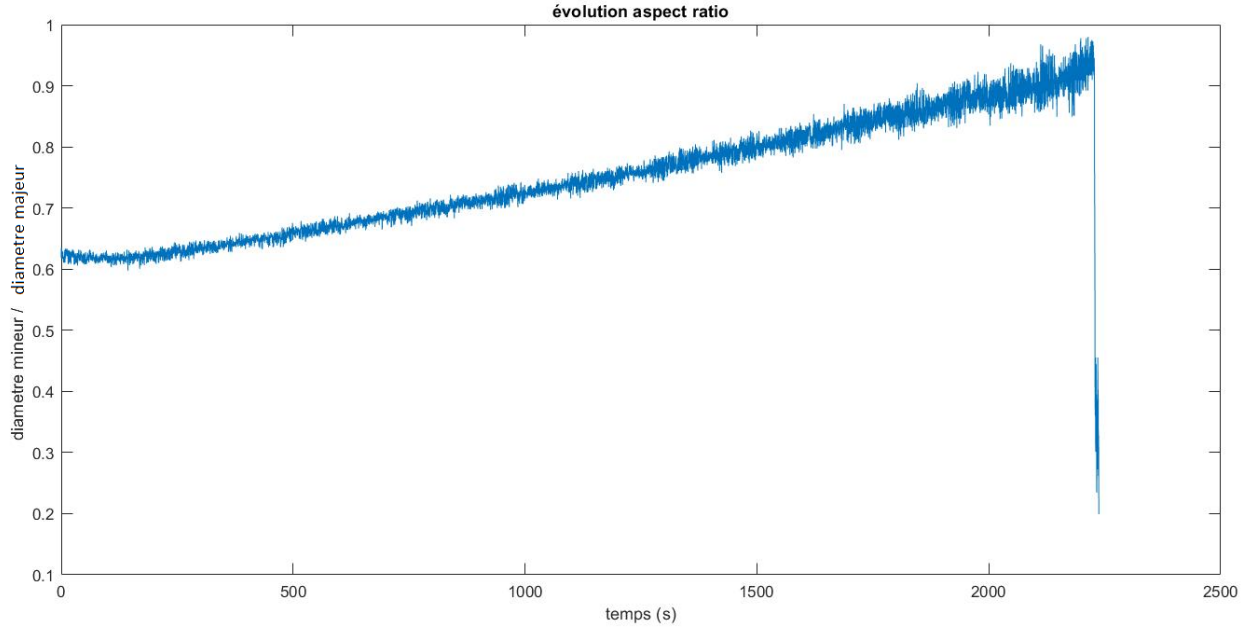

Figure 6.19: Sample a

6.2.4. Arabica-Robusta 70%-30% - hot brewed (T_{fin}=65°C) not centrifuged, let sediment naturally

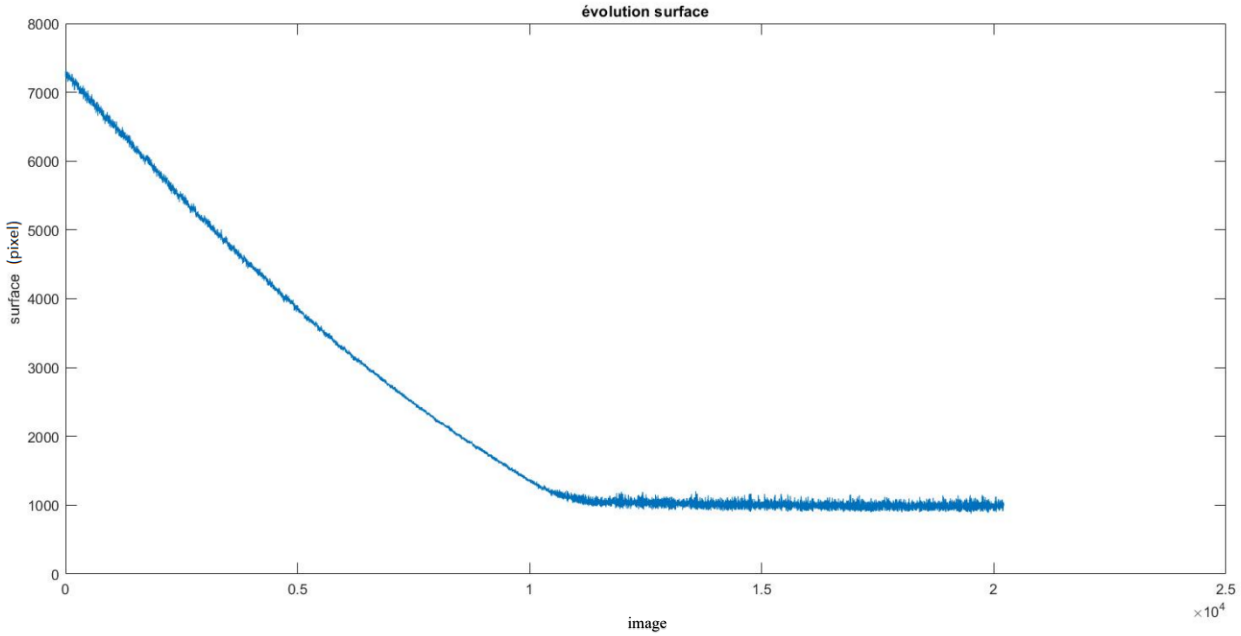

Figure 6.20: Sample a

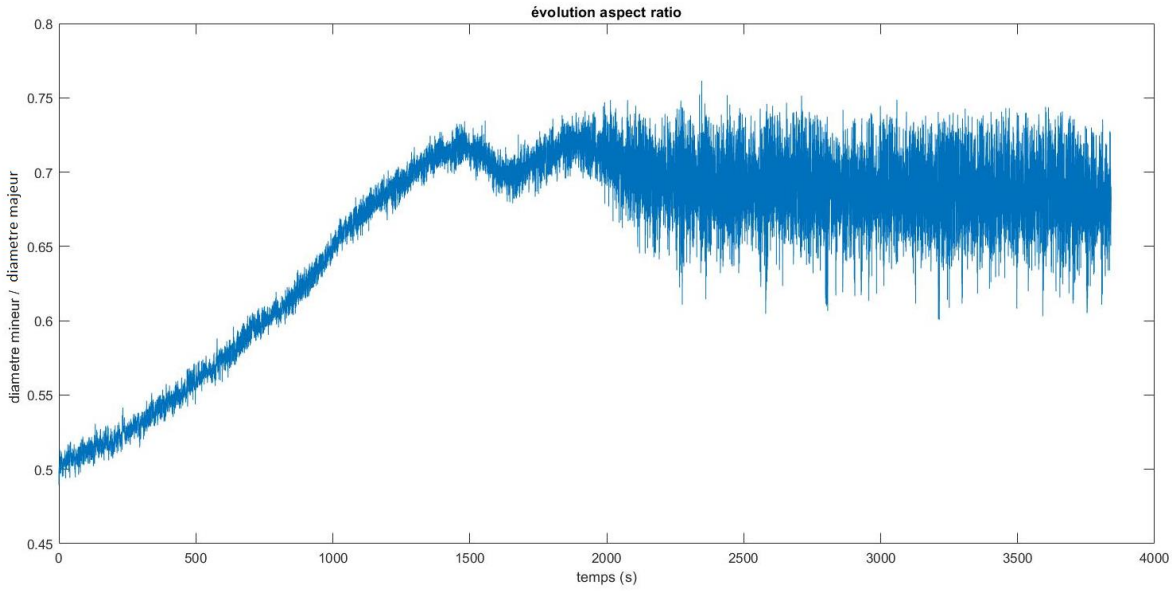

Figure .21: Sample a

6.2.5. Vergnano's *"Granaroma" moka mixture – extracted via Bialetti's Moka*

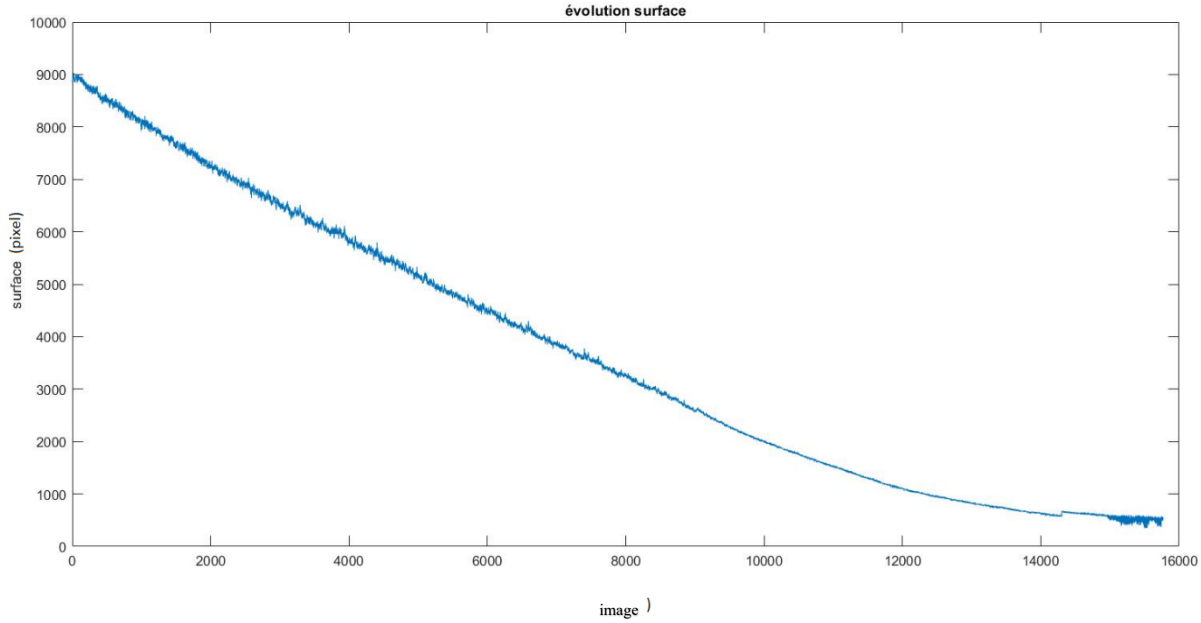

Figure 6.22: Sample a

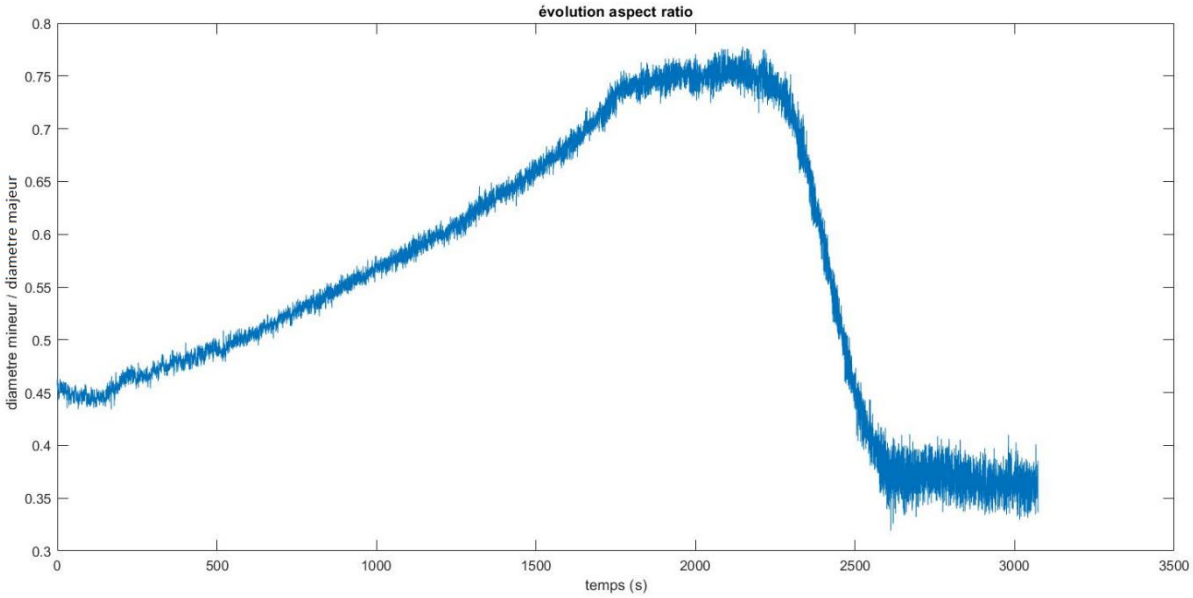

Figure 6.23: Sample b

6.3. *Whole milk*

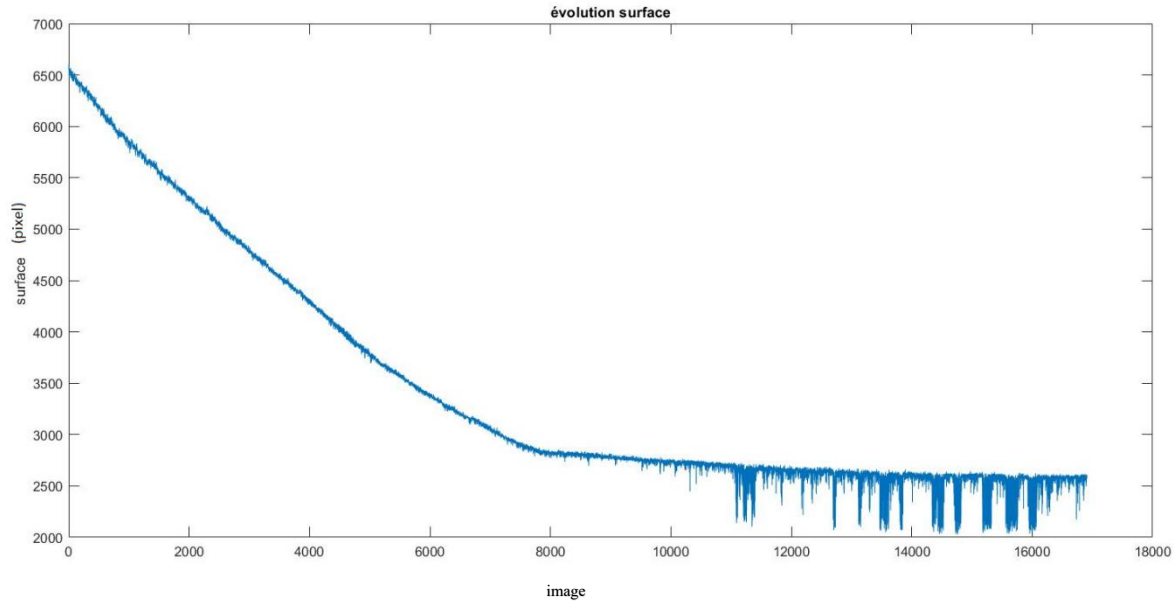

Figure 6.24: Sample a

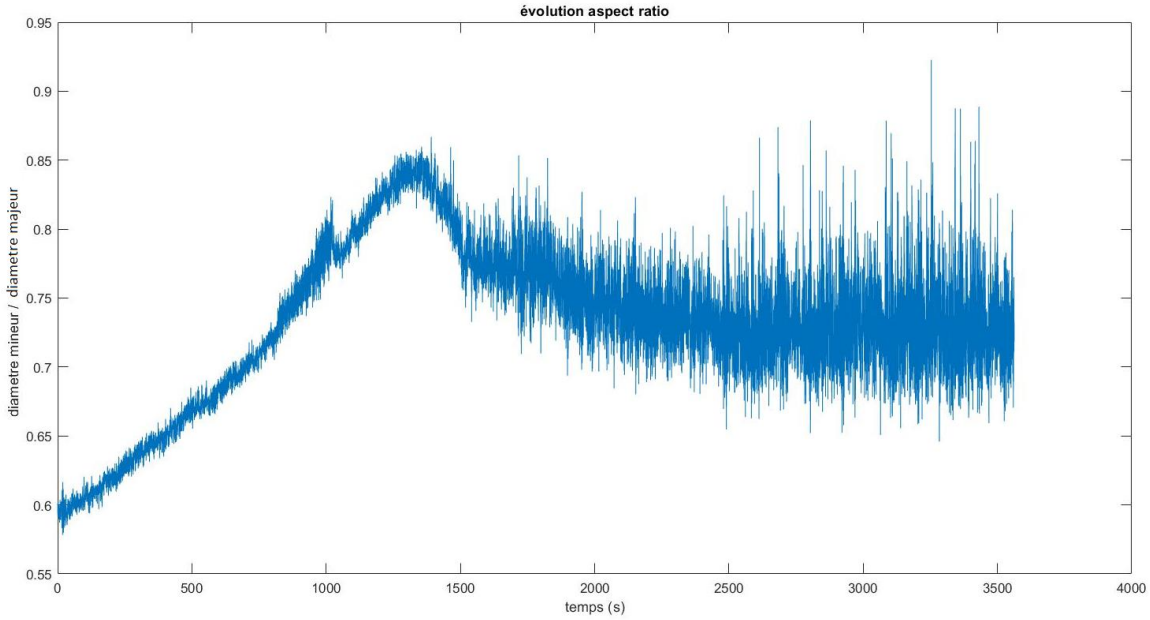

Figure 6.25: Sample b

6.4. *Recapitulative table*

Label	Sample	Massic composition (g)				N°	slope α ($m^2.s^{-1}$)	Sh	St. Deviation
		Water	Arabica	Robusta	Milk				
1	Pure water	-	-	-	-	A	-1.13E-08	8.185	-
2	100% Arabica T=55°C centrifuged	50.0000	3.6100	-	-	A	-2.06E-08	14.964	2.8035655
						B	-1.25E-08	9.110	
						C	-1.23E-08	8.927	
3	100% Robusta T=43°C centrifuged	100.0000	-	7.1810	-	A	-1.10E-08	8.011	0.24109001
						B	-1.18E-08	8.576	
						C	-1.12E-08	8.144	
4	100% Arabica T=21°C centrifuged	50.0000	3.6031	-	-	A	-1.32E-08	9.617	0.87368041
						B	-1.03E-08	7.478	
						C	-1.17E-08	8.503	
5	100% Robusta T=21°C centrifuged	50.0000	-	3.6070	-	A	-1.40E-08	10.142	0.37799695
						B	-1.44E-08	10.474	
						C	-1.31E-08	9.560	
6	mix 50/50 Robusta Arabica T=21°C non centrifuged	50.0000	1.8000	1.8000	-	A	-1.46E-08	10.630	1.00084033
						B	-1.21E-08	8.800	
						C	-1.14E-08	8.302	
7	mix 50/50 Robusta Arabica T=59°C centrifuged	50.0000	1.8000	1.8000	-	A	-7.98E-09	5.799	3.33866186
						B	-1.42E-08	10.291	
						C	-1.92E-08	13.964	
8	mix 50/50 Robusta Arabica T= 65°c non centrifuged	50.0000	1.8000	1.8000	-	A	-1.56E-08	11.321	0.39861795
						B	-1.62E-08	11.797	
						C	-1.69E-08	12.297	
9	mix 7/3 Arabica Robusta T=21°C filtered	35.7000	3.5867	1.5371	-	A	-2.05E-08	14.911	1.06750155
						B	-1.96E-08	14.280	
						C	-1.71E-08	12.398	
10	Vergnano Granaroma Bialetti's Moka					A	-2.13E-08	15.495	0.22436549
						B	-2.07E-08	15.059	
						C	-2.06E-08	14.987	
11	Whole milk				50.0000	A	-7.46E-09	5.420	0.22217746
						B	-8.07E-09	5.865	

Table 6.1

6.5. Considerations

6.5.1. The graphs

First, let us consider the graphs. I chose to show here every sample, but not every take. This to avoid useless redundancy and to focus on interesting outtakes, trying to highlight results that I found interesting.

Let us start by commenting the graphs. By an easy comparison with the sample of pure water it is clear that in the case of a non-pure liquid mixture the slope is not anymore linear. These graphs show a good concordance with the theory, as it happened at the beginning of the section. Depending by the case, the changing in the slope from the linear behaviour to the non linear can be more or less clear. In any case roughly all experiments tend to a sort of a plateau, reached after the period of transition. Exceptions are also shown and will be justified. Please notice that the speculation upon the graphs is merely qualitative. Precise interpretation could be extrapolated only after analysis of the quantitative data showed in the recapitulative table. Nonetheless is interesting to see what those graphs could show, for it is a quick and visual way to finally understand the phenomena that we discussed earlier and that are taking place.

Observe Figure 5.6. This may be the most perfect result obtained. A perfect linearity with little noise is observed just until the half of the experiment, around the image n° 8000 (we are in the order of the 1500 s). This is when the d^2 law applies, and the evaporation is not yet compromised by the formation of the crust. Then a progressive flattening occurs, followed by the plateau. This completely flat zone was not observed in the sample of pure water, simply because the absence of dissolved solids could not bring to a residual body to the evaporation of the liquid. Instead, in this case, at the end we obtain the particle of the dissolved solid now completely dry and condensed. Now, as I said, this graph represents the “perfectly theory-coherent” example of an experiment. Naturally, not all the experiences led to such results. It is the case for example of Figures 5.10, 5.14 and 5.18, where the experiments come to a premature end, with an abrupt interruption. Here we have an undesired yet typical phenomenon, that is the explosion of the droplet or its fall due to some unexpected interference. However, whether it is certainly a theoretical problem, this happened always after a relatively long period of observation, in any case sufficient to collect significative data on the first-period evaporation.

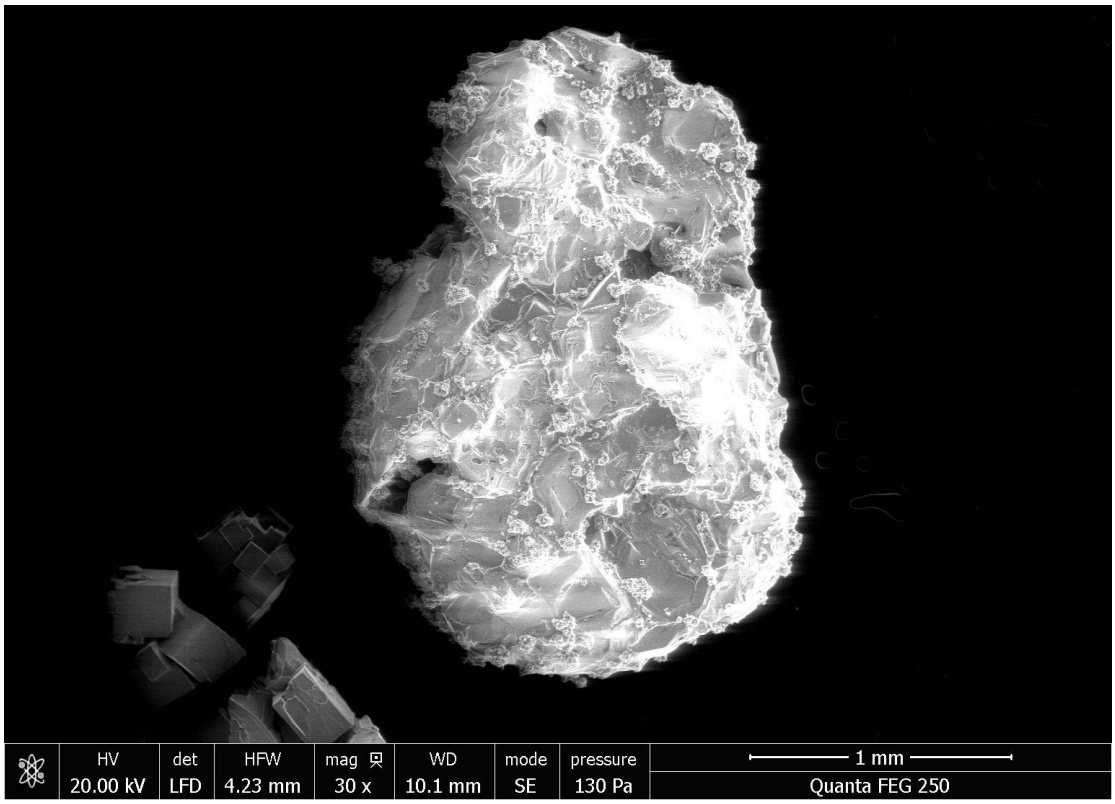

Figure 6.26: SEM-TEM microscopy image of an amorphous residue of a mixture of sucrose and sodium chloride, result from a precedent experiment. It is presumable that the residue from the evaporation of coffee and milk would not differ from this picture, that shows the irregularities of the shape, and the porousness of the surface.

Then, the graphs reporting the evolution of the aspect ratio. The theory tells us that the droplet, initially of an oblate shape, tends to get more and more spherical whilst evaporating, thus reaching a ratio of the minor and major axis equal to one. From a quick overview of the graphs, we firstly notice that there is a certain degree of noise in the line. So, before even focusing on the various shape of the curves here presented, we can state this: even if the levitating droplet is stable from a macroscopic point of view, meaning that is (normally) stable on the pressure point and segregated in a limited space, it is not stable on a smaller scale. The noise represented by the vertical peaks on the tendency line can be interpreted in different ways. The droplet can vibrate internally or be subjected to rotation. It is not possible to state exactly what are the instabilities due to whit the with the instrumentation used, because to witness the rotation it would be necessary a system able to capture images on at least two different axes. This was a sifted possibility, that unfortunately was impossible to actuate due to the exceptional emergency conditions. Details of it will be shown at the end of this work. Hypothesis can be done. Let us interpret for example some graphs. Take Fig. 5.9: the ideal behaviour is shown. But observe Fig. 5.15 and 5.17. Why does the graph shows those two humps? Maybe a rotation, maybe an anomaly in the acoustic field. Finally, for Fig. 5.21 and 5.25 the best supposition is the formation of a relatively big amorphous solid particle that rotates under the influence of the field. Again, no certain proof can be produced of this, for a microscopy picture of the solid particle would have been required, but even if the samples were correctly collected and ready for the SEM-TEM lab, time was cruel. In any case, the evolution of the aspect ratio clearly shows how the evaporation is a phenomenon intrinsically subjected to a high instability.

6.5.2. *The table*

The recapitulative table shows quantitatively the results, namely the Sherwood number. Basically, the greater the number, the higher is the mass transfer, and so the evaporation. The shows how results labelled from 1 to 6 are all around $Sh \cong 8$ that is the result obtained for the sample of pure water. This blank sample is to be taken as point of reference, to record a regular evaporation, not yet conditioned by external and heterogeneous content. From labels 6 to 9, the Sh deviates consistently, coming back to a more suitable value for the milk sample.

6.6. *Interpretation*

Now, those numbers raise issues. First, naturally, is the meaning that we have to give to them; then, the implications that could follow from a particular interpretation.

One last time, let us remember that the environment of the experiment is stagnant, meaning that no convective stream of gas was blown to enhance the evaporation or to remove the vapour enriched gas surrounding the droplet. Amongst numerous factors, this was one of main difference with respect to the other studies I encountered in my bibliography research. Again, even though this is an evaporation occurring in a virtually stagnating gas medium, the correlation of Ranz and Marshall is clearly not to be applied in this case, being the forecasted value of $Sh = 2$ far from the obtained. So, from Yarin et al we are to use the definition for the acoustic Sherwood

$$\langle \overline{Sh} \rangle = \langle \overline{h_c} \rangle \frac{2a}{D_0} = \left(\frac{45}{4\pi}\right)^{\frac{1}{2}} \frac{B}{(\omega D_0)^{\frac{1}{2}}} = K \frac{B}{(\omega D_0)^{\frac{1}{2}}} \quad (5.1)$$

as listed in Sec. 3.1.1. Still we need to define the group B that was left behind with no other label than gas particle velocity amplitude in the acoustic wave. Now, this group is actually represented by the formula

$$B = \frac{A_{0e}}{\rho_0 \, C_0} \quad (5.2)$$

where

- A_{0e} is the amplitude of the incident sound wave
- ρ_0 and C_0 are respectively the unperturbed air density and the sound velocity in air

The value of A_{0e} is to be obtained from the sound pressure level SPL. Now this is usually a measure done in real time. However, this was not the case, because the instrumentation was not available. Thanks to the work and the availability of the designer of the device, I was able to get access to the data of his experiments.

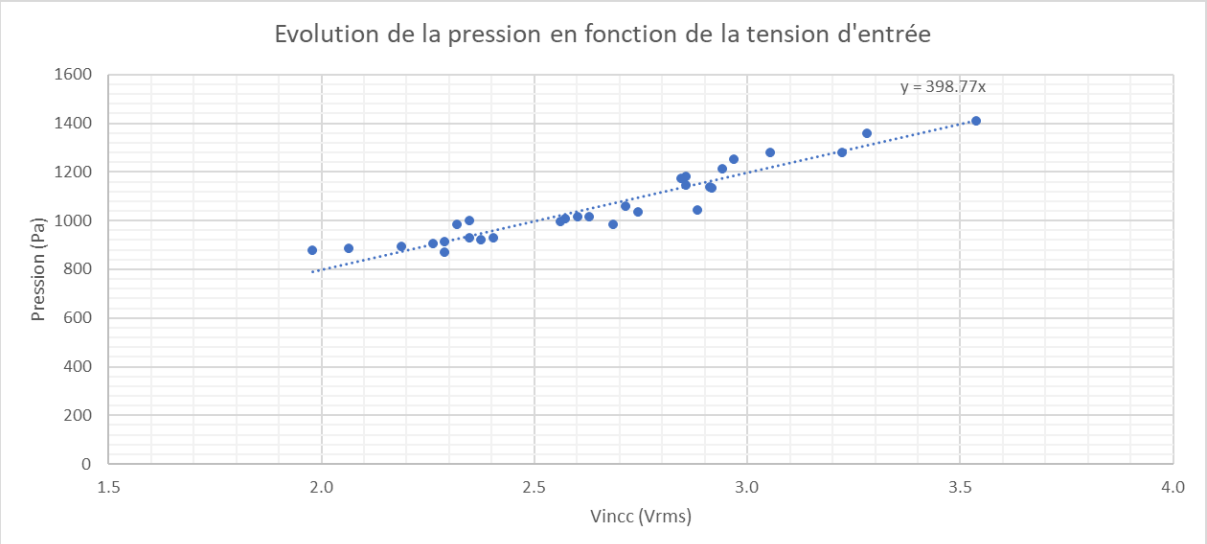

Figure 6.27 pressure vs the tension given to the device (Courtesy of M. Buot de l'Epine, PhD)

The device works at a tension of 6.35 Vrms, meaning a pressure of roughly 2500 Pa, or 161 dB. From the formula we have

$$A_{0e} = 10^{\frac{SPL-74}{20}} \quad (5.3)$$

And so, what we obtain is:

Vincc (rms)	pressure (Pa)		ro air (kg m^{-3})	Co (m s^{-1})	K	D0 (m^{2}s^{-1})
6.35	2532.1895		1.177	340	1.89	2.63E-05
SPL (dB)		Aoe			B	
162.049324		25261.9114	dyne cm-2		6.31263717	
		2526.19114	Pa			
Sh						
11.32						

Table 6.2

Clearly, a number of Sherwood distant from we obtained with the trial of pure water. In any case this out-of-a-prediction result should not be taken as truly valid; in fact we have to consider that the pressure value was extrapolated at a tension never tested before, so it could not correspond to reality. With an easy reverse calculation, I inputted the obtained Sh, and this resulted in SPL=159 to 160 dB, not so far away from the hypothesis.

We may continue now with talking of those numbers in the table above. Apart from two cases (N° 2 and 7), the standard deviation seems to be little enough. A good degree of repeatability was achieved, although always keeping in mind that the experiments were performed one after the other in a short period of time, not allowing then to the characteristics of the chamber to change significatively. Still, the main question is on the value assumed by those Sh numbers. The sample with just water, label N° 1, should present the highest value. For that one, in fact, evaporation is not affected in any case by the dissolved solids, and this is also proven by the linearity of the graph of Fig 1. Experiments performed by Yarin, Tropea et al. are reporting similar results on water samples. Yet, it is not clear why the coffee samples should show equal whether not higher values, when the change in viscosity and surface tension should inhibit the evaporation (Kim & Weon, 2018).

We therefore have to justify those results. First: the Sh of the pure water sample. Being my first attempt on the procedure and on the machine, I may have done some mistakes unintentionally. For example, with time I understood that the degree of humidity of the chamber needs time to set completely, so when the interface shows to have reach the set point, more time is required to stabilize it. Also, disposable syringes need practice to be handled perfectly. Hence: it is remarkable that the value that I obtained is not out-of-a-scale, partially in line with previous experiences, but I cannot exclude errors. Second: the Sh of the samples from N° 2 to 10. If we exclude the values that seem to be off range, (e.g. N° 2a), we appreciate, as mentioned before, a certain homogeneity amongst the three attempts of every sample. Still, we obtain values ranging from ≈ 8 to more than 15. Again, as mentioned before the value indicating the adimensional mass transfer should be lower for a liquid-solid mixture, because the evaporation would lead to phenomena of increase in viscosity and of crust formation that in fact would represent an obstacle to the evaporation itself. On the contrary, they seem sometimes to evaporate faster; no crust is interfering in the span of time analysed, being always in the firs-stage of evaporation, but this result is in any case at least curious. Third, sample of whole

milk, N° 11. Eventually we have some results that are in line with what the theory make us to expect: a Sh clearly smaller than the reference, showing interference of the fluid in the evaporation process, even before the actual formation of a crust.

7. Conclusions

Along the short period of time of less than a month, I carried out experiments trying to study the evaporation of small levitating liquid particles. Purpose of the research was to evaluate the number of Sherwood of every experience, and to use it as indicator of the mass transfer, to see if the dissolution of solids in water affects in some way the evaporation of the droplet. The focus was on the first stage of evaporation, when no actual crust formation is noticed. Experiences were performed with samples of pure water, coffee and whole milk, and the conditions of relative humidity and temperature were kept the same. The water provided the reference, and the results of all the other samples were interpreted with respect to that.

The results obtained for the milk prove that the heterogeneous nature of the fluid actually interfere on the evaporation, being the obtained Sh smaller than the one for water. On the other hand, the results on the coffee may raise some question, for a higher value of the mass transfer is obtained, therefore implying a higher evaporation rate. This result differs from previous studies, that although were carried out under different conditions.

7.1. Remarks

A number of remarks have to be made concluding this work. First of all, the most impacting factor on the development of this final project was for sure the outbreak of the Covid-19 emergency. Forecasting the closing of the university and the labs, I tried to perform the maximum number of experiments with the time that I was given. However, all those problems and interrogatives arose during the processing of the data during the lockdown, that would have required more or collateral experiments to solve, remained, eventually, unsolved.

In the end, after having mentioned all he difficulties encountered, I would like to present an idea of mine that, if applied, would have improved the procedure and probably apported different data.

During the observation process, I noticed an important flaw, that seems all previous studies have neglected. The image processing measures the evolving of the surface of the droplet; to do so, since we used a single camera, we have to approximate the suspended droplet with ad oblate spheroid. Yet, we have no certainty that that idealised shape is actually the shape taken. This is then an intrinsic limit if the capturing is always performed in one plane. It seemed strange to me that no one else thought of this problem, but it is understandable considering the high cost of the PIV camera. Imagining to place two of those, displaced at 90°, is not only cost-intensive, but even unrealizable with the setup the UTC has, because the camera, is placed outside the chamber. To overcome this problematic I took into consideration to use a game of mirrors that would have been both cheap and easy to place.

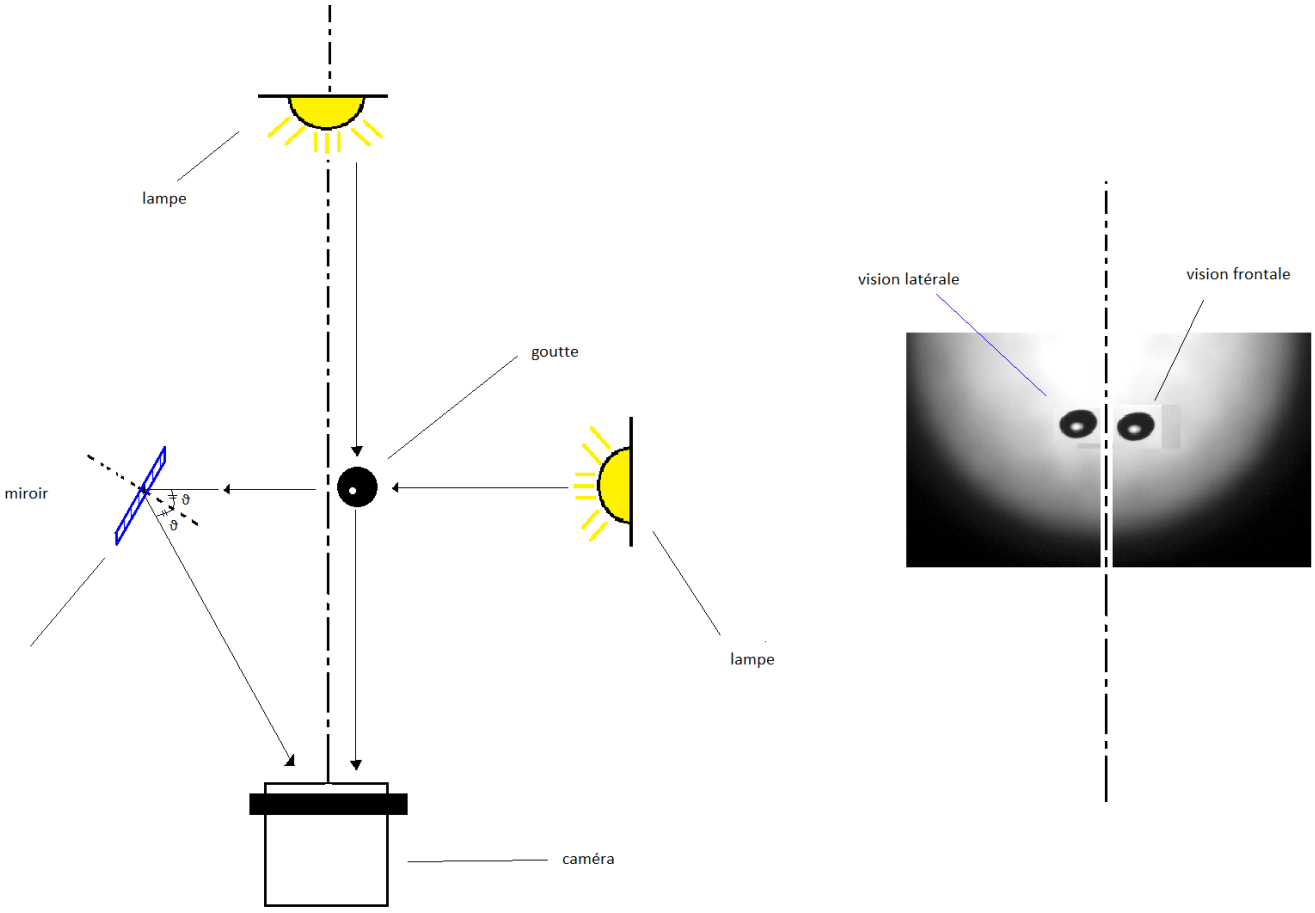

Figure 7.1 on the left, a sketch of a possible configuration for the image capturing of more orthogonal planes at the same time. On the right, what would have appeared on the camera view.

The idea was discussed with my tutor and other researchers from the department of optics and informatics. This was found realizable; quick tests that I performed to test the feasibility shown that the mirrors would not have introduced interferences, and the levitation was still possible. The frontal image of the droplet would have been captured directly by the camera, and the lateral view would have been projected from the mirror. From that point, a new Matlab code would have been developed, able to process simultaneously the two images, and thereby to evaluate possible deviation from the ideality on the shape of the droplet. Once again, the project remained a project unfortunately.

8. Appendix

8.1. Matlab code

8.1.1. Image interpretation

```
      clear all
close all
clc
```

Determination of the ROI (region of interest) on first image

```
      img = im2bw(imread("Image_000000.tif"));
% Find connected components
% Largest component is the one with bigest Area in CC.PielIdxList
CC = bwconncomp(img);
props = regionprops(CC,'BoundingBox','Area');
[sortedAreas,indexes]=sort(vertcat(props.Area),'descend');
props = props(indexes(1));
bb = props(1).BoundingBox;
% extend bottom limit by 10%
bb(4) = floor(bb(4)*1.1);
```

Determine the drop position on successive images

```
      range = 1:20320;
volume = zeros(length(range),1);
S_proje=zeros(length(range),1);
draw = true;
A=readtable('Imagetime.csv');
% replace for by parfor if parallel execution is desired
% parfor i = 1:length(range)
shg
tic
for i = 1:length(range)
    limitsX = floor([bb(2)+floor(bb(4)/2), bb(2)+bb(4)]);
    limitsY = floor([bb(1), bb(1)+bb(3)]);
    % Read ROI of image
    img = imread(sprintf("Image_%06d.tif",range(i)),'PixelRegion',{limitsX,limitsY});
    % Convert to black and white and invert
    imgbw = 1-imbinarize(img);
    % Fill holes and find connected components of inverted image
    CC = bwconncomp(imfill(imgbw,'holes'));
    % get properties of connected components
    props = regionprops(CC,'MinorAxisLength','MajorAxisLength',...
    'Centroid','Orientation','Area');
    if length(props) > 1
        % Sort CC by area
        [sortedAreas,indexes]=sort(vertcat(props.Area),'descend');
        % Largest CC is the large bottom white zone
        % Second CC is the drop
        % others are just dust in the wind...
        props = props(indexes(2));
        volume(i) = 4/3*pi*props.MajorAxisLength^2*props.MinorAxisLength;
        e=(sqrt((props.MajorAxisLength/2)^2-
(props.MinorAxisLength/2)^2)/(props.MajorAxisLength/2)^2);
        S(i) = 2*pi*(props.MajorAxisLength/2)^2+(pi*(props.MinorAxisLength/2)^2/e)*log((1+e)/(1-
e));
        D(i)=props.MajorAxisLength;
        d(i)=props.MinorAxisLength;
        S_proje(i)=D(i)/2*d(i)/2*pi;
        if draw
            imshow(img)
            plotEllipse(props)
            drawnow
        end
    end
```

```
end
toc

i=1;
for i = 1:length(range)
    rap_S_star(i)=S(i)/S(1);
end

i=1;
t=1;
for i = 1:length(range)
    if rap_S_star(i)>0;
        t=t+1;
    else
        break
    end
end
i=1;

aspect_ratio=d./D;
aspect_ratio=aspect_ratio.';
S=S.';

B=A(1:t-1,2);
b=table2array(B);
rapS=rap_S_star(1:t-1);
rapS1=rapS.'

format long
plot(volume)
title('évolution volume')
ylabel('volume')
pause
plot(S)
ylabel('surface')
title('évolution surface')
pause
p=polyfit(b,rapS1,1)

% plot(b,rapS1,'.')
% xlabel('temps (s)')
% ylabel('A/A0')
% hold on
% y= p(1) * b + p(2);
% plot(b,y,'r')
% txt=['y=' num2str(p(1)) '*x+' num2str(p(2))];
% text(1000,0.9,txt)
% pause

plot(b,aspect_ratio(1:t-1))
title('évolution aspect ratio')
xlabel('temps (s)')
ylabel('diametre mineur / diamï¿½tre majeur')
pause
```

utilitary function

```
      function plotEllipse(p)
    a = p.MajorAxisLength/2;
    b = p.MinorAxisLength/2;
    Xc = p.Centroid(1);
    Yc = p.Centroid(2);
    phi = deg2rad(-p.Orientation);
    t = linspace(0,2*pi,128);
    x = Xc + a*cos(t)*cos(phi) - b*sin(t)*sin(phi);
    y = Yc + a*cos(t)*sin(phi) + b*sin(t)*cos(phi);
    hold on
    plot(x,y,'r','Linewidth',2)
    hold off
end
```

8.1.2. Spatial calibration

(https://it.mathworks.com/matlabcentral/answers/261513-how-to-display-an-image-in-mm, s.d.)

```
      9.    function spatial_calibration_demo()
% This demo allows you to spatially calibrate your image and then make distance or area
measurements.

global originalImage;
% Check that user has the Image Processing Toolbox installed.
clc;    % Clear the command window.
close all;  % Close all figures (except those of imtool.)
workspace;  % Make sure the workspace panel is showing.
format long g;
format compact;
fontSize = 20;

hasIPT = license('test', 'image_toolbox');
if ~hasIPT
      % User does not have the toolbox installed.
      message = sprintf('Sorry, but you do not seem to have the Image Processing Toolbox.\nDo you
want to try to continue anyway?');
      reply = questdlg(message, 'Toolbox missing', 'Yes', 'No', 'Yes');
      if strcmpi(reply, 'No')
            % User said No, so exit.
            return;
      end
end

% Read in a standard MATLAB gray scale demo image.
folder = fullfile(matlabroot, '\toolbox\images\imdemos');
button = menu('Use which demo image?', 'CameraMan', 'Moon', 'Eight', 'Coins', 'Peppers', 'My
own...', 'Exit');
switch button
      case 1
            baseFileName = 'cameraman.tif';
      case 2
```

```
            baseFileName = 'moon.tif';
      case 3
            baseFileName = 'eight.tif';
      case 4
            baseFileName = 'coins.png';
      case 5
            baseFileName = 'peppers.png';
      case 6
            % Get the name of the file that the user wants to use.
            defaultFileName = fullfile(cd, '*.*');
            [baseFileName, folder] = uigetfile(defaultFileName, 'Select an image file');
            if baseFileName == 0
                  % User clicked the Cancel button.
                  return;
            end
      case 7
            return;
end

% Get the full filename, with path prepended.
fullFileName = fullfile(folder, baseFileName);
% Check if file exists.
if ~exist(fullFileName, 'file')
      % File doesn't exist -- didn't find it there.  Check the search path for it.
      fullFileName = baseFileName; % No path this time.
      if ~exist(fullFileName, 'file')
            % Still didn't find it.  Alert user.
            errorMessage = sprintf('Error: %s does not exist in the search path folders.',
fullFileName);
            uiwait(warndlg(errorMessage));
            return;
      end
end
% Read in the chosen standard MATLAB demo image.
originalImage = imread(fullFileName);
% Get the dimensions of the image.
% numberOfColorBands should be = 1.
[rows, columns, numberOfColorBands] = size(originalImage);
% Display the original gray scale image.
figureHandle = figure;
subplot(1,2, 1);
imshow(originalImage, []);
axis on;
title('Original Grayscale Image', 'FontSize', fontSize);
% Enlarge figure to full screen.
set(gcf, 'units','normalized','outerposition',[0 0 1 1]);
% Give a name to the title bar.
set(gcf,'name','Demo by ImageAnalyst','numbertitle','off')

message = sprintf('First you will be doing spatial calibration.');
reply = questdlg(message, 'Calibrate spatially', 'OK', 'Cancel', 'OK');
if strcmpi(reply, 'Cancel')
      % User said Cancel, so exit.
      return;
end
button = 1; % Allow it to enter loop.

while button ~= 4
```

```
	if button > 1
		% Let them choose the task, once they have calibrated.
		button = menu('Select a task', 'Calibrate', 'Measure Distance', 'Measure Area', 'Exit
Demo');
	end
	switch button
		case 1
			success = Calibrate();
			% Keep trying if they didn't click properly.
			while ~success
				success = Calibrate();
			end
			% If they get to here, they clicked properly
			% Change to something else so it will ask them
			% for the task on the next time through the loop.
			button = 99;
		case 2
			DrawLine();
		case 3
			DrawArea();
		otherwise
			close(figureHandle);
			break;
	end
end

end

%====================================================================
function success = Calibrate()
global lastDrawnHandle;
global calibration;
try
	success = false;
	instructions = sprintf('Left click to anchor first endpoint of line.\nRight-click or double-
left-click to anchor second endpoint of line.\n\nAfter that I will ask for the real-world distance
of the line.');
	title(instructions);
	msgboxw(instructions);

	[cx, cy, rgbValues, xi,yi] = improfile(1000);
	% rgbValues is 1000x1x3.  Call Squeeze to get rid of the singleton dimension and make it
1000x3.
	rgbValues = squeeze(rgbValues);
	distanceInPixels = sqrt( (xi(2)-xi(1)).^2 + (yi(2)-yi(1)).^2);
	if length(xi) < 2
		return;
	end
	% Plot the line.
	hold on;
	lastDrawnHandle = plot(xi, yi, 'y-', 'LineWidth', 2);

	% Ask the user for the real-world distance.
	userPrompt = {'Enter real world units (e.g. microns):','Enter distance in those units:'};
	dialogTitle = 'Specify calibration information';
	numberOfLines = 1;
	def = {'microns', '500'};
	answer = inputdlg(userPrompt, dialogTitle, numberOfLines, def);
```

```
	if isempty(answer)
		return;
	end
	calibration.units = answer{1};
	calibration.distanceInPixels = distanceInPixels;
	calibration.distanceInUnits = str2double(answer{2});
	calibration.distancePerPixel = calibration.distanceInUnits / distanceInPixels;
	success = true;


	message = sprintf('The distance you drew is %.2f pixels = %f %s.\nThe number of %s per pixel
is %f.\nThe number of pixels per %s is %f',...
		distanceInPixels, calibration.distanceInUnits, calibration.units, ...
		calibration.units, calibration.distancePerPixel, ...
		calibration.units, 1/calibration.distancePerPixel);
    dist=1/calibration.distancePerPixel

	uiwait(msgbox(message));
catch ME
	errorMessage = sprintf('Error in function Calibrate().\nDid you first left click and then
right click?\n\nError Message:\n%s', ME.message);
	fprintf(1, '%s\n', errorMessage);
	WarnUser(errorMessage);
end

return;	% from Calibrate()
end

%======================================================================
% --- Executes on button press in DrawLine.
function success = DrawLine()
try
	global lastDrawnHandle;
	global calibration;
	fontSize = 14;

	instructions = sprintf('Draw a line.\nFirst, left-click to anchor first endpoint of
line.\nRight-click or double-left-click to anchor second endpoint of line.\n\nAfter that I will ask
for the real-world distance of the line.');
	title(instructions);
	msgboxw(instructions);
	subplot(1,2, 1); % Switch to image axes.
	[cx,cy, rgbValues, xi,yi] = improfile(1000);
	% Get the profile again but spaced at the number of pixels instead of 1000 samples.
	hImage = findobj(gca,'Type','image');
	theImage = get(hImage, 'CData');
	lineLength = round(sqrt((xi(1)-xi(2))^2 + (yi(1)-yi(2))^2))
	[cx,cy, rgbValues] = improfile(theImage, xi, yi, lineLength);

	% rgbValues is 1000x1x3.  Call Squeeze to get rid of the singleton dimension and make it
1000x3.
	rgbValues = squeeze(rgbValues);
	distanceInPixels = sqrt( (xi(2)-xi(1)).^2 + (yi(2)-yi(1)).^2);
	distanceInRealUnits = distanceInPixels * calibration.distancePerPixel;

	if length(xi) < 2
		return;
	end
```

```
	% Plot the line.
	hold on;
	lastDrawnHandle = plot(xi, yi, 'y-', 'LineWidth', 2);

	% Plot profiles along the line of the red, green, and blue components.
	subplot(1,2,2);
	[rows, columns] = size(rgbValues);
	if columns == 3
		% It's an RGB image.
		plot(rgbValues(:, 1), 'r-', 'LineWidth', 2);
		hold on;
		plot(rgbValues(:, 2), 'g-', 'LineWidth', 2);
		plot(rgbValues(:, 3), 'b-', 'LineWidth', 2);
		title('Red, Green, and Blue Profiles along the line you just drew.', 'FontSize', 14);
	else
		% It's a gray scale image.
		plot(rgbValues, 'k-', 'LineWidth', 2);
	end
	xlabel('X', 'FontSize', fontSize);
	ylabel('Gray Level', 'FontSize', fontSize);
	title('Intensity Profile', 'FontSize', fontSize);
	grid on;

	% Inform use via a dialog box.
	txtInfo = sprintf('Distance = %.1f %s, which = %.1f pixels.', ...
		distanceInRealUnits, calibration.units, distanceInPixels);
	msgboxw(txtInfo);
	% Print the values out to the command window.
	fprintf(1, '%\n', txtInfo);

catch ME
	errorMessage = sprintf('Error in function DrawLine().\n\nError Message:\n%s', ME.message);
	fprintf(1, '%s\n', errorMessage);
	WarnUser(errorMessage);
end
end  % from DrawLine()

%====================================================================
function DrawArea()
global originalImage;
global lastDrawnHandle;
global calibration;
try
	txtInfo = sprintf('Left click to anchor vertices.\nDouble left click to anchor final point of
polygon.');
	title(txtInfo);
	msgboxw(txtInfo);

	% Get size information.
	[rows, columns, numberOfColorBands] = size(originalImage);

	% Get a gray scale version.
	if numberOfColorBands > 1
		grayImage = rgb2gray(originalImage);
	else
		grayImage = originalImage;
	end
```

```
      subplot(1,2, 1); % Switch to image axes.
      % Ask user to draw a polygon.
      [maskImage, xi, yi] = roipolyold();

      % Draw the polygon over the image on the main screen.
      hold on;
      lastDrawnHandle = plot(xi, yi, 'r-', 'LineWidth', 2);
      numberOfPixels = sum(maskImage(:));
      area = numberOfPixels * calibration.distancePerPixel^2;

      % Get the mean gray level of the gray scale image.
      mean_GL = mean(grayImage(maskImage)); % Of the gray scale version.

      % Print the area values out to the command window.
      txtInfo = sprintf('Area = %8.1f square %s.\nMean gray level = %.2f.', ...
            area, calibration.units, mean_GL);
      fprintf(1,'%s\n', txtInfo);
      title(txtInfo, 'FontSize', 14);

      % Done with measurement of area.
      % Now, just for fun, get the mean value and display the histogram.
      if numberOfColorBands >= 3
            % It's a color image.  Get the mean RGB Values.
            redPlane = double(originalImage(:, :, 1));
            greenPlane = double(originalImage(:, :, 2));
            bluePlane = double(originalImage(:, :, 3));
            mean_RGB_GL(1) = mean(redPlane(maskImage));
            mean_RGB_GL(2) = mean(greenPlane(maskImage));
            mean_RGB_GL(3) = mean(bluePlane(maskImage));
            fprintf('%s\nRed mean = %.2f\nGreen mean = %.2f\nBlue mean = %.2f', ...
                  txtInfo, mean_RGB_GL(1), mean_RGB_GL(2), mean_RGB_GL(3));
      end

      % Just for fun, let's get its histogram within the masked region.
      [pixelCount, grayLevels] = imhist(grayImage(maskImage));
      subplot(1,2, 2); % Switch to plot axes.
      cla;
      bar(pixelCount);
      grid on;
      caption = sprintf('Histogram within area.    Mean gray level = %.2f', mean_GL);
      title(caption, 'FontSize', 14);
      xlim([0 grayLevels(end)]); % Scale x axis manually.
      % Show the mean as a vertical red bar on the histogram.
      hold on;
      maxYValue = ylim;
      line([mean_GL, mean_GL], [0 maxYValue(2)], 'Color', 'r', 'linewidth', 2);
catch ME
      errorMessage = sprintf('Error in function DrawArea().\n\nError Message:\n%s', ME.message);
      fprintf(1, '%s\n', errorMessage);
      WarnUser(errorMessage);
end

end % od DrawArea()

%=====================================================================
function msgboxw(message)
      uiwait(msgbox(message));
end
```

```
%=========================================================================
function WarnUser(message)
      uiwait(msgbox(message));
end
```

9. Special thanks

I would like to thank all the IMID department of the UTC for the kindness they used to me, particularly Prof. M. Saleh Khashayar, who was a tutor, a mentor, a brilliant professor, and believed in me for more than this project.

Thanks to Prof. Stefania Specchia for all the help, not only strictly related to this project, but also to all the collateral details needed to fulfil my Erasmus request, my departure and my arrival.

Thank you, all of you, from the deep of my heart to let me live the most wonderful experience of my life so far.

10. Abbreviation and Symbols

- CCD charged couple device
- SDD Single Droplet Drying technique
- SPL Sound Pressure Level
- λ wavelength of the sound wave
- p_1 first order perturbation pressure field
- u_1 first order perturbation velocity field
- ρ_1 first order perturbation density field
- $\mathbf{F_{rad}}$ acoustic radiation force
- ρ_p sphere density [g cm^{-3}]
- c_p speed of sound in the sphere [m s^{-1}]
- p_0 pressure amplitude
- ω the angular frequency of the wave
- $$k = \frac{\omega}{c_0}$$
- a radius of the droplet [m]
- α_l thermal diffusivity [m^2 s^{-1}]
- τ_1 characteristic heat transfer time [s]
- τ_2 typical lifetime of an acoustically levitated droplet [s]
- T temperature inside the droplet [°C]
- T_s surface temperature [°C]
- $\langle\overline{h_c}\rangle$ time average mass transfer coefficient
- D_0 diffusion coefficient of vapor in air [cm^2 s^{-1}]
- ω angular frequency of the ultrasound. [s^{-1}]
- B gas particle velocity amplitude in the acoustic wave [cm s^{-1}]
- A_{0e} effective pressure amplitude of the acoustic field [dyne cm^{-2}]
- ρ_0 unperturbed gas density [g cm^{-3}]
- c_0 gas sound velocity [cm s^{-1}]

- $\frac{dm}{dt}$ drying rate [kg/s]
- h_m mass transfer coefficient [m/s]
- A surface of the droplet [m^2]
- $\rho_{v,s}$ vapor density at the surface of the droplet [kg/m^3]
- $\rho_{v,b}$ vapor density in the bulk of air [kg/m^3]
- ρl density of the liquid [kg/m^3]
- C_{total} total molar concentration [mol m^{-3}]
- D_{AB} gas/liquid diffusivity coefficient [$m^2 s^{-1}$]
- M_{water} molar mass [kg mol^{-1}]

11. Bibliography

https://www.piezodrive.com/ultrasonic-drivers/intro-ultrasonic/. (n.d.).

Aissa, A., ABDELOUAHAB, M., NOUREDDINE, A., EL GANAOUI, M., & PATEYRON, B. (2015). RANZ AND MARSHALL CORRELATIONS LIMITS ON HEAT FLOW BETWEEN A SPHERE AND ITS SURROUNDING GAS AT HIGH TEMPERATURE. *THERMAL SCIENCE,*, 1521-1528.

Al Zaitone, B., & Tropea, C. (2011). Evaporation of pure liquid droplets: Comparison of droplet evaporation in an acoustic field versus glass-filament. *Chemical Engineering Science*, 3914-3921.

Andrade, M. A., Pérez, N., & Adamowski, J. C. (2018). Review of Progress in Acoustic Levitation. *Brazilian Journal of Physics*, 190-213.

Andrade, Pérez, & Adamowski. (2018). Review of Progress in Acoustic Levitation. *GENERAL AND APPLIED PHYSICS*, 190-213.

Brant. (2001). Acoustic Physics: suspended by sound. *Nature*, 474-475.

Bücks, & Müller . (1933). Über einige Beobachtungen an schwingenden Piezoquarzen und ihrem Schallfeld. *Zeitschrift für Physik volume* , 75-86.

Buot de l'Epine, Y. (2017). *Réalisation d'un dispositif de lévitation acoustique.* Compiègne: UTC- Université de Technologie de Compiègne.

de Souza Lima, Ré, & Arlabosse. (2019). Drying droplet as a template for solid formation: A review. *Powder Technology*, 161-171.

Fang, Rogers, Selomulya, & Chen. (2012). Functionality of milk protein concentrate: Effect of spray drying temperature. *Biochemical Engineering Journal*, 101-105.

Ferrari, G. (1989). Drying Kinetics for a Single Droplet of Skim-Milk. *Journal of Food Engineering*, 215-230.

Foresti, D., Nabavi, & Poulikakos. (2012). On the acousic levitation stability of spherical and ellipsoidal particles. *Journal of Fluid Mechanics*, 581-592.

Fu, N., Wai Woo, M., & Dong Chen, X. (2012). Single Droplet Drying Technique to Study Drying Kinetics Measurement and Particle Functionality: A Review. *Drying Technology*.

Giorgiutti-Dauphiné, & Pauchard. (2018). Drying drops containing solutes: From hydrodynamical to mechanical instabilities. *THE EUROPEAN PHYSICAL JOURNAL*.

Goharzadeh, A., & Molki, A. (2015). Measuerement of fluid velocity development behind a circular cylinder using particle image velocimetry (PIV). *European Journal of Physics*.

Hilgenfeldt, Rallabandi, Agarwal, & Raju. (n.d.). Beyond acoustophoresis: Attractive and repulsive forces on particles. *The Journal of the Acoustical Society of America*, 2017.

https://it.mathworks.com/matlabcentral/answers/261513-how-to-display-an-image-in-mm. (n.d.).

https://soe.rutgers.edu/sites/default/files/imce/pdfs/gset-2016/acoustic-levitation-theoretical.pdf. (n.d.).

Kim, J. Y., & Weon, B. M. (2018). Evaporation of strong coffee drops. *Applied Physics Letters*.

Lin, & Chen. (2004). CHANGES IN MILK DROPLET DIAMETER DURING DRYING CHANGES IN MILK DROPLET DIAMETER DURING DRYING USING THE GLASS-FILAMENT METHOD. *Food and Bioproducts Processing*, 213-218.

Marzo, Barnes, & Drinkwater. (2017). TinyLev: A multi-emitter single-axis acoustic levitator. *Review of Scientific Instruments*.

Masters, K. (1972). *Spray drying Handbook.* TBS The Book Service Ltd.

Mecham, R. D. (2018). *Langevin Transucer Analysis and Acoustic Levitatio.* Lake Forest College Pubblication. Retrieved from 2018.

Mezhericher, Levy, & Borde. (2020). Theoretical Models of Single Droplet Drying Kinetics: A Review. *Drying Technology*, 278-293.

Mezhericher, M., & Borde, I. (2010). Theoretical Models of Single Droplet Drying Kinetics: A Review. *ResearchGate*.

Moreno, E., Acevedo, P., & Leija, L. (2005). Design and construction of a bolt-clamped Langevin transducer. *ResearchGate*.

Renksizbulut, Nafziger, & Li. (1991). A mass transfer correlation for droplet evaporation in high-temperature flows. *Chemical Engineering Science*, 2351-2358.

Shamaei, S., Kharaghani, A., Seiiedlou, S. S., Aghbashlo, M., Sondej, F., & Tsotsas, E. (2016). Drying behaviour and locking point of single droplets containing functional oil. *Advanced Powder Techology*, 1750-1760.

Sloth, J., Kiil, S., Jensen, A. D., Andersen, S. K., Jorgensen, K., Schiffter, H., & Lee, G. (2006). Model based nalysis of the drying of a single solution droplet in an ultrasonic levitator. *Chemical Engineering Science*, 2701-2709.

Thu Hang, Jaskulski, & Peglow. (2015). A NEW VALIDATED MODEL FOR SINGLE DROPLET DRYING PROCESS. *Thermal Process Engineering* (p. 12). Magdeburg: Otto von Guericke University.

Trinh, E. H., & Hsu, C.-J. (1986). Equilibrium shapes of acoustically levitated drops. *The journal of the acoustical society of America*.

Vasileiou, T. F. (2016). Toward Contactless Biology: Acoustophoretic DNA Transfection. *Sci Rep*.

WHITEHEAD, BALL, FINE, & LANGOLF. (2010). Solvent Vapor Exposures in Booth Spray Painting and Spray Glueing, and Associated Operations. *American Industrial Hygiene Association Journal*, 767-772.

Whymark. (1975). Acoustic field positioning for containerless processing. *Ultrasonics*.

Yarin, Brenn, Kastner, & Tropea. (2002). Drying of acoustically levitated droplets of liquid–solid suspensions: Evaporation and crust formation. *PHYSICS OF FLUIDS*.

YARIN, BRENN, KASTNER, RENSINK, & TROPEA. (1999). Evaporation of acoustically levitated droplets. *Journal of Fluid Mechnics*, 151-204.

YARIN, PFAFFENLEHNER, & TROPEA. (1998). On the acoustic levitation of droplets. *Journal of Fluid Mechanics*, 65-91.